

T-3383

GRAVITY DATA REDUCTION AND INTEGRATED INTERPRETATION  
IN A RUGGED MOUNTAINOUS AREA

**ARTHUR LAKES LIBRARY**  
**COLORADO SCHOOL of MINES**  
**GOLDEN, COLORADO 80401**

by

HENGREN XIA

ProQuest Number: 10796322

All rights reserved

INFORMATION TO ALL USERS

The quality of this reproduction is dependent upon the quality of the copy submitted.

In the unlikely event that the author did not send a complete manuscript and there are missing pages, these will be noted. Also, if material had to be removed, a note will indicate the deletion.



ProQuest 10796322

Published by ProQuest LLC (2019). Copyright of the Dissertation is held by the Author.

All rights reserved.

This work is protected against unauthorized copying under Title 17, United States Code  
Microform Edition © ProQuest LLC.

ProQuest LLC.  
789 East Eisenhower Parkway  
P.O. Box 1346  
Ann Arbor, MI 48106 – 1346


T-3383

A thesis submitted to the Faculty and the Board of Trustees of the Colorado School of Mines in partial fulfillment of the requirements for the degree of Doctor of Philosophy, Geophysics.

Golden, Colorado


Date 1/4/1988

Signed:   
Hengren Xia

Approved:   
Thomas LaFehr  
Thesis Advisor

Golden, Colorado

Date: 4 January 1988

  
Phillip R. Romig, Head  
Geophysics Department

ABSTRACT

It is difficult to reduce and interpret gravity anomalies in rugged mountainous areas. This thesis discusses three specific aspects of the use of the gravity method in areas of rugged topography: terrain corrections with variable density distributions, reduction of data to a common datum, and anomaly separation.

Using a constant density to calculate the simple Bouguer and terrain corrections in preparing of a complete Bouguer anomaly map can lead to substantial errors in areas where rock densities vary across the mapped region. The approach described in this thesis uses a linear regression method to calculate the minimum correlation between Bouguer anomaly and elevation in Nettleton profiles. After computing the variable reduction densities, variable-density terrain corrections are calculated using a fast Fourier transform (FFT) technique.

The method is tested on a gravity data set which encompasses the Klamath Mountains and Cascades volcanic chain boundary in northern California. The results show a reasonable density map calculated from the Bouguer anomaly

map. The complete Bouguer anomaly map using variable reduction density shows distinct differences from the complete Bouguer anomaly calculated using constant density.

Reduction of data to a datum is an interesting problem to geophysicists. Two synthetic data sets, a step with a sphere and real topography with a sphere, were used to compare three methods in the thesis: those of Dampney (1969), Bhattacharyya and Chan (1977), and Henderson and Cordell (1971). The Dampney method is found to be the most accurate, but it is expensive. The Bhattacharyya and Chan method can only be used for upward continuation, but it is a fast method. When the datum is close to a station, an accurate numerical integration method should be used; otherwise a false anomaly will be created. This change will slow the computation. The accuracy and computation speed of the Henderson and Cordell method is between those of the other two methods. The key problem is truncation of the harmonic series.

Anomaly separation is very important for anomaly interpretation. So far, no method can solve the inherent non-uniqueness in separation except forward modeling, which can only be used for areas where the geologic environment is

well-known. After analyzing modeling, filtering, and upward continuation methods, upward continuation, with the help of the filtering method, was used to separate regional and local anomalies. The results of this anomaly separation are geologically reasonable.

Finally, the new complete Bouguer anomaly data set using variable reduction density was interpreted in combination with other geophysical data. The differences between the variable density data and the constant density data lead to a different tectonic model, which is supported by seismic refraction, heat flow, and aeromagnetic data.

The main features of the new interpretation are the following: First, the relationship between the Klamath Mountain and the Cascade Range is not a normal fault contact, but a direct deposit contact. Second, there is a normal fault zone with a north-south trend passing beneath Mount Shasta. Third, there is another normal fault zone with a north-south trend to the east of the Medicine Lake Highland. These two normal fault zones imply a half-graben tectonic model for the Cascade Range.

TABLE OF CONTENTS

	Page
TITLE PAGE.....	i
SUBMITTAL SHEET.....	ii
ABSTRACT.....	iii
TABLE OF CONTENTS.....	vi
LIST OF FIGURE CAPTIONS.....	vii
LIST OF TABLE CAPTIONS.....	xi
ACKNOWLEDGEMENTS.....	xii
INTRODUCTION.....	1
GEOLOGIC SETTING.....	6
TERRAIN CORRECTIONS WITH VARIABLE DENSITY DISTRIBUTIONS.....	19
COMPARISON OF CONTINUATION TECHNIQUES FOR POTENTIAL FIELDS.....	34
GRAVITY ANOMALY SEPARATION.....	58
INTEGRATED INTERPRETATION.....	70
CONCLUSIONS AND FUTURE WORK.....	107
REFERENCES.....	112
APPENDIX.....	117

## LIST OF FIGURE CAPTIONS

Figure		Page
1	Physiographic provinces of the north-central California study area (after Huppunen, 1984)....	7
2	A perspective view of the topography in the study area.....	8
3	Geologic map of Klamath Mountains province (after Irwin, 1981).....	9
4	Schematic diagram showing sequential ages of suturing of accretion plates of the Klamath Mountains and adjacent Coast Ranges (after Irwin, 1981).....	11
5	Geologic map of the Cascades Range province (after Hammond, 1979).....	13
6.	Nettleton density profile, showing the correlation between topography and gravity anomaly (after Nettleton, 1939).....	21
7	Relationship between station height, and terrain and Bouguer correction values.....	23
8	Reduction density distribution map of the study area. Contour interval: $0.2 \text{ g/cm}^3$ .....	26
9	Complete Bouguer anomaly map with variable density distribution. Contour interval: 5 mGal.....	32
10	Complete Bouguer anomaly map with a constant density ( $2.67 \text{ g/cm}^3$ ). Contour interval: 5 mGal.....	33
11	Synthetic model 1: A. A step with a sphere (the step is one grid unit high, the sphere is 2 grid units deep); B. Theoretical gravity anomaly on the step surface.	



	Contour interval: 1 mGal.....	36
12	Synthetic model 2: A. Real relief (from Mount Shasta) with a sphere at 1 km depth; B. Theoretical gravity anomaly on the real relief surface. Contour interval: 1 mGal.....	37
13	A. Anomaly of the step model reduced to the top surface of the step using the Dampney method. B. Theoretical anomaly on the top surface of the step. Contour interval: 1 mGal.....	42
14	A. Anomaly of the real relief model reduced to the 4 km datum using the Dampney method. B. Theoretical anomaly on 4 km datum. Contour interval: 1 mGal.....	43
15	Anomaly of the real relief model reduced to a 1 km datum using the Dampney method. Contour interval: 5 mGal.....	45
16	A. Anomaly of the step model reduced to the top surface of the step using the Bhattacharyya and Chan method. B. Theoretical anomaly on the top surface of the step. Contour interval: 1 mGal.....	49
17	A. Anomaly of the real relief model reduced to the 4 km datum using the Bhattacharyya and Chan method. B. Theoretical anomaly on 4 km datum. Contour interval: 1 mGal.....	50
18	A. Contour map of location term values in Equation 4.11. Contour interval: 2 units. B. Equivalent source value contour map. Contour interval: 0.005 units.....	51
19	Anomaly of the real relief model reduced to a 5 km datum using the Bhattacharyya and Chan method.	

	Contour interval: 1 mGal.....	52
20	A. Anomaly of the step model reduced to the top surface of the step using the Henderson and Cordell method. B. Theoretical anomaly on the top surface of the step. Contour interval: 1 mGal.....	55
21	Anomaly of the real relief model reduced to a 5 km datum using the Henderson and Cordell method. Contour interval: 1 mGal.....	56
22	Isostatic anomaly map of the study area. Contour interval: 5 mGal.....	64
23	Isostatic residual anomaly map of the study area. Contour interval: 5 mGal.....	65
24	Radially averaged power spectrum of the isostatic residual anomaly for the study area....	66
25	Filtered gravity anomaly map of the isostatic residual anomaly for the study area (filter pass band: 250-80 km). Contour interval: 5 mGal.....	67
26	Gravity anomaly on plane 7.5 km above sea level. Contour interval: 5 mGal.....	69
27	Northern California refraction line location map (after Zucca and others, 1986).....	74
28	Heat flow map of Northern California (after Mass and others, 1982).....	76
29	Calculated density section of Klamath Mountains and Cascade Range area (after Zucca and others, 1986).....	79
30	Interpreted section from magnetotelluric data in Northern California (after Stanley, 1982)....	83

31	Aeromagnetic anomaly map of Northern California. Contour interval: 100 nT.....	86
32	Filtered reduced-to-pole aeromagnetic anomaly for Northern California (filter pass band: 1000-20 km). Contour interval: 100 nT.....	87
33	Aeromagnetic anomalies on plane 7.5 km above sea level. Contour interval: 100 nT.....	88
34	Basement depth contour map of Cascade Range. Contour interval: 0.5 km.....	95
35	Reduced gravity anomaly on datum 4 km above sea level. Contour interval 5 mGal.....	96
36	Forward model section of regional structure in Klamath Mountains and Cascades Range. solid line: anomaly reduced to 4 km datum; dotted line: calculated anomaly.....	97
37	Gravity anomaly map of Medicine Lake Highland. Contour interval: 2 mGal.....	99
38	Forward model profile through Medicine Lake Highland. Solid line: calculated anomaly; dotted line: observed anomaly.....	101
39	Diameter versus Bouguer gravity anomaly for 18 calderas. M: mafic rock; I: intermediate rock; S: silicic rock (after Finn and Williams, 1985).....	104
40	Geologic model of regional profile in the Klamath Mountains and Cascades range area. 1. High Cascades, 2. Western Cascades, 3. Eastern Klamath plate, 4. Central Metamorphic plate, 5. Western Paleozoic and Triassic plate, 6. Granite, 7. Basalt, 8. Upper Mantle, 9. Intrusion, 10. Fault.....	106

T-3383

41	Place Location Map, (transparency at back of this thesis) .....	126
----	--	-----

## LIST OF TABLE CAPTIONS

Table		Page
1	Relationship between the truncation order of of the harmonic series and data size.....	54
2	Rock sample densities in the Klamath Mountain and Cascade Range area (after Chong and Blank, 1972).....	77
3	Rock densities in the Klamath Mountain and Cascade Range area from the variable reduction density distribution map.....	80

ACKNOWLEDGEMENTS

Without the spirited support of my wife, Ms. Ruzhen Yan, I could not have completed my Ph.D. program. I cordially devote this dissertation to her.

There is a Chinese adage: when we drink the water, we cannot forget the man who dug the well. It is a pleasant task to remember and thank those who have helped me with this thesis work. I first want to thank Dr. Thomas LaFehr for his support, orientation and advice. I also wish to thank Dr. Tomas Grose, Dr. Walter Whitman, Dr. Norman Harthill, Dr. Richard Hansen and Dr. Donald Dickinson. All of them gave me valuable help and encouragement. Especially, I want to thank Dr. Norman Harthill and Dr. Richard Hansen; through them I have greatly widened my knowledge in different areas.

I appreciate Ms. Helen Leek's help with English, typing, and daily assistance. I also wish to thank all of the students in the Center for Potential Fields Studies who assisted me in accomplishing various research work.

Finally, I want to thank all the sponsors of CPFS: AGIP, AMOCO, ARCO, Chevron Research, EXXON, Mobil Oil, Standard Oil, Tenneco Oil, and Unocal. It would have been

T-3383

impossible to finish the research work without their  
sponsorship.

## INTRODUCTION

Gravity data are increasingly acquired in rugged mountainous areas where it is more difficult to acquire, reduce, and interpret gravity data than in the flat areas. This thesis is concerned with gravity data reduction and interpretation in such areas of rugged topography, especially terrain corrections with variable density, reduction of data to a datum, and anomaly separation.

Observed gravity data are affected by two groups of factors: factors external to the subsurface geology and factors directly caused by subsurface geology. The external factors include gravimeter drift, solar and lunar effects, station elevation effects (free air and simple Bouguer), terrain effects, and normal earth effects. The effective removal of the external factors is the purpose of gravity data reduction. The internal factors are the effects of the anomalous subsurface geology. Determining this distribution is the goal of gravity data interpretation. The difficulty is that the terrain and simple Bouguer effects are mixed with the effects of the anomalous subsurface geology in rugged topographic areas. The purpose of this dissertation is to try to solve this problem.



### Terrain correction with variable density

In areas of rugged topography, the values of Bouguer and terrain corrections are very large. Conventional data reduction with a constant density can cause distortion in rugged mountainous areas. For example, in the Klamath Mountains and Cascade Range area, the relief is very rugged, and relative elevations are very large (nearly 4000 m). Also, the geology is complicated. The densities of rocks are variable, from less than  $2.25 \text{ g/cm}^3$  (volcanic rocks) to more than  $3.0 \text{ g/cm}^3$  (ultramafic rocks). The maximum Bouguer correction values are as large as 450 mGal, and the terrain correction exceeds 100 mGal at Mount Shasta (T. LaFehr, personal communication). In such areas, data reduction using a constant density,  $2.67 \text{ g/cm}^3$ , may cause errors as large as 50 mGal. Thus, we need to use variable densities to perform the Bouguer and terrain corrections on gravity data in such areas.

Many geophysicists contributed to the solution of this problem. Hammer (1939) created terrain correction charts, which do not, however, anticipate relief as large as that at the study area. Nettleton (1939) proposed a density determination method for profiles, which has been used by many geophysicists since then. Vajk (1956) proposed a method for handling variable density, emphasizing the importance of using a constant density below the lowest

elevation. Grant and Elsharty (1962) used a least-squares fit of a polynomial function to obtain variable densities from residual Bouguer anomaly and elevation data. During the course of this project (Xia and Dewhurst, 1986), Francine, Jean-Claude and Lakshmanan (1987) developed a procedure similar to the one used here to estimate density distributions from residual Bouguer anomaly and elevation data.

#### Reduction of data to datum

Where gravity measurements are not made on a constant elevation datum, interpreters must either incorporate the terrain in their final model or actually reduce the gravity data to a common level. The latter is a subject which has attracted many geophysicists.

Dampney (1969) determined an equivalent source distribution of discrete point masses on a plane from Bouguer anomaly measurements on an irregular surface, using a system of linear equations. Henderson and Cordell (1971) described a method for reduction of unevenly spaced gravity and magnetic data at elevations to a common level using the finite Fourier series. Emilia (1973) adopted the concept of equivalent sources, (i.e., a distribution of line dipoles), for processing and analyzing total magnetic field profiles. Courtillot et al. (1974) considered the problem of finding

the geometrical distribution of sources responsible for an observed magnetic anomaly. Bhattacharyya and Chan (1977) generated an equivalent source layer on the topographic surface using a Fredholm integral equation of the second kind. Hansen and Miyazaki (1984) developed equivalent dipole layers under the topographic surface. Following Evjen (1936), Cordell and Grauch (1984) created a Taylor expansion method for the drape-to-level problem.

#### Anomaly separation

Anomaly separation means the separation of regional anomalies and residual anomalies. The definition of regional anomalies and residual anomalies depends on the geologic targets which we want to study. Sometimes there are several orders of regional anomaly. In general, there are two orders of regional anomalies in rugged mountainous areas: the regional anomaly of the Moho and the regional anomaly of basement structures.

Isostatic correction is a commonly-used method for separating the Moho effect. Since Pratt (1855) and Airy (1855) published their papers, many geophysicists have made contributions to this subject (Heiskanen and Vening Meinesz 1958; Woollard, 1966). Recently, the case for applying isostatic corrections to Bouguer gravity data has been presented by Jachens and Griscom (1985).

The filtering method for separating regional anomalies has been an active subject in gravity and magnetics for decades. Nettleton (1954) used a convolution technique to separate regional and residual fields. Gupta and Ramani (1980) used a Wiener filter to separate gravity anomalies in Precambrian terrain. Upward continuation is a special case of the filtering method. The paper by Jacobsen (1987) showed that the upward continuation operator is physically comprehensible when applied to real, nonrandom anomalies.

#### Purpose

Although many geophysicists have made contributions to the study of gravity data reduction in areas of rugged topography, the methods are still impractical, especially those for terrain corrections with variable density distributions. The intent of this dissertation is to promote these techniques to a practical stage. The organization of the thesis is as follows: first, to generate an algorithm for density calculation; second, to make a comparison of continuation techniques; and third, to create a procedure for anomaly separation. Then, using the data set from the Klamaths and Cascades as an example, to prove the advantages of these techniques.

## GEOLOGIC SETTING

The Klamaths and Cascades area is located in northern California. The study area extends from  $41^{\circ}\text{N}$  to  $42^{\circ}\text{N}$  latitude and from  $121^{\circ}\text{W}$  to  $123^{\circ}\text{W}$  longitude. Two major physiographic provinces are partially included in the study area: the Cascade Range and the Klamath Mountains (Figure 1). The study area is a rugged mountainous area, especially the Klamath Mountains province, where is characterized by rugged mountains and narrow valleys. However, the highest peak in the study area is Mount Shasta, which is in the Cascade Range province. The peak is 4200 meters high. Figure 2 is a perspective view of the topography in the study area.

## Klamath Mountain province

The Klamath Mountains lie west of and adjacent to the Cascade Range. Figure 3 is the geologic map of the Klamath Mountains. The geology of the area is complicated. The area is an accretion zone, which was formed by plate subduction. It is composed of four plates: the Eastern Klamath Plate, the Central Metamorphic Plate, the Western Paleozoic and Triassic Plate, and the Western Jurassic Plate. These plates range in age from Devonian to Jurassic (Irwin, 1981) (Figure 4).

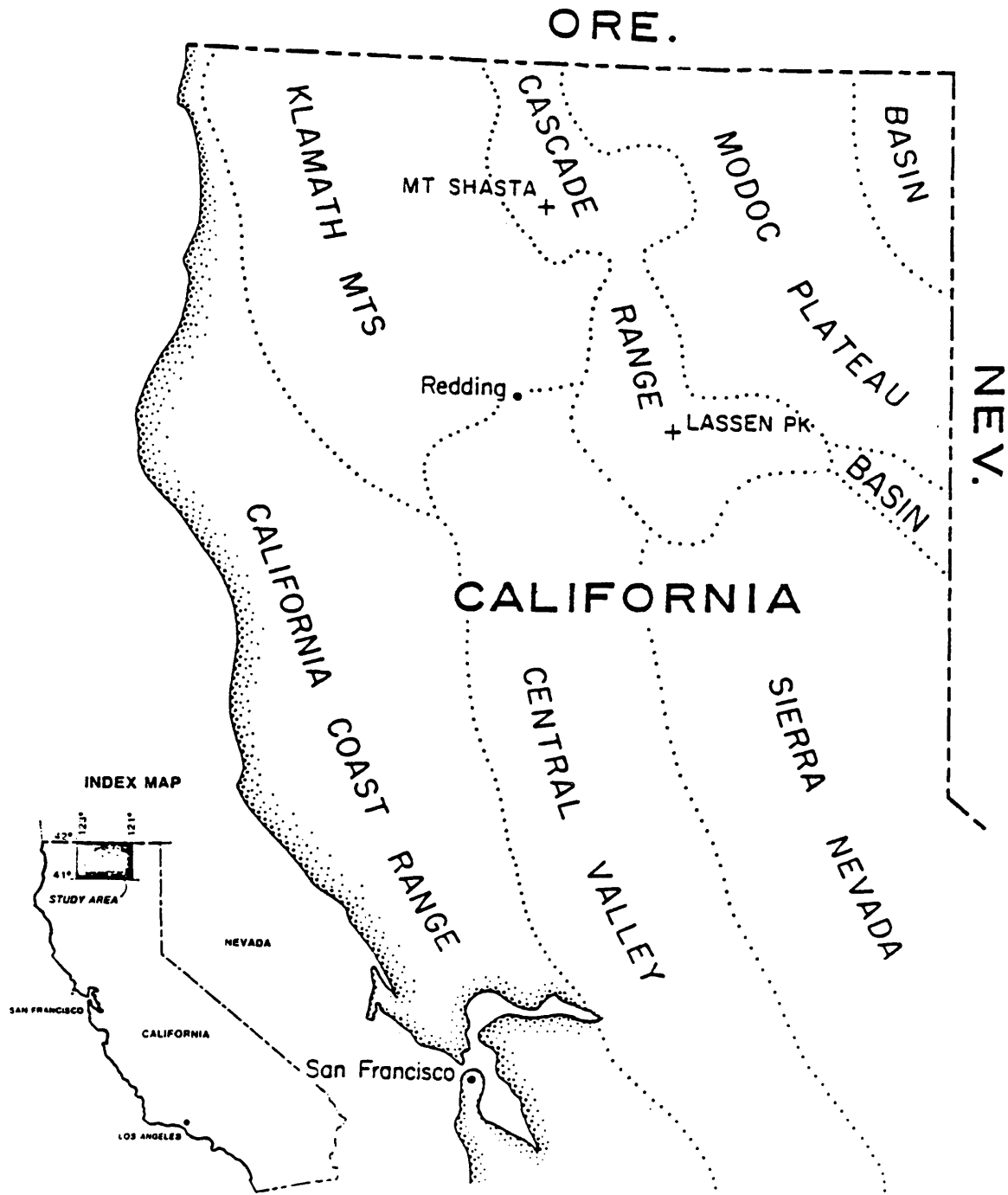


Figure 1. Physiographic provinces of the north-central California study area (after Hupponen, 1984).

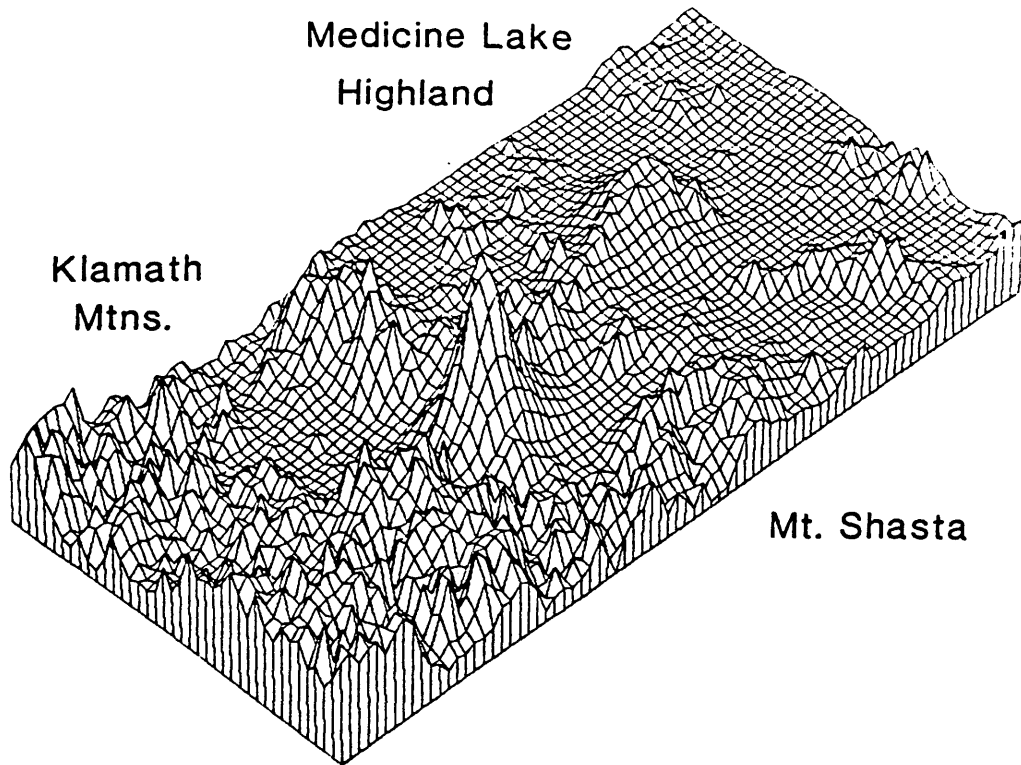


Figure 2. A perspective view of the topography in the study area.

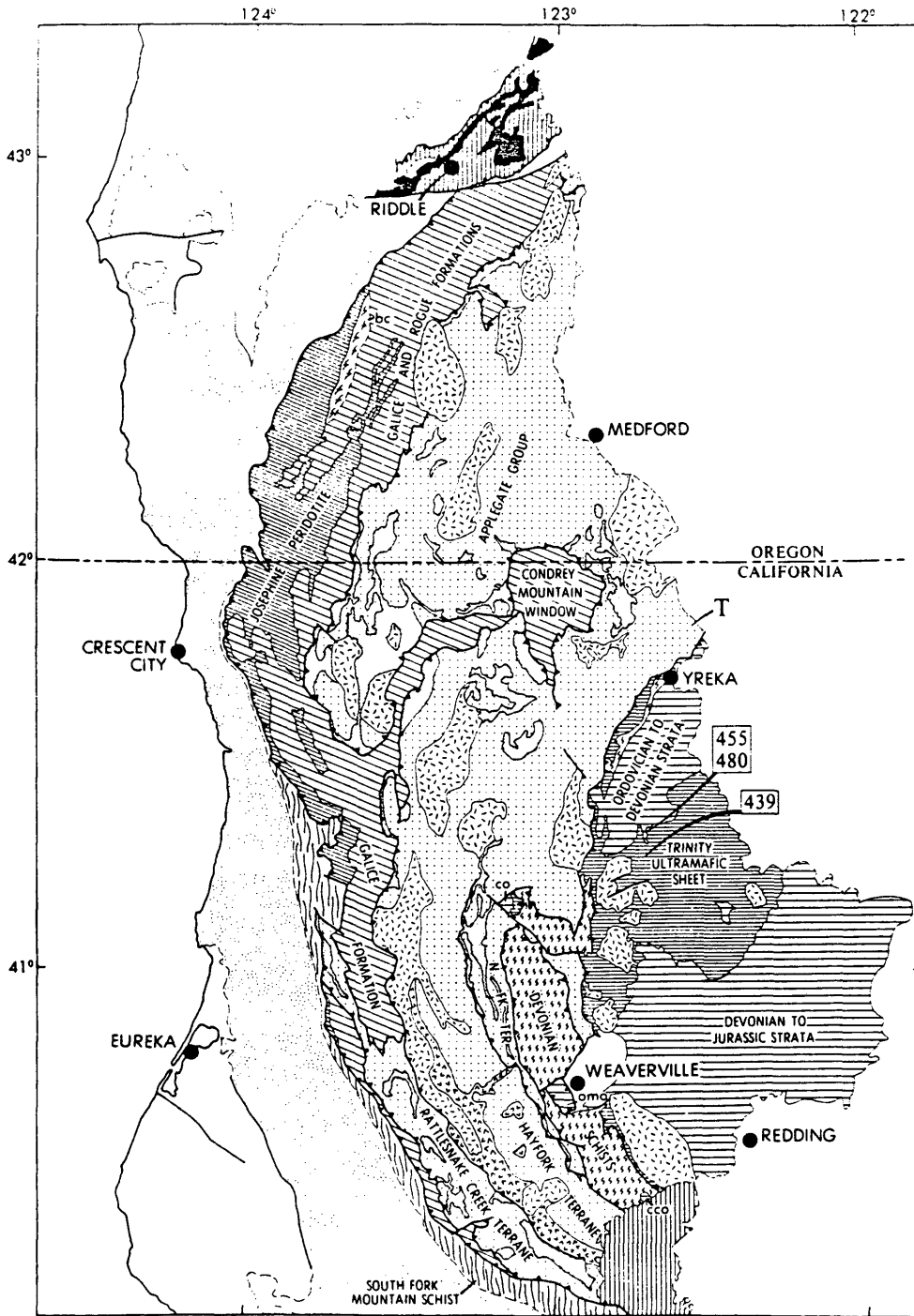


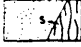

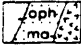

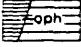
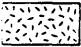
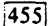



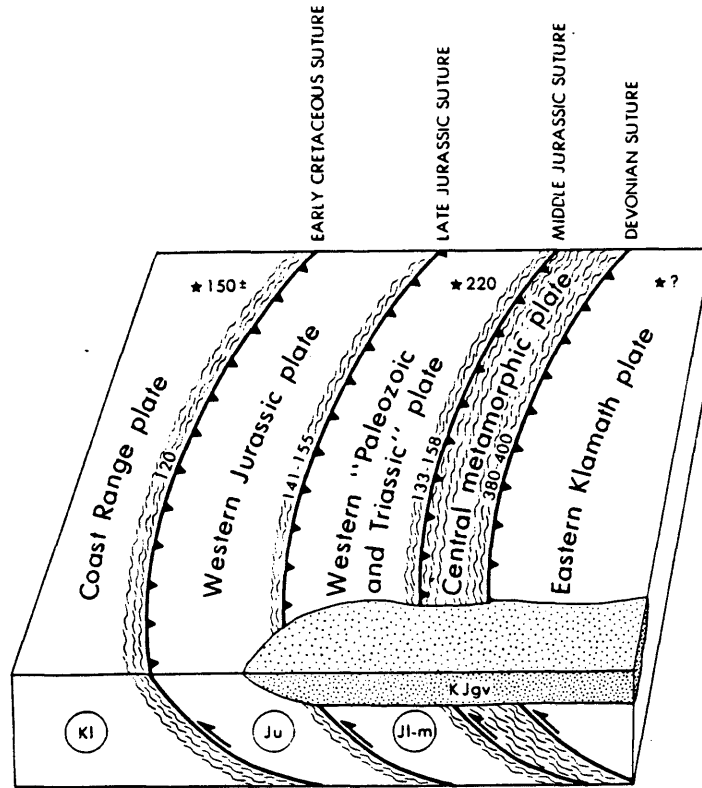
Figure 3. Geologic map of Klamath province (after Irwin, 1981). (continued on next page)



Figure 3. continued

## EXPLANATION

-  Tertiary and younger strata; includes minor Upper Cretaceous in California Coast Ranges
-  Great Valley sequence in California and Myrtle Group in Oregon; Upper Jurassic and Cretaceous; includes Upper Jurassic ophiolitic rocks(oph)
-  Mesozoic rocks of Coast Range province; mostly Franciscan and Dothan Formations, but includes klippen of Klamath Mountains rocks and Great Valley sequence in Oregon; South Fork Mountain Schist(s) is shown only adjacent to the Klamath Mountains province and includes some semischistose metagraywacke
-  Western Jurassic plate: mainly Galice and Rogue Formations; includes Josephine Peridotite and related ophiolitic rocks(oph), amphibolite of Briggs Creek(bc), and schist of Condrey Mountain
-  Western Paleozoic and Triassic plate: mainly rocks of North Fork, Hayfork, and Rattlesnake Creek terranes in southern part of province, undivided rocks in central part, and Applegate Group in Oregon; includes ophiolitic rocks(oph); Hayfork Bally Meta-andesite(ma) shown in Hayfork terrane
-  Central metamorphic plate: Abrams Miça Schist and Salmon Hornblende Schist of Devonian metamorphic age
-  Eastern Klamath plate: early Paleozoic strata in the Yreka-Callahan area; Devonian to Jurassic in the Redding area; includes Trinity ultramafic sheet of ophiolitic rocks(oph); klippen of eastern Klamath plate on central metamorphic plate include Cecilville outlier(co), Oregon Mountain outlier(oma), and Cottonwood Creek outlier(cco)
-  Calc-alkaline plutonic rocks; Jurassic age
-  Radiometrically dated samples of ophiolitic rock
-  Permian limestone of Tethyan faunal affinity



EXPLANATION

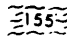

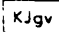
-  Isotopic age of rock regionally metamorphosed during underthrusting.
- ★ 220 Isotopic age of blueschist knockers.
-  Paleontologic age of youngest strata in underthrust (lower) plate. J1-m (Lower or Middle Jurassic); Ju (Upper Jurassic); K1 (Lower Cretaceous - Valanginian)
-  Great Valley sequence: deposited on accreted plates of Klamath Mountains.

Figure 4. Schematic diagram showing sequential ages of suturing of accretion plates of the Klamath Mountains and adjacent Coast Ranges (after Irwin, 1981).

The discussion by Hammond (1979) points out the uncertainty in the tectonic relationship between the provinces of the Klamath Mountains and the Cascade Range. Magill and Cox (1980) described the geologic contact between the Klamath Mountains and the Western Cascades in northern California as being a depositional contact rather than a fault contact. The basalt rocks of the Cascade Range are observed to lie unconformably on the pre-Tertiary rocks of the Klamath Mountains. Dickinson (1976) suggested that the Klamath Mountains are part of the remains of a pre-Tertiary island arc which extends eastward beneath the Modoc Plateau region. An eastward projection of the Klamath Mountains between Mount Shasta and Lassen Peak nearly bisects the Cascade Range and marks the transition from the north-south trend of the Cascade axis north of, and including, Mount Shasta to a southeast trend which continues south to end near Lassen Peak.

#### The Cascade Range

Figure 5 is the geologic map of the Cascade Range. MacDonald (1966) gave the following description of the Cascade Range in California.

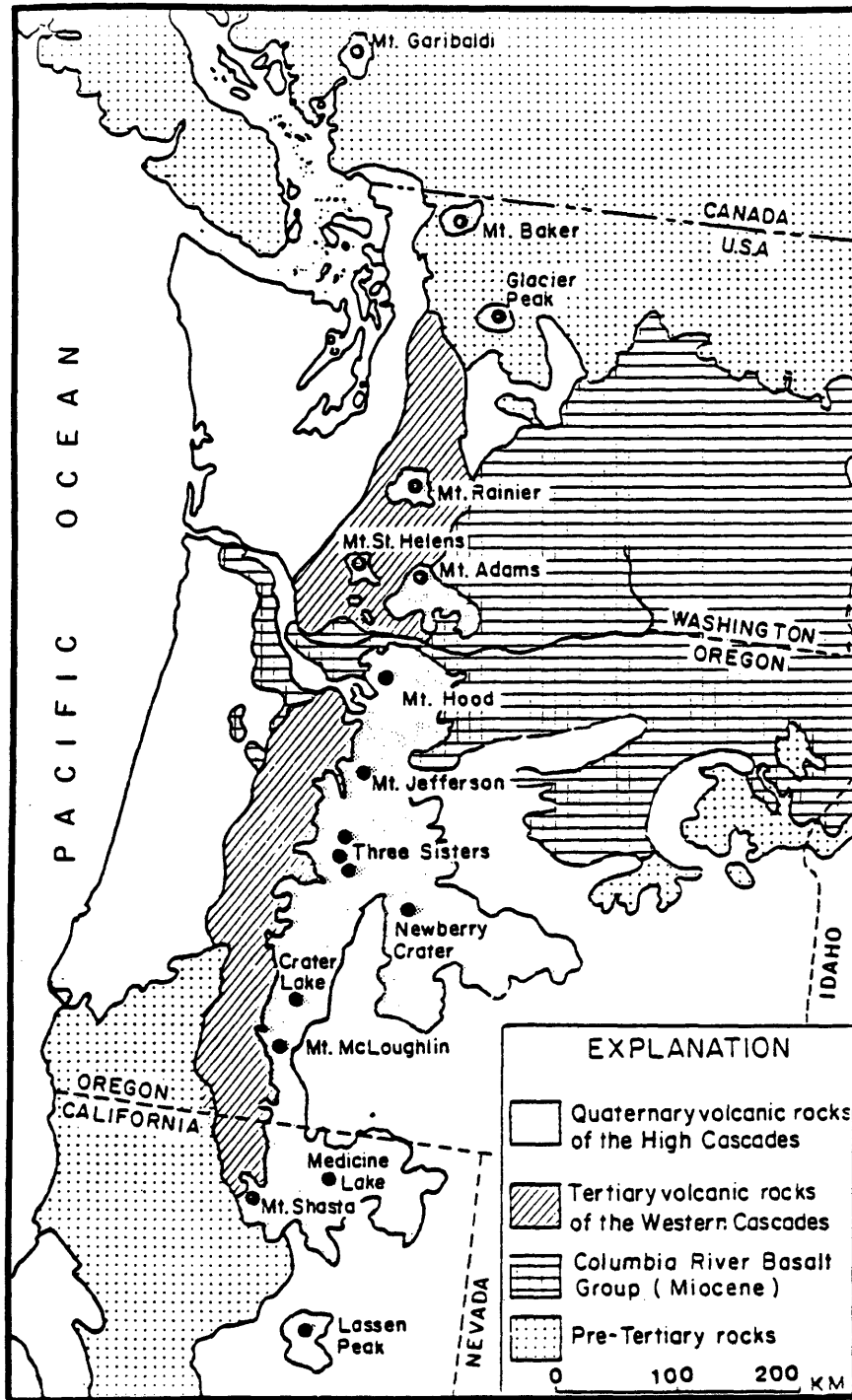


Figure 5. Geologic map of the Cascade Range province (after Hammond, 1979).

The range may be divided into the Western Cascade Range and the High Cascade Range. The sequences range in age from late Eocene to late Miocene. The rocks of the Western Cascade Range extend along the west edge of the High Cascade Range for approximately 55 miles south of the northern California border. The rocks of the High Cascade Range extend southward from the California border across the entire length of the study area and include two elongate lobes of high topography with axes oriented east-west that are associated with the volcanic centers of the Mount Shasta, Medicine Lake, and Lassen Peak volcanoes.

A more detailed study of the Cascade range was carried out by Hammond (1979) and the following description is taken substantially from that work. The Western Cascade Group is divided into three parts: the lower part, middle part, and upper part (Hammond, 1979). The lower part is about 1.5 to 5 km thick, and consists of andesite, basalt and silicic volcanic rocks. This part is found mainly along the western margin of the range. The thick sequences of basalt lava flows comprise broad shield volcanoes. The andesite lava flows form the broad base of stratovolcanoes. The lava sequences give way eastward to a thick accumulation of volcanoclastic rocks, including lithic-rich mudflow deposits, well-bedded lacustrine, fluvial, and minor air-fall tuff beds.

The middle part is 0.5 to 3 km thick and consists of interstratified light-colored pyroclastic flows and beds of volcanoclastic rocks, including mudflow deposits. Dark-colored pyroclastic rocks and lava flows form about equal volumes. The middle part is separated from the underlying part by a regional unconformity marked generally by a basalt pyroclastic flow. The pyroxene andesite lava flows, 200 to 800 m thick, commonly form the base and apron of the broad stratovolcanoes. In areas where the lavas are thin or lacking, the stratigraphic interval is occupied by a distal volcanoclastic facies, consisting chiefly of andesitic mudflow and conglomerate deposits. The interstratified sequences of pyroclastic and andesitic lava flows are the main characteristics of the middle part. This indicates that volcanism consisted chiefly of eruptions from stratovolcanoes and probably calderas. The greater abundance of pyroclastic flows in the middle part compared with the lower part indicates increasing emplacement of silicic magma. The middle part ranges in age from 30 to 15 Ma.

The upper part of Western Cascade Group is 0.25 to 0.75 km thick, consisting of interstratified varicolored hornblende dacite and andesite pyroclastic flows, mudflows, and fluvial volcanoclastic deposits, and brown-to-gray pyroxene andesite porphyry lava flows. The rocks of this

part may be the most silicic of the Western Cascade Group. Most rocks of the upper part appear to have erupted from stratovolcanoes and probable calderas. The silicic volcanic rocks represent a continuation of the high level magnetism of the middle part. The rocks of the upper part range in age from 15 to 5 Ma.

The granitic intrusions were emplaced during the formation of the Western Cascade Group between 50 and 10 Ma. The major intrusions consist of biotite-hornblende quartz diorite and granodiorite, pyroxene diorite, and less quartz monzonite and/or pyroxene andesite porphyry and dacite dikes. The granitic plutons form two belts: an eastern belt and a western belt. The western belt is slightly younger.

The High Cascade Group is composed of about 85% high-alumina olivine basalt and basaltic andesite and 15% hornblende and/or pyroxene andesite and less dacite. Rocks of different compositions are interstratified and unconformably overlie the Western Cascade Group. The high-alumina olivine basalt and basaltic andesite erupted from many cinder cones and shield volcanoes coalesced to form a platform about 0.5 to 1 km thick. Dating of rock samples shows that the High Cascade Group is about 5 Ma to Recent time.

Epizonal plutons form two north-trending belts underlying the northern part of the range. Folding in the northern part of the range was along northwest to north trends, while broad subsidence prevailed in the southern part for the period 50 to 12 Ma. Eastward-trending Yakima folds were superimposed on the northern part of the range while the southern part continued subsiding during the period 12 to 5 Ma.

Two principal fault directions occur in the volcanic Cascade Range: northwest and north-south. The northwest trend parallels the older northwest fold pattern and is believed to have developed concurrently with that fold system. East-west extension on the these north-south faults seem to be the dominant tectonic pattern affecting the High Cascade Group and, locally, the Western Cascade Group. The east-west trending Honey Lake shear zone is the probable southern termination of the range. It lies within a zone of marked crustal thinning north of the Sierra Nevada, and the fault possibly offsets Mesozoic structures of the Klamath Mountains on the west.

Uplift began in the North Cascades possibly as early as 50 Ma, in southern Washington 20 Ma, attaining as much as 1.5 km elevation. In the south uplift has been negligible, and the volcanic accumulation of the High Cascade Group forms the topography.



Rotation occurred during 50 Ma to 15 Ma. The tectonic history of the Cascade Range started with the growth of the Cascade volcanic arc on the back side of the Coast Range-Klamath Mountains block. The Cascades rifted from the continent along the Olympic-Wallowa Lineament and together rotated about a pivot in the Olympic Mountains, with the Olympic-Wallowa Lineament becoming a transition zone between the southern Cascade arc and stationary North Cascades. Active subduction pressed the northern pivotal end of the block against the continent. This rotation caused an extensive environment in the South Cascades. The northern and north-south trending normal faults indicate such an environment. These faults within the High Cascade Group most likely correspond to Basin and Range faulting. In addition, a great number of cinder cones cover the study area, in particular over the Medicine Lake Highland. The cones probably mark the location of normal faults and volcanic vents (LaFehr, 1965; MacDonald, 1966).

TERRAIN CORRECTION  
WITH VARIABLE DENSITY DISTRIBUTIONS

Following the density determination of Harkness (1889), simple Bouguer and terrain correction are usually calculated using a standard density of  $2.67 \text{ g/cm}^3$ . Although using a single reduction density is obviously unrealistic, there have been relatively few attempts to devise a method by which variable densities could be used to reduce gravity data. Nettleton (1939) devised the density profile technique to determine reduction densities. In this technique, a spatial density function which minimizes the coherence between the reduced complete Bouguer anomaly and surficial topography is established visually. Following the Nettleton technique, a linear regression model has been generated to automatically calculate surficial density distributions.

Having established the variable density distribution, terrain corrections are calculated using a fast Fourier transform (FFT) technique. The method is used to correct the gravity data set from the Klamath Mountains/Cascade Range boundary. The results show a reasonable density map, and the new terrain corrections with variable density distribution yield an improved Bouguer anomaly map.

### Density determination

The Nettleton density profile technique for determining density uses the fact that the correct reduction density may be determined by minimizing the coherence between the complete Bouguer anomaly and elevation of the profile under consideration. It is possible that minimum correlation may exist for different reduction densities in different parts of the profile. Certain assumptions must be true so that the minimum correlation occurs for the correct reduction density:

- 1) Within a limited region, variations in surficial rock densities are small enough that the rock units can be characterized by an average density.
- 2) The gravity data within the limited region are sampled sufficiently densely that a spatial wavelength band can be defined within which the effects of spatial aliasing of the free air gravity field are minimal.
- 3) No anomaly correlated with geology exists in the limited region.

Figure 6 is a Nettleton density profile (Nettleton, 1939). This profile reflects the coherence between the

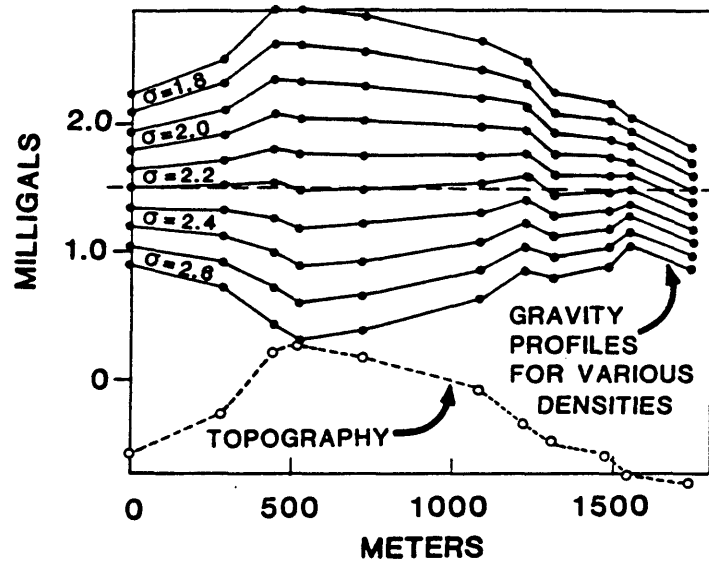


Figure 6. Nettleton density profile, showing the correlation between topography and gravity anomaly (after Nettleton, 1939).

gravity distortion of topography and elevation. The Bouguer gravity anomaly is:

$$g = g_o + g_e + g_b + g_t \quad (3.1)$$

where  $g_o$  is the observed of gravity anomaly,

$g_e$  is the earth effect,

$g_b$  is the Bouguer correction,

and

$g_t$  is the terrain correction.

In Equation (3.1),  $g_t$  and  $g_b$  are related to the elevation. The relationship between  $g_t$  and the elevation is parabolic, and the relationship between  $g_b$  and the elevation is linear. However,  $g_t$  is much smaller than  $g_b$  (Figure 7). Therefore, over a limited region of the earth's crust, the correlation between the Bouguer anomaly and the elevation can be considered to be characterized by the following linear relationship:

$$g(\rho) = a + bh$$

where  $g(\rho)$  is the complete Bouguer anomaly, a function of density,  $\rho$ ;  $h$  is the station elevation; and  $a$  and  $b$  are coefficients of the linear function. This relationship allows the use of a linear regression method to estimate

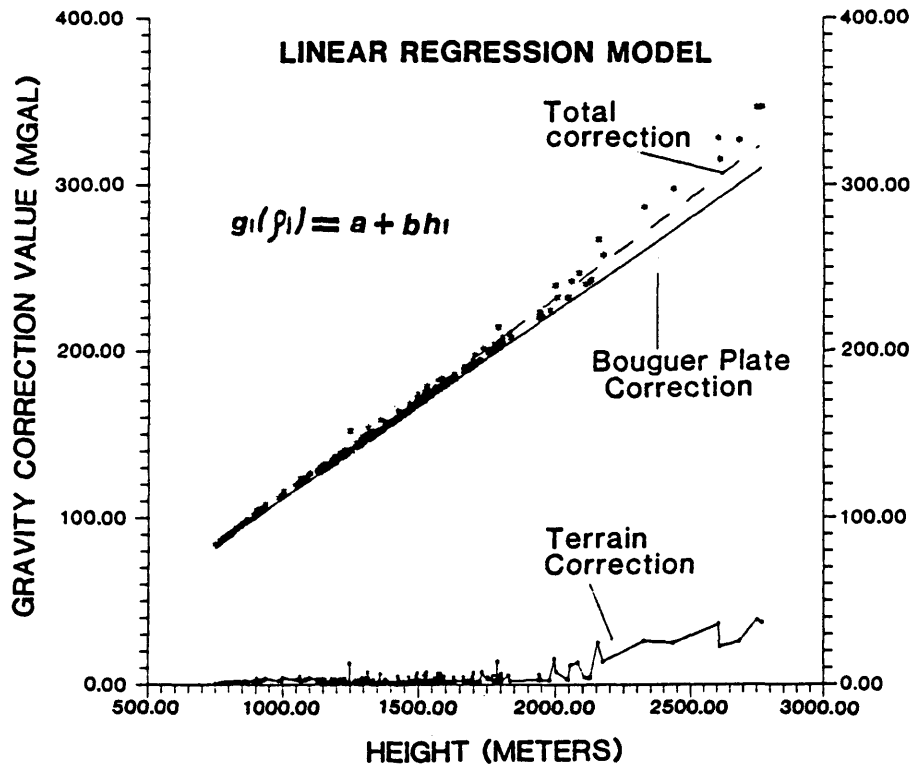


Figure 7. Relationship between station height, terrain and Bouguer correction values.

the density for a limited region. The correlation coefficient between the complete Bouguer anomaly and the station elevation is

$$R(\rho_j) = \frac{\Sigma(h_i - h)[g_i(\rho_j) - g(\rho_j)]}{\{\Sigma(h_i - h)^2 \Sigma[g_i(\rho_j) - g(\rho_j)]^2\}^{1/2}} \quad (3.3)$$

where  $\rho_j$  is the reduction density for the limited region;  $h$  is the average value of the station elevations; and  $g$  is the average complete Bouguer anomaly of the limited region. The optimum reduction density is given by minimizing this correlation coefficient.

Equation (3.3) is only valid for regions where no anomaly is caused by geologic bodies. However, gravity anomalies are generally caused by geologic bodies everywhere. These anomalies will cause this method to fail to calculate the correct density. The most serious problem is where regional anomalies exist, because most regional anomalies have high amplitudes. To suppress such regional anomalies, the derivative of the Bouguer anomaly and elevation are used in formula (3.3) for computing the correlation coefficient instead of the Bouguer anomaly and station elevation. Based on (3.3), the following steps are then to compute densities:

- 1) Pick a profile from the gridded gravity data set, including elevation, free air anomaly, and terrain correction data.
- 2) Based on the elevation data, separate each peak as a limited segment for density estimation.
- 3) Re-reduce each segment of gravity data using a suite of constant densities.
- 4) Compute the correlation coefficient using the derivatives of elevation and complete Bouguer anomaly.
- 5) Minimize the correlation coefficient, obtain an optimum density and verify whether the density is reasonable.
- 6) Repeat steps 3)-5) until the profile is finished.
- 7) Repeat steps 1)-6) until the whole area is finished.

The calculation of density should be carried out along different directions, then an average density data set obtained as the final reduction density data.

#### Density distribution map

The method was used on the gravity data set from the Klamath Mountains and the Cascade Range area (Figure 8). Smith (1984) mapped a region which encompassed the boundary between the Klamath Mountains province and the Cascade Range



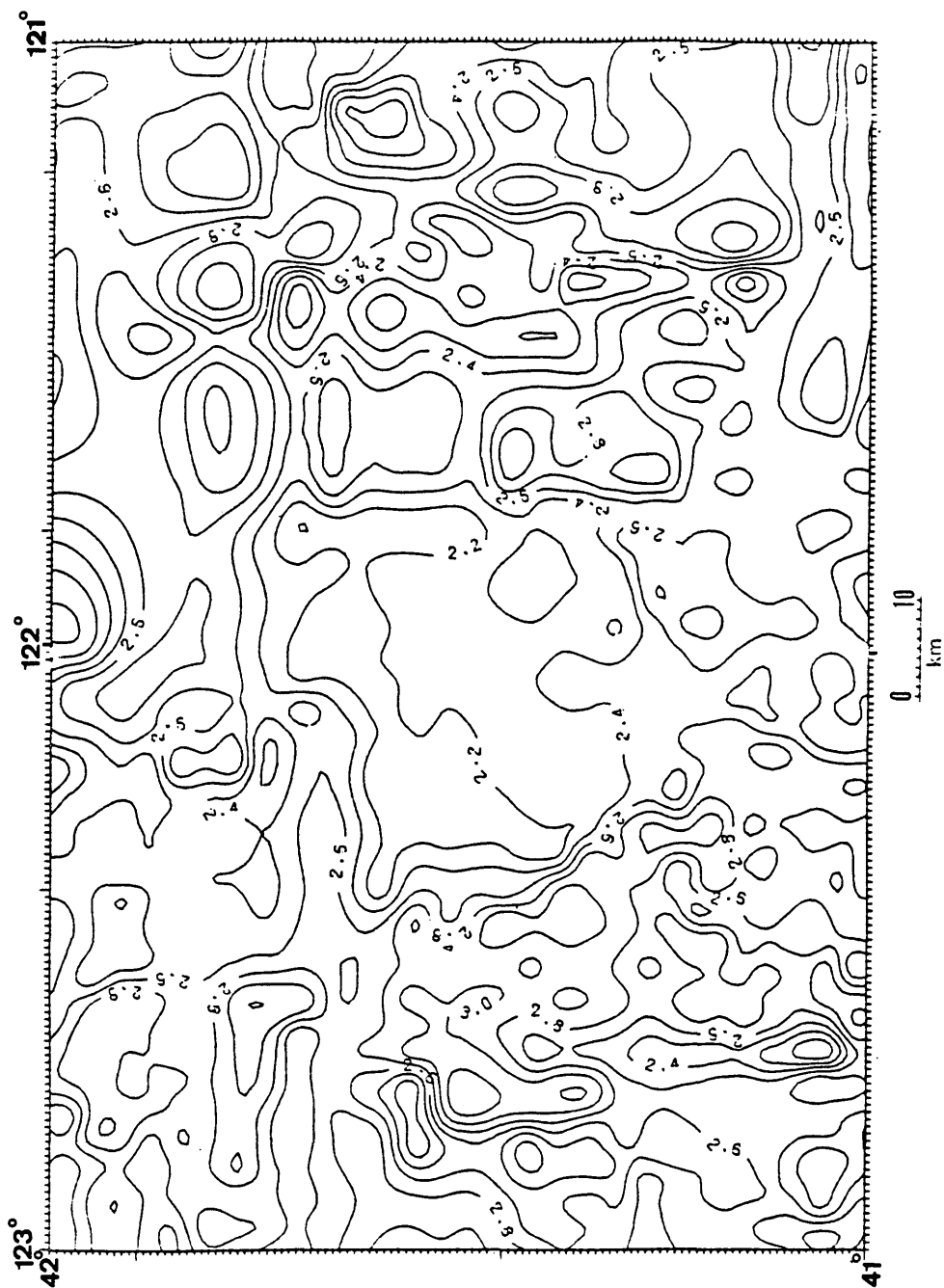


Figure 8. Reduction density distribution map of the study area.  
Contour interval: 0.2 g/cm<sup>3</sup>.

province in Northern California. In the density map, the higher densities (greater than  $2.67 \text{ g/cm}^3$ ) are mainly located on the west side of the map, whereas the lower densities (less than  $2.67 \text{ g/cm}^3$ ) occur on the east side of the  $1^\circ \times 2^\circ$  area. The boundary between the two density sets matches the geologic boundary between Klamath Mountains and the Cascade Range almost perfectly. Within these two areas there are several anomalous regions. The first is the southwest quadrant of the Klamath area where an area of low density strikes north-south; the origin of this low-density area is unknown. In the Cascade Range region to the east, there are two high-density zones. One zone strikes north-south; the other is north-west to south-east trending. The two intersect at the Medicine Lake Highland. The latter zone coincides with the Medicine Lake Highland, where a shallow intrusion exists (Finn, 1985). The former zone is coincident with a widespread outcrop of Tertiary basalt with north-west to south-east trend which, on satellite imagery, can be seen to have volcanic centers and perhaps a collapse feature associated with it.

#### Calculation of terrain corrections using the FFT

Classical methods of calculating terrain correction in the spatial domain are slow. However, Sideris (1984) and Forsberg (1985) introduced a technique in which the terrain

integral is computed using an FFT algorithm, giving a rapid and accurate means of calculating terrain data. This method involves using equally spaced terrain data. A brief review of the technique is presented below.

The nonlinear terrain correction integral can be written as

$$T_c(x_p, y_p, z_p) = \frac{G}{2} \iint \frac{\rho(x, y)(z - z_p) dz ds}{r^3} \quad (3.4)$$

where  $r(x_p, y_p, z_p, x, y, z) = [(x_p - x)^2 + (y_p - y)^2 + (z_p - z)^2]^{1/2}$ ,  $\rho(x, y)$  is the density function,  $G$  is the universal gravitation constant, and  $s$  is the planar surface of integration.

Moritz (1980) showed that the computation is vastly simplified when the integral in Equation (3.5) is evaluated locally on a plane and the assumption made that the slope of the terrain immediately surrounding the point of evaluation is small, i.e.,

$$\frac{1}{r^3} \approx \frac{1}{r_o^3} \quad (3.5)$$

where  $r_o = [(x_p - x)^2 + (y_p - y)^2]^{1/2}$ . The terrain correction integral equation (3.5) then reduces to

$$T_c(x_p, y_p, z_p) = \frac{G}{2} \int \frac{\rho(x, y) [z - z_p]^2}{r_o^3} ds \quad . \quad (3.6)$$

Forsberg (1985) reported that the errors associated with the use of this approximation are very small, typically less than 1 mGal. The integral equation (3.7) can now be evaluated as a linear combination of two-dimensional spatial convolutions:

$$T_c = \frac{G}{2} \rho [h^2 * r_o - 2h_p (h * r_o) + h_p^2 r_o] \quad , \quad (3.7)$$

where  $r_o$  is the DC value of the Fourier transform of the function,  $r_o, h_p$  is the height at the point of computation, and  $h$  is the elevation of the neighboring points which affect the terrain correction at  $(x_p, y_p, z_p)$ .

The most effective way to evaluate these convolution integrals is in the frequency domain. The computation of the discrete convolution in the frequency domain involves calculating the Fourier transform of the elevation data, the square of the elevation data, and the radial distances from the point of computation to each of the grid points which affect the points of computation. Note that in Equation (3.8) the density function is not assumed to be constant; thus, if a variable density distribution model is either assumed or known, and a digital elevation data set is

available in the region of interest, then a variable density terrain correction may be computed. The procedure to arrive at a complete Bouguer anomaly map using variable density terrain correction is to (1) calculate the density map as explained previously, (2) use the density map to compute a new set of terrain corrections, (3) recompute the complete Bouguer anomaly map, and (4) carry out a geologic interpretation of the new complete Bouguer anomaly map.

The terrain data and the variable reduction density data are gridded at a 1 km interval. Both data sets are 30 km wider than the study area on each side. The original complete Bouguer anomaly map is modified into a new complete map with variable reduction density using these two data sets.

The terrain correction of the original data set is composed of two parts: the inner zone correction, from station to 0.59 km, and the outer zone correction, from 0.59 to 166.7 km. The new terrain correction with variable reduction densities is carried out in the following way. The terrain correction values from 0.5 to 30 km are computed using the FFT method with variable reduction densities, and the terrain correction values for the inner zone are modified from the USGS inner zone data using variable density. The terrain correction values outside 30 km are made using a constant reduction density of  $2.67 \text{ g/cm}^3$ .

The simple Bouguer correction with variable reduction density is used only for the region inside a 30 km radius and above the lowest station elevation (413 m). The Bouguer slab correction in other areas uses the constant density.

Figure 9 is the new complete Bouguer anomaly map for the Klamath Mountains and the Cascade Range area using terrain corrections with variable density distributions. In comparison with the data set with a constant reduction density ( $2.67 \text{ g/cm}^3$ ) (Figure 10), there are three main differences. The first is that the gravity anomaly amplitudes change. In the Klamath Mountains area, the gravity anomaly amplitudes are less than those of the data set with a constant density, while in the Cascade Range the situation is the opposite. The second is that the correlations between the gravity anomaly and the topography are reduced, especially in the Mount Shasta area. The gravity low of Mount Shasta is moved eastward, and the peak of Mount Shasta is located on an eastward-dipping slope of the gravity low, but not at the center of the gravity low. The third is that the north-south strike structure is more obvious and the north-west trend persists in the Cascade Range area. The new complete Bouguer anomaly map will be interpreted in detail in Chapter 6.

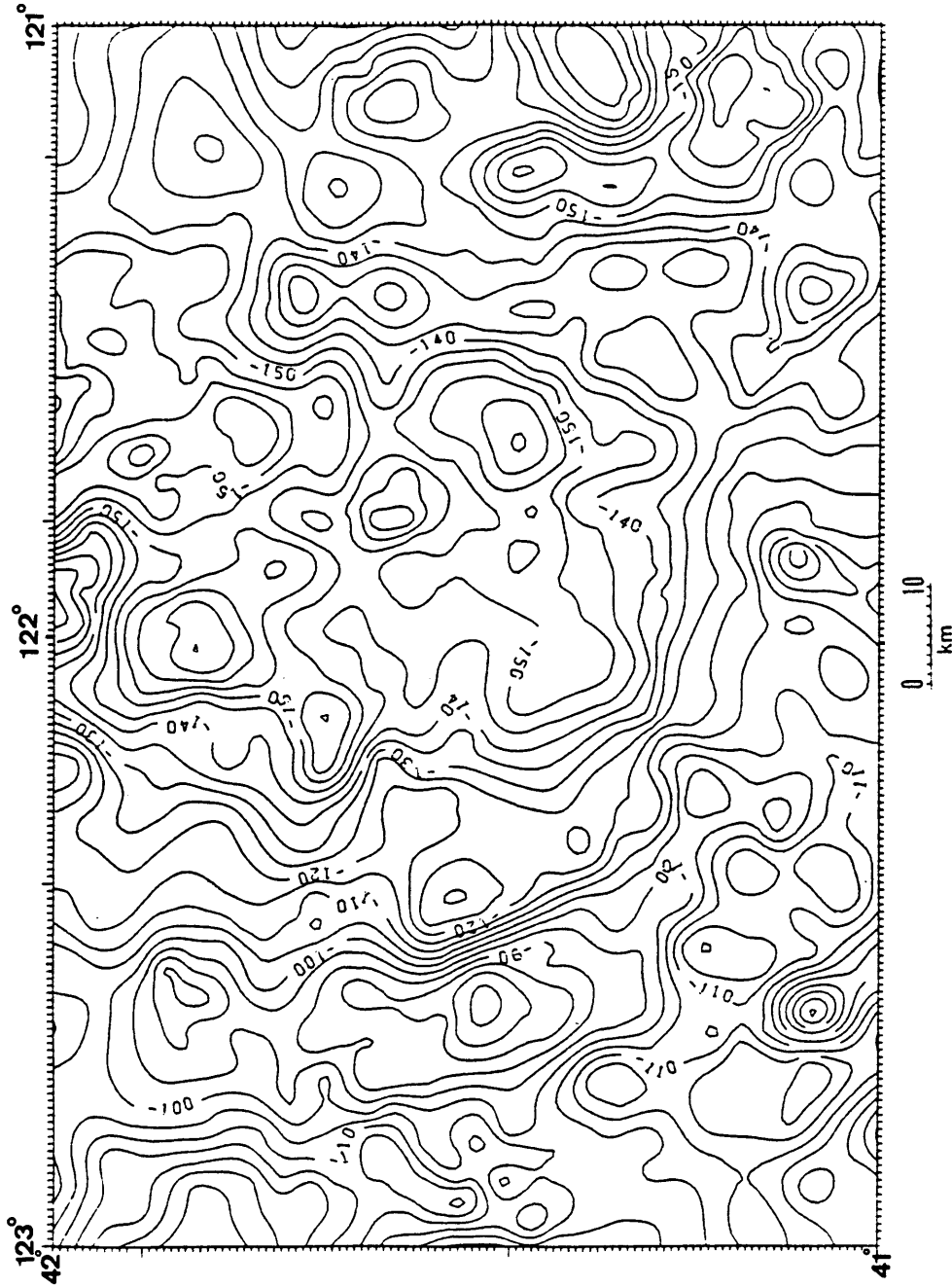


Figure 9. Complete Bouguer anomaly map with variable density distribution. Contour interval: 5 mGal

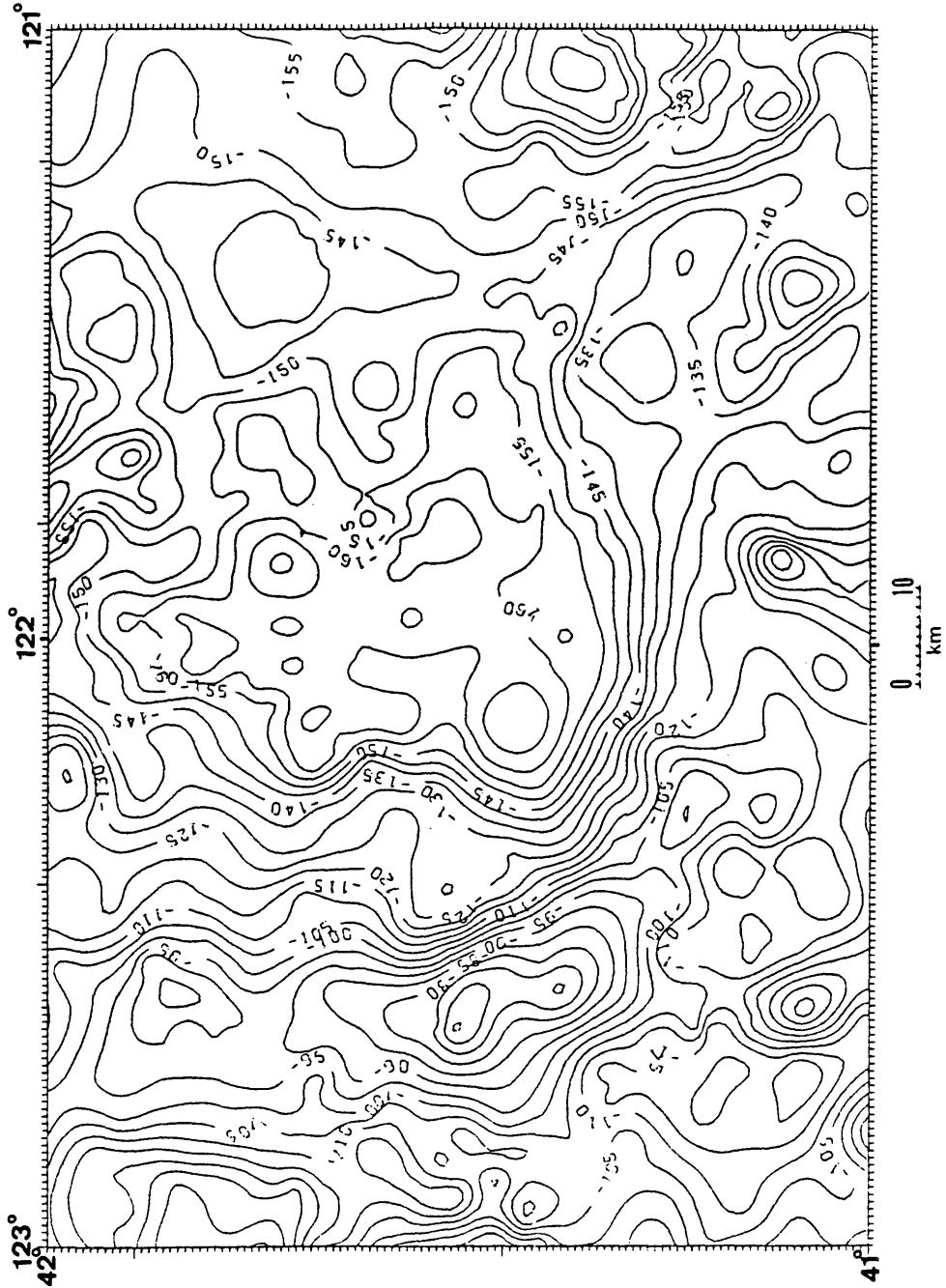


Figure 10. Complete Bouguer anomaly map with a constant density (2.67 g/cm<sup>3</sup>). Contour interval: 5 mGal.



COMPARISON OF CONTINUATION TECHNIQUES  
FOR POTENTIAL FIELDS

In rugged topography, it is generally desirable to have the data reduced to a datum. Of the many different methods which have been developed to solve the problem, three have been chosen for testing. Two use equivalent source methods, and the other uses a series expansion method.

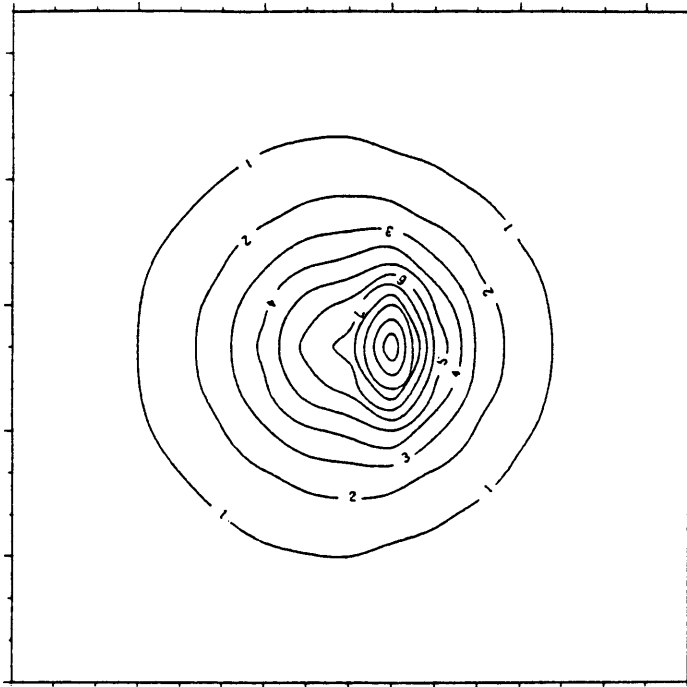
Dampney (1969) used an equivalent source layer of discrete point masses on a plane determined from Bouguer anomaly measurements on an uneven surface. The Bouguer anomaly can then be easily projected on a regular gridded horizontal datum. Henderson and Cordell (1971) developed a different method for reduction of gravity and magnetic data at variable elevation to a common level. For this reduction, the observations are represented by a finite Fourier series and the coefficients of the series are determined by inversion of a 2-D matrix. Bhattacharyya and Chan (1977) used an equivalent source on the observation surface determined by a Fredholm integral equation of the second kind.

In this thesis, two synthetic data sets are used to compare the three techniques objectively. The purposes of the comparison are to understand the features of each method and to choose a method suitable for use with the Bouguer

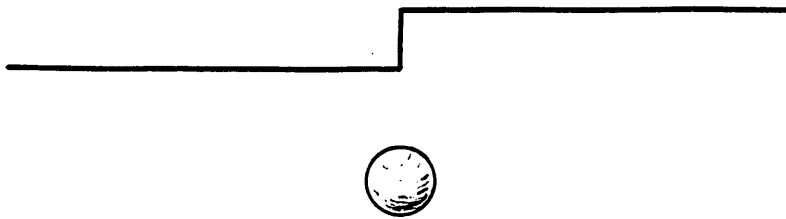
gravity data set from the Klamath Mountains and Cascade Range area.

#### Synthetic data set

Two synthetic data sets were generated for testing the three techniques. The first is the gravity anomaly of a sphere distributed on a step surface (Figure 11). The step is one grid unit high, and the depth of the sphere is 2 units deeper than the surface of the lower plane. This model was used by Dampney (1969). The second data set is the anomaly of a sphere distributed on real relief (Figure 12), which is a part of the Klamath Mountains-Cascades region in northern California. The grid unit is 1 km. The highest elevation is 3.9 km and the lowest 0.7 km. The sphere is located at the center of the area and the depth of the sphere center is 1 km below sea level.



A



B

Figure 11. Synthetic model 1: A. Step with a sphere (the step is one grid unit high, the sphere is 2 grid units deep); B. Theoretical gravity anomaly on the step surface. Contour interval: 1 mGal.

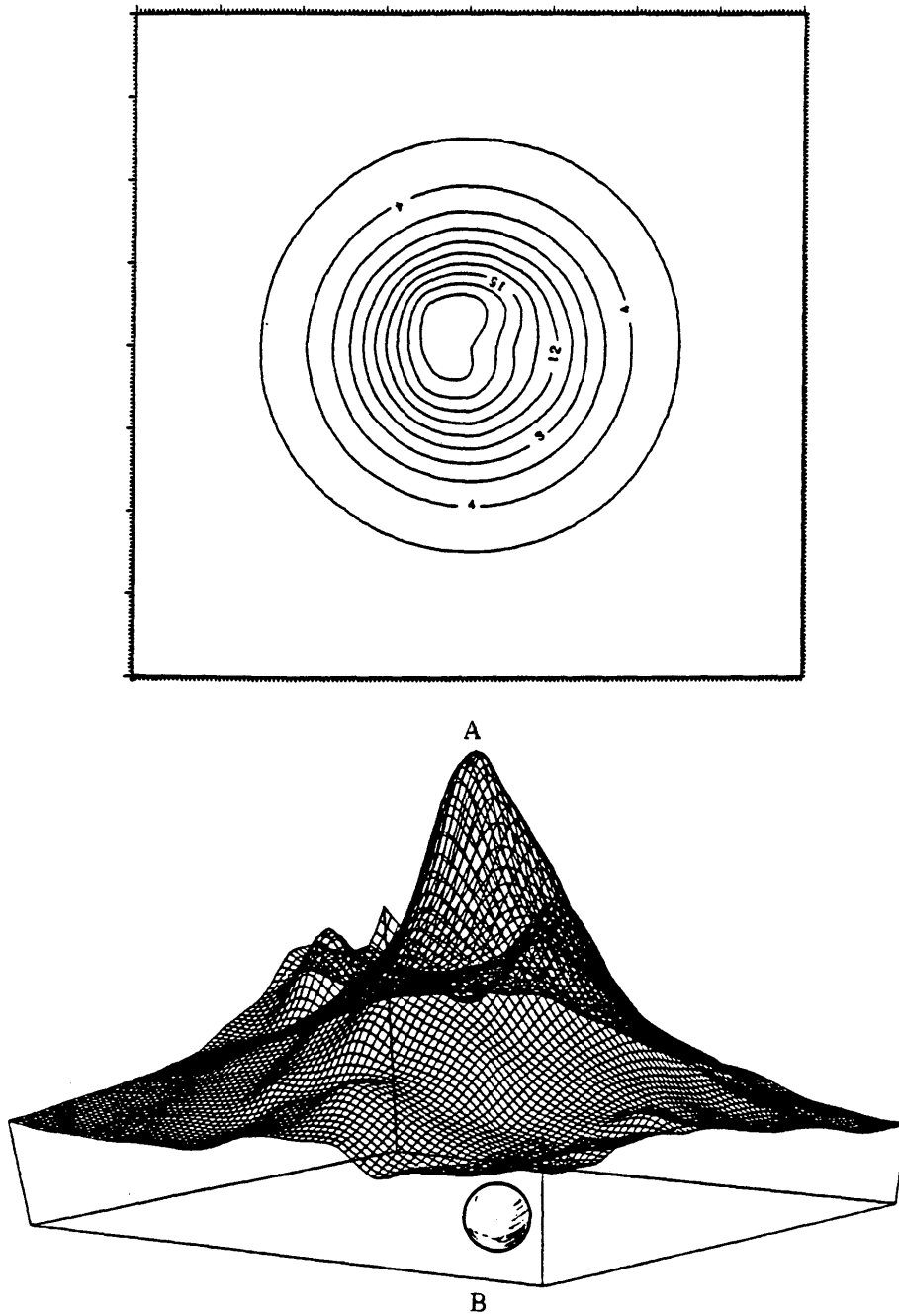


Figure 12. Synthetic model 2: A. Real relief (from Mount Shasta) with a sphere at 1 km depth; B. Theoretical gravity anomaly on the real relief surface. Contour interval: 1 mGal.

## Analysis of techniques

*Dampney's method*

The following equation is the the relationship between  $g_z(x,y,z)$  and  $\sigma(\alpha,\beta,\tau)$ :

$$g_z(x,y,z) = G \iint \frac{\sigma(\alpha,\beta,h)(h-z) \, d\alpha d\beta}{\{(x-\alpha)^2 + (y-\beta)^2 + (z-h)^2\}^{3/2}} \quad (4.1)$$

where  $\sigma(\alpha,\beta,\gamma)$  is the surface density constant distribution over the plane  $z = h$ ,  $G$  is the universal gravitational constant and the positive direction of  $z$  is downward. The depth  $h$  of the equivalent source layer layer take any value. To perform the inversion of Equation (4.1), it is sufficient to have a complete knowledge of  $g_z$  on a plane  $z = z_1$ ,  $z_1 < h$ . Therefore a unique correspondence exists between the function  $g_z(x,y,z = z_1)$  and  $\sigma(\alpha,\beta,\gamma)$ ; and, furthermore, as a result of equation (4.1), the value of  $g_z(x,y,z)$  for  $z < h$  is similarly uniquely defined.

Thus, a surface density contrast distribution is found on an arbitrary plane which synthesizes a known gravity field. It is then possible to calculate the gravity field at any other point in space from the gravity measurement at one height. By using the equivalent source  $\sigma(\alpha,\beta,\gamma)$  as an integral part of gravity field computations, two advantages result: (1) all available information contained in the



masses  $m_k$  at  $(\alpha, \beta, h)$ . The position of  $g_i$  is  $(x_i, y_i, z_i)$ . This can be written in matrix form as

$$\bar{g} = A\bar{m} \quad (4.4)$$

where  $x, y, z$  are the station coordinates,  $\alpha, \beta$  are the equivalent source coordinates, the subscript  $i$  indicates the  $i$ th station, the subscript  $j$  corresponds to the  $j$ th equivalent source, and  $h$  is the depth of the equivalent source plane.

The diagonal of the matrix is

$$a_{ii} = 1/(z_i - h)^2 \quad (4.5)$$

According to the theory of linear equations, the relaxation method for solving a linear equation is absolutely convergent if the value of each diagonal element is larger than the sum of all the off-diagonal terms in its row; that is, if

$$a_{ii} > \sum_{\substack{j=1 \\ j \neq i}}^n a_{ij} \quad (4.6)$$

Therefore, each diagonal element must be large enough to satisfy the convergence condition. For this condition to

hold, the vertical distance from the equivalent source plane to the highest station,  $(z_i - h)$ , should be less than 3.3 times the station spacing or grid unit, based on my model tests. If  $(z_i - h)$  is larger than about 3.3 grid units, the singular value decomposition method can be used to solve the linear equations.

The results of using the technique are shown in Figures 13 and 14. Figure 13 is the data reduced to the top surface of the step. The result is perfectly coincident with the theoretical data. Figure 14 is the data reduced to 4 km level from the real topographic model with a sphere. The center part of the map matches the theoretical data very well: the maximum error is only 0.02 mGal (the amplitude is 19.7 mGal). However, in the part surrounding the center, the error is larger than in the center. These errors are caused by edge effects. The higher the distance of upward continuation is, the larger the error.



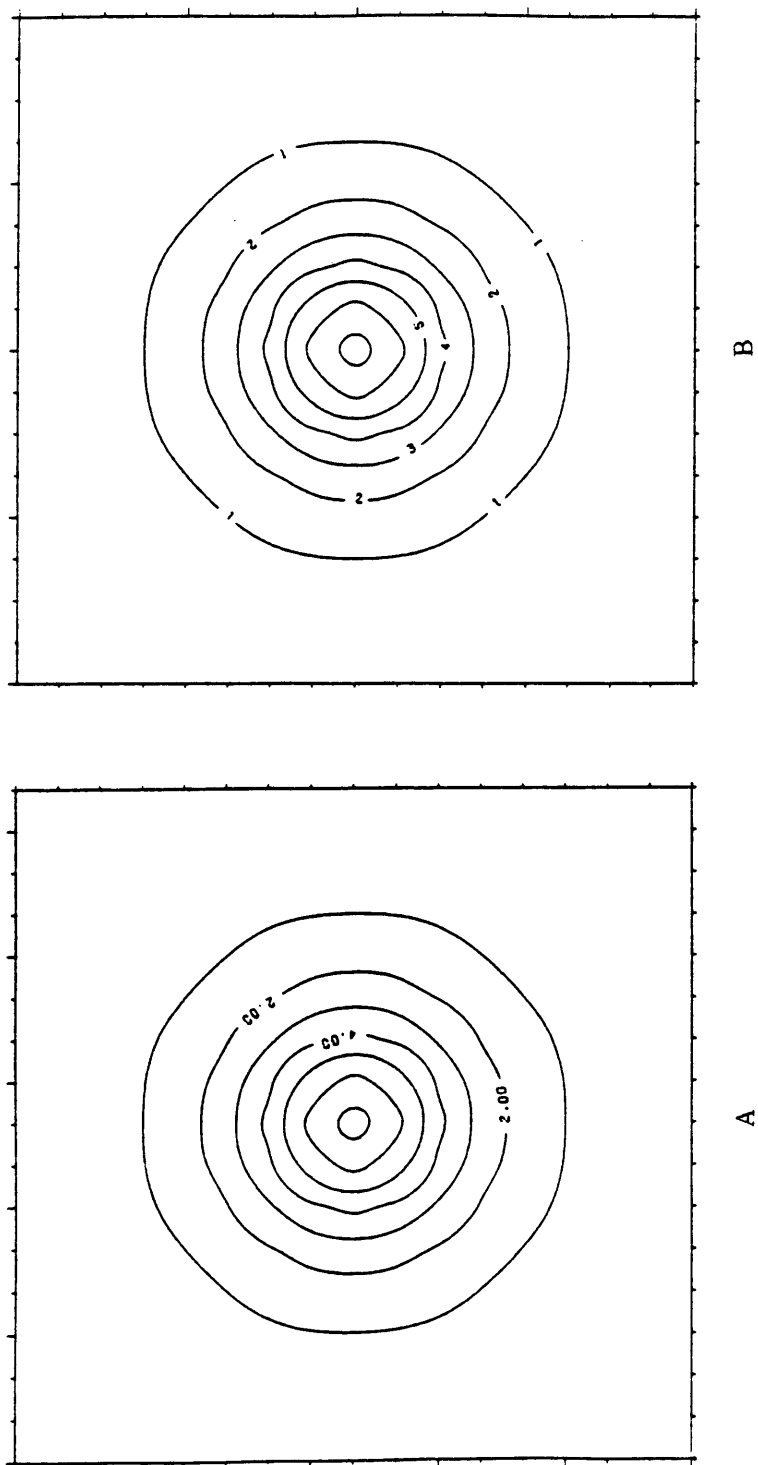
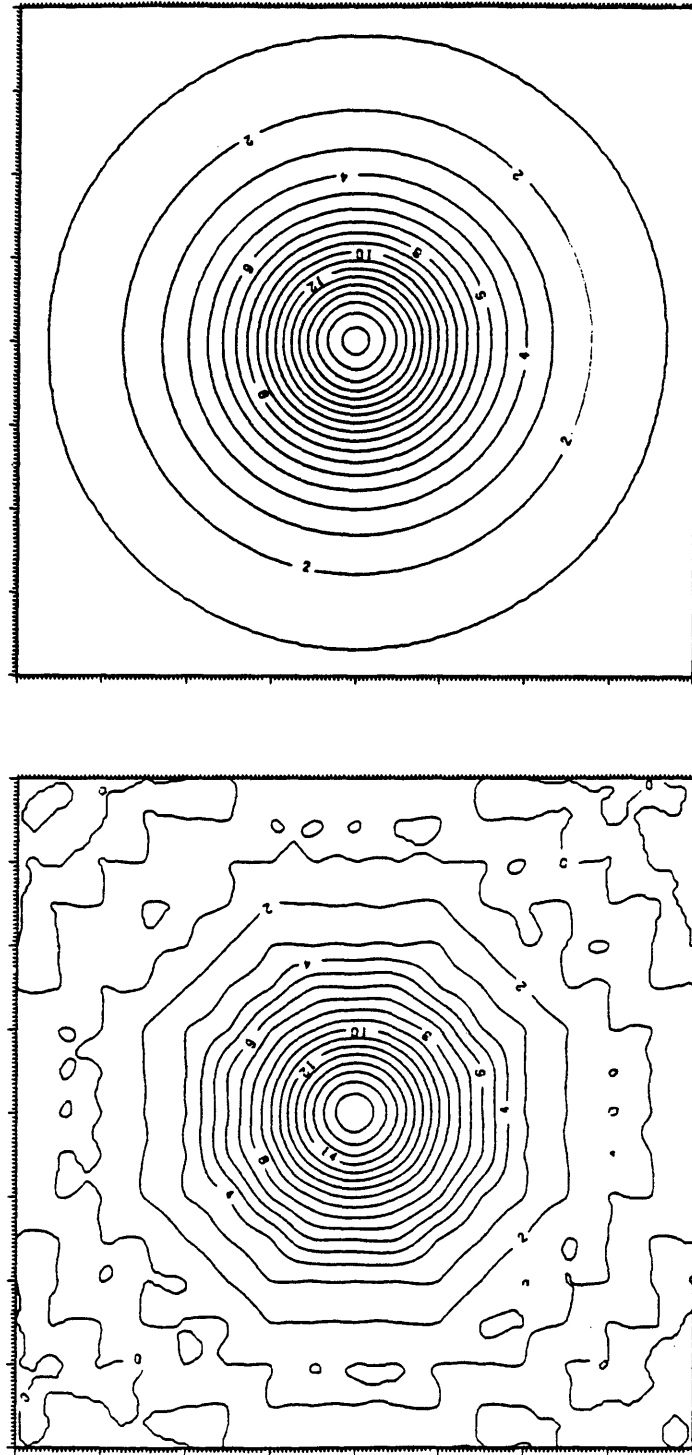


Figure 13. A. Anomaly of the step model reduced to the top surface of the step using the Dampney method. B. Theoretical anomaly on the top surface of the step. Contour interval: 1 mGal.



A

B

Figure 14. A. Anomaly of the real relief model reduced to the 4 km datum using the Dampney method. B. Theoretical anomaly on 4 km datum. Contour interval: 1 mGal.

The Dampney technique requires solving a system of linear equations. Any method for solving a linear equation system is subject to the following problems: limited matrix size for particular computers, and convergence speed. For example, if we use the Gaussian elimination method or singular value decomposition method to solve a linear equation system, the maximum matrix size is 300 x 300 for the Apollo DN300 and 1000 x 1000 for the Gould 9050. This means that each solution can only compute 300 or 1000 points. If the data set is bigger than that, it must be divided into several overlapping subsets or computation. In this way, more computer CPU time is required.

Based on the theory, the equivalent source surface generated by the Dampney technique is accurate. If a data set has no noise in it, we may use the technique to do downward continuation. Figure 15 is the data reduced to a 1 km level. It is downward-continued at the center of the map by about 3 km. The maximum error is 16.7 mGal, but the maximum amplitude is 97 mGal; thus the error is only about 17% of the maximum amplitude. This is an acceptable result. Therefore this technique may be used for downward continuation.

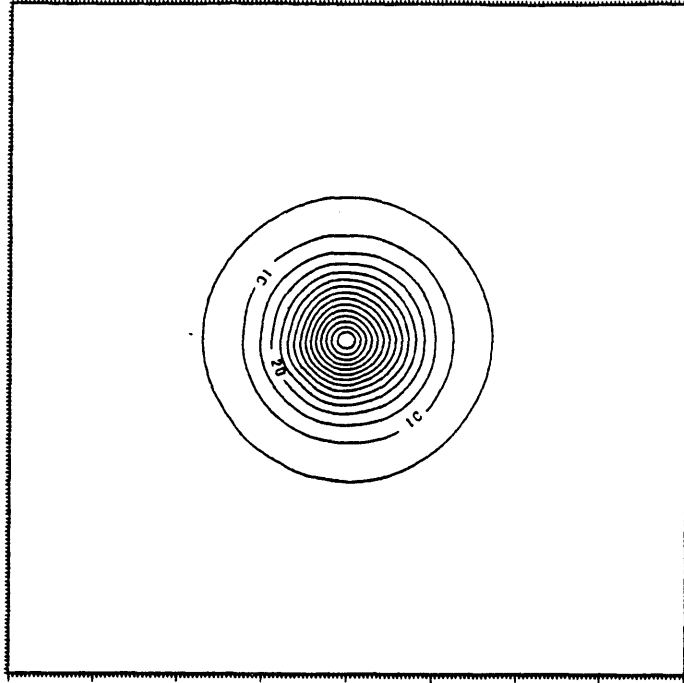


Figure 15. Anomaly of the real relief model reduced to a 1 km datum using Dampney method.  
Contour interval: 5 mGal.

*Bhattacharyya and Chan's method*

This method is based on the determination of a distribution of equivalent sources on the observation surface. For this reason, the method may only be used to reduce data to a datum which lies everywhere above the observation surface.

The method is based on Equation (4.1), but it is necessary to determine the limiting form of  $g(x,y,z)$  as the point  $p(x,y,z)$  approaches  $Q(\alpha',\beta',\gamma')$  on the surface  $S$  along the normal at  $(\alpha',\beta',\gamma')$ . Since the surface  $S$  is irregular, the vertical direction given by the  $z$ -axis is not generally coincident with the normal  $N$  to the surface  $S$  at a point  $Q(\alpha',\beta',\gamma')$ . For this reason, the method uses a new system of coordinates  $(x',y',z')$  such that the  $z'$  axis is along the normal and  $x',y'$  plane is the tangent plane at  $Q$ . This system is variable in the sense that the directions of the coordinate axes change as  $Q$  moves.

In these coordinates, Bhattacharyya and Chan (1977) derived the following formula:

$$g(\alpha',\beta',\gamma') = 2\pi G n \rho(\alpha',\beta',\gamma') - G \iint_{S'} \frac{\rho(\alpha,\beta,\gamma)}{n} \cdot \frac{\gamma' - \gamma}{r^3} d\alpha d\beta \quad (4.7)$$

where

$$n = \frac{1}{[1 + f_{\alpha}^2 + f_{\beta}^2]^{1/2}} \quad (4.8)$$

$f_{\alpha}$  and  $f_{\beta}$  are the horizontal derivatives of  $\tau = f(\alpha, \beta)$ , and  $\tau$  is the vertical height. Introducing the notation

$$\sigma = G\rho/n, \quad (4.9)$$

Formula (4.7) can be expressed in the form of a Fredholm integral equation of the second kind:

$$\begin{aligned} \sigma(\alpha', \beta', \gamma') &= \frac{g(\alpha', \beta', \gamma')}{2\pi n^2} \\ &+ \frac{1}{2\pi n^2} \iint \sigma(\alpha, \beta, \gamma) \frac{\gamma' - \gamma}{r^3} d\alpha d\beta \quad . \end{aligned} \quad (4.10)$$

The equivalent source on the topographic surface may be computed using an iterative method based on equation (4.10). Here  $\alpha, \beta, \tau$  are the coordinates of the station with the current station excluded, and  $\alpha', \beta', \gamma'$  are the coordinates of the current station.

Equation (4.1) can be expressed in terms of  $\sigma$ :

$$g(x,y,z) = - \iiint \sigma(\sigma, \beta, \gamma) \frac{z - \gamma}{r^3} d\alpha d\beta \quad (4.11)$$

Thus, Equation (4.11) can be used to calculate the gravity anomaly at a point on another surface external to the surface S, which is the surface of observation.

Figure 16 is the step model reduced to the top surface of the step. The result is almost identical to the input data. This shows that the method is not effective for data on a cliff. Figure 17 is the reduced data on a datum 4 km above sea level from the model data on real relief. There is a false anomaly at the center of the map. The largest difference from the theoretical data is 3254.9 mGal (the real amplitude is 19.1 mGal). This result reveals a problem with the method. The reason for the false anomaly is that the term  $1/(z-\gamma)^2$ , which is the main part of the summation value for  $(z-\gamma)/r^3$ , becomes very large (Figure 18 A) when the datum is close to the station, that is when  $(z-\gamma)$  is small. However, the value of the equivalent source will only change a little (Figure 18 B). Therefore, the false anomaly appears at the places where the datum is too close to the highest station of the topography. Fortunately the false anomaly is reduced very rapidly as the datum is moved further from the station.

We can use two methods to avoid this false anomaly. One method is to move the datum upward. Figure 19 is the

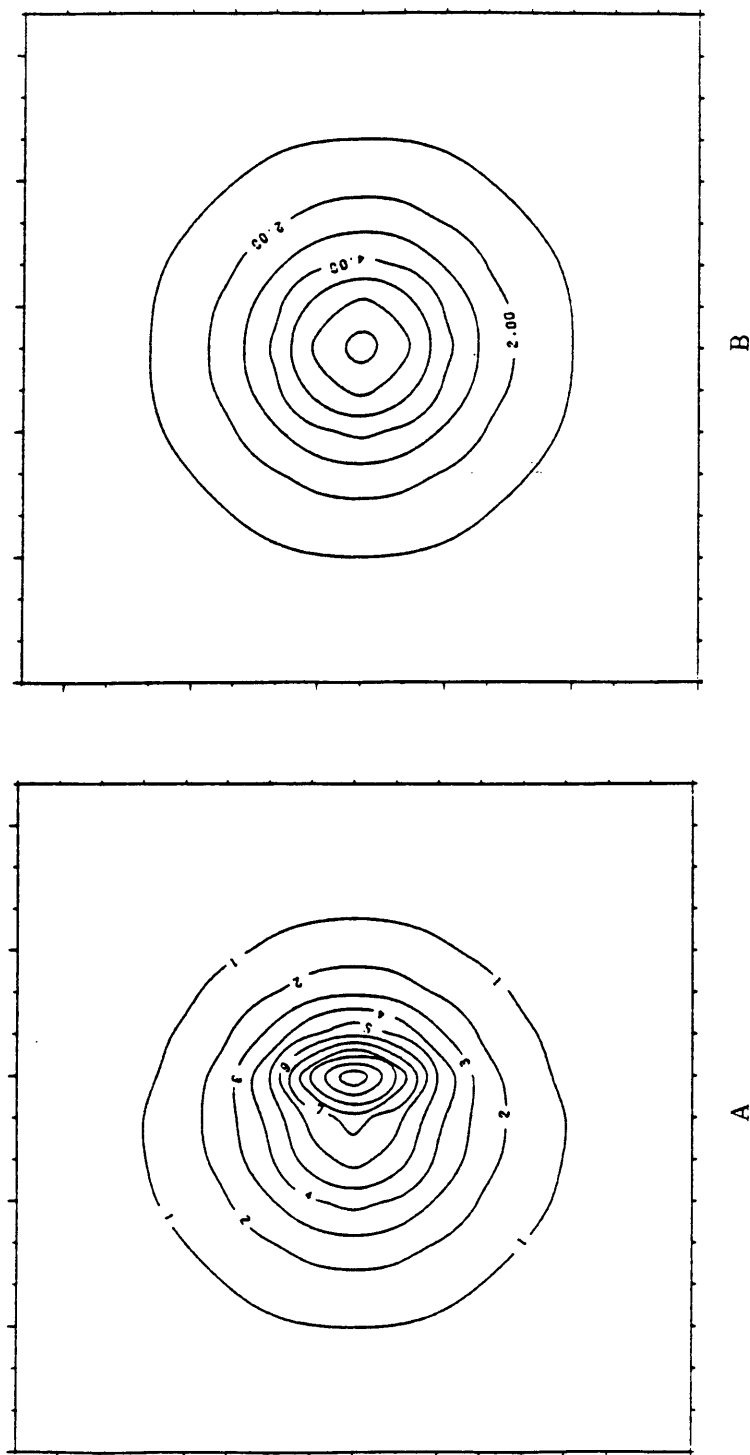


Figure 16. A. Anomaly of the step model reduced to the top surface of the step using the Bhattacharyya and Chan method. B. Theoretical anomaly on the top surface of the step. Contour interval: 1 mGal.



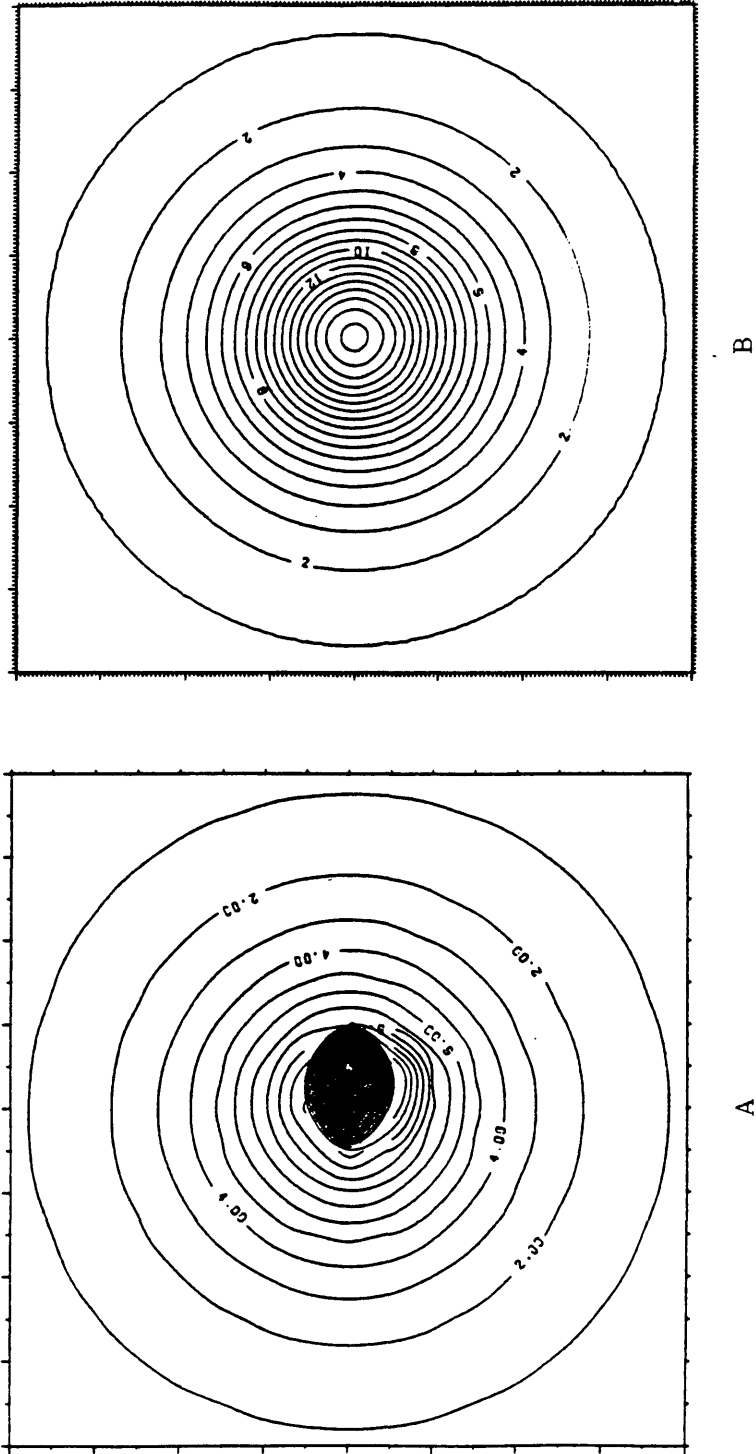


Figure 17. A. Anomaly of the real relief model reduced to the 4 km datum using the Bhattacharyya and Chan method. B. Theoretical anomaly on 4 km datum. Contour interval: 1 mGal.

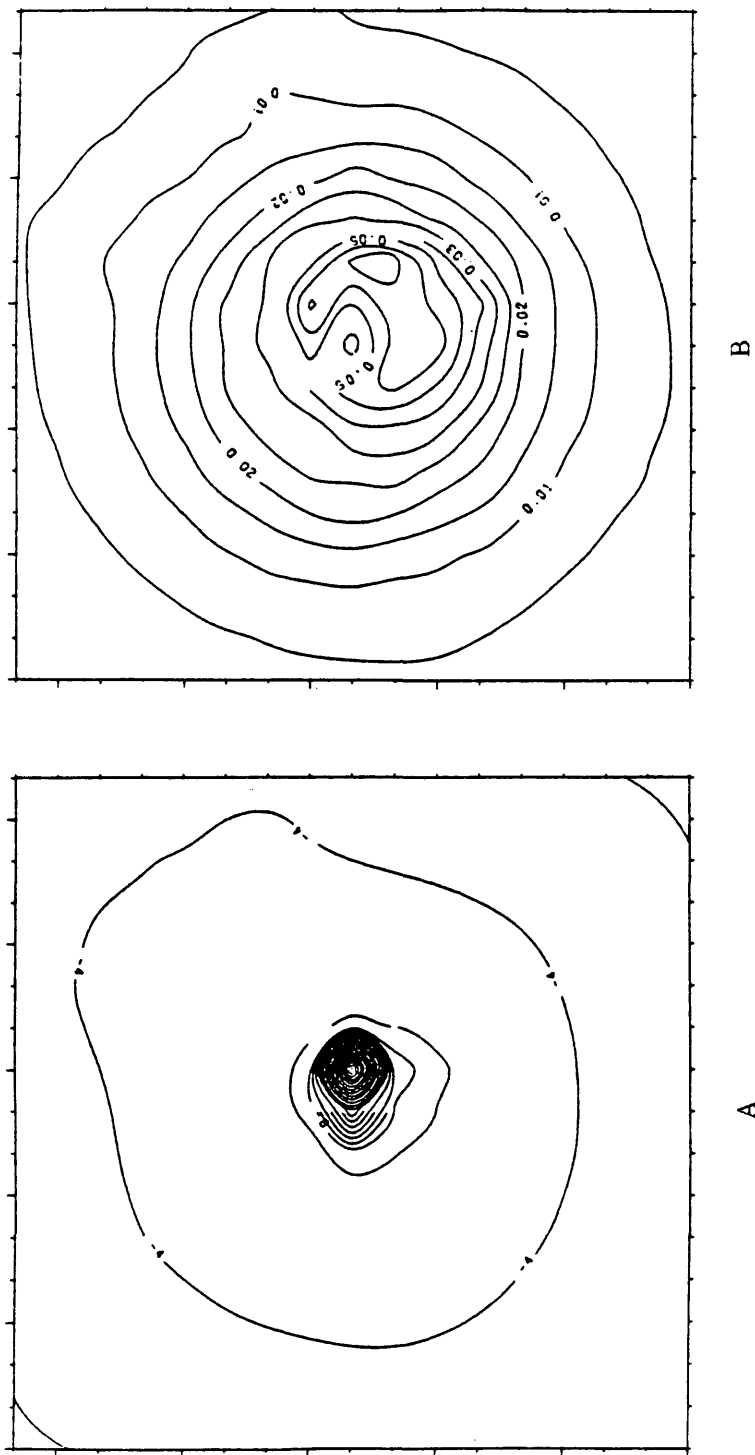


Figure 18. A. Contour map of location term values in Formula 4.11.  
Contour interval: 2 units.  
B. Equivalent source value contour map.  
Contour interval: 0.005 units.

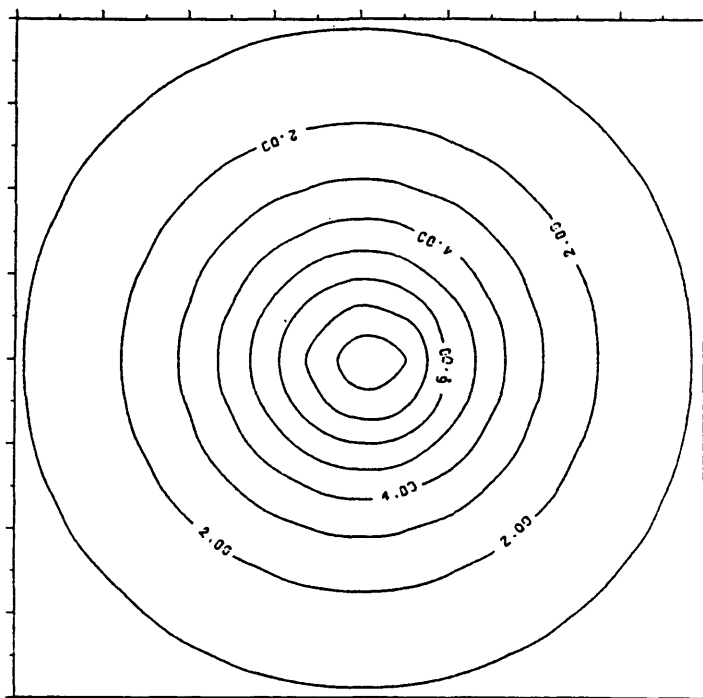


Figure 19. Anomaly of the real relief model reduced to the 5 km datum using the Bhattacharyya and Chan method. Contour interval: 1 mGal.

result of reduction to a 5 km datum; it is much better than Figure 17. Another method is to use a numerical integration technique with higher accuracy to compute the areas where stations are close to the datum. Hansen and Miyazaki (1984) derived an accurate formula for this integral.

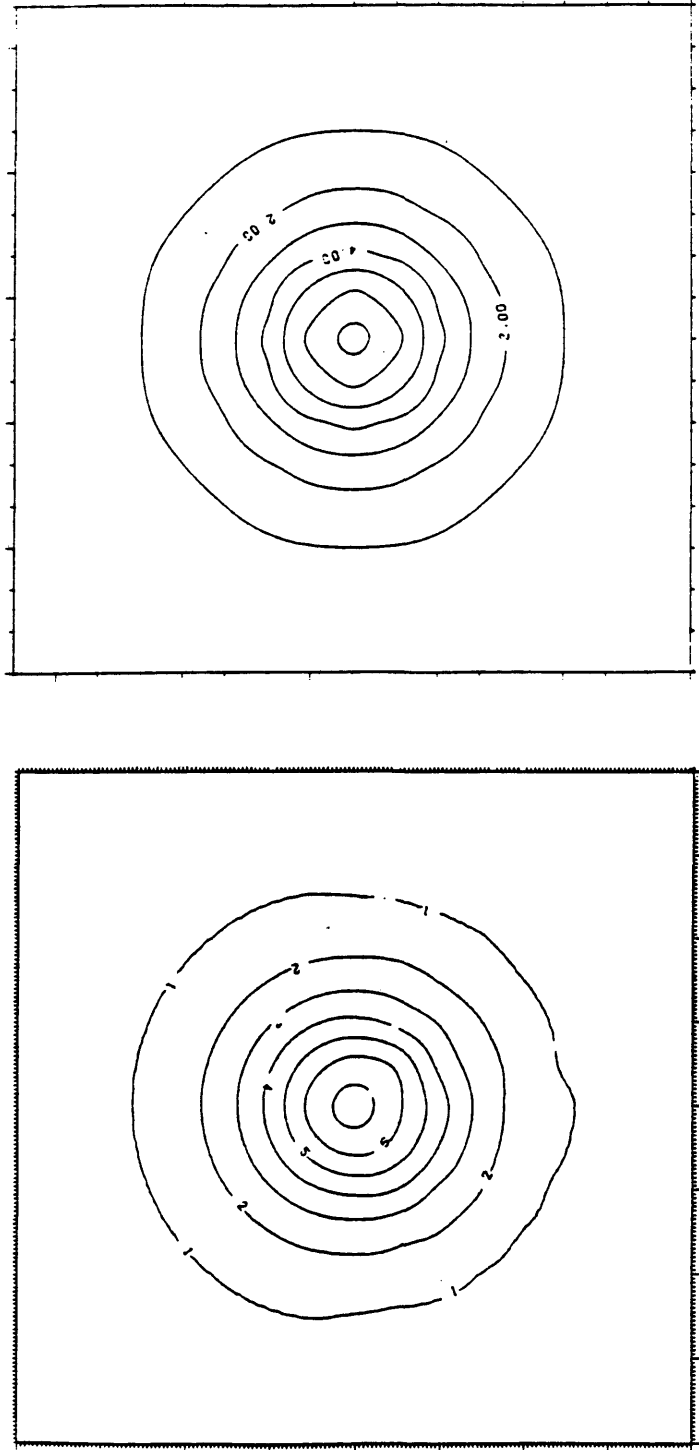
*Henderson and Cordell's method*

Pawłowski (1986) has studied this method in detail. Most of the results in this section are obtained from his report. The Henderson and Cordell method is based on a finite Fourier series expansion, so there is a term truncation problem in the method. Pawłowski points out that: 1) the larger the data set, the higher the order of the harmonic series which is required to fit the large wavenumber features of the data; 2) the broader the features are in the data, the larger the required area of coverage; 3) the finite series expansion for a magnetic field will require higher -order terms than the expansion for a gravity field. He gives a table (Table 1) of the relationship between the maximum order of harmonic series and the size of the data set in practice.

The data size of the synthetic model is 289 points, so order 8 was taken to test the data set. Figures 20 and 21 are the reduced data for the step model and real relief model, respectively. The results are good enough for upward

Table 1. The relationship between the truncated term order of harmonic series and data size.

Order	Size of Data set
1	9
2	25
3	49
4	81
5	121
6	169
7	225
8	289
9	361
10	441
11	529
12	625
13	729
14	841
15	961



B

A

Figure 20. A. Anomaly of the step model reduced to the top surface of the step using the Henderson and Cordell method. B. Theoretical anomaly on the top surface of the step. Contour interval: 1 mGal.

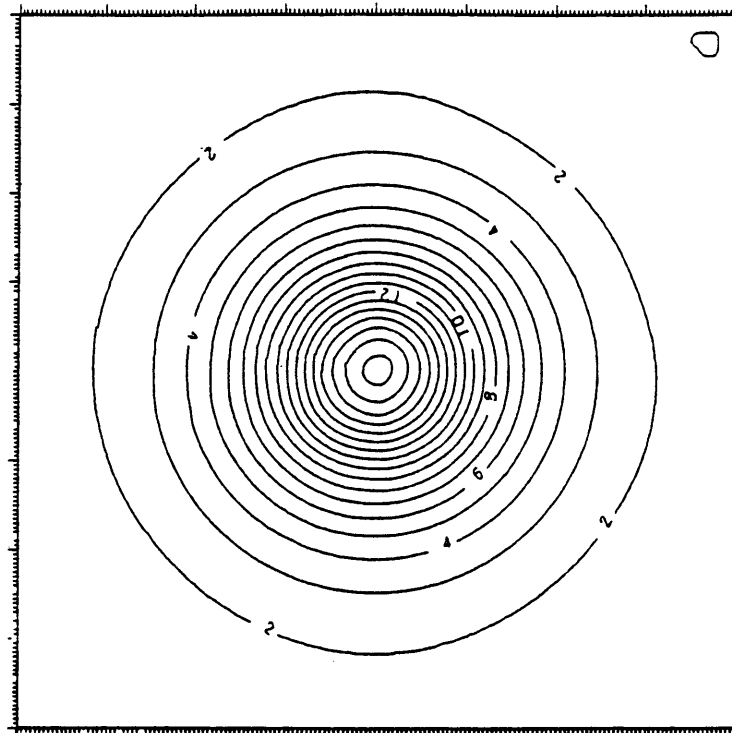


Figure 21. Anomaly of the real relief model reduced to 4 km datum using the Henderson and Cordell method. Contour interval: 1 mGal.

continuation, although the errors are larger than the errors from Dampney's method.

#### Comparison

1. Dampney's method is the most effective of the four methods, but a supercomputer is required for large data set.
2. Bhattacharyya and Chan's method may be used to reduce the data to a datum lying above the observation surface, but the minimum value of  $(z-\gamma)$ , the vertical distance between the datum and the highest station, must be larger than one grid unit. Otherwise, a numerical integration method with high accuracy must be used to treat the areas which are close to stations. The advantage of this method is that convergence is fast when an iterative method is used to solve the Fredholm integral equation of the second kind.
3. Henderson and Cordell's method may be used for upward continuation, but the size of data set and the truncation order must be chosen based on Table 4.1.



## GRAVITY ANOMALY SEPARATION

The purpose of this part of the project is to understand the nature of techniques for anomaly separation, and to find a reasonable procedure for separating the anomalies in the Klamaths and Cascades regions. Three methods are discussed in this chapter. They are: the modeling method, the filtering method, and the upward continuation method.

## Philosophy of anomaly separation

Obtaining a good result from an anomaly separation depends on two factors: knowledge of the geological environment and the separation technique.

The first step in separating anomalies is to understand the geological environment of the area under study. This means understanding the causal relationship between the anomalies and the geological environment. After that, the geological environment needs to be simplified in order to formulate a geological model.

The second step is to understand the features of each technique for anomaly separation. Generally speaking, the techniques of anomaly separation include three kinds of methods: the modeling method, the filtering method, and the upward continuation method. The features of each method

will be discussed in the next section.

Based on the geological model and the features of methods for anomaly separation, an optimum method is selected and a reasonable procedure set up.

The features of separation methods

#### *Modeling Method*

If the geological environment is well-known, this is the best method. It is a simple method, but obtaining sufficient knowledge of the environment is difficult. Well log and seismic data are the most commonly-used sources of data for this method. The technique is to generate a geological model which is as exact as possible based on known geology, and then to compute the forward gravity model based on this data. Thus, this method can only be used in areas where the geology is well-known.

The isostatic method can be considered one of the modeling methods. Most geophysicists and geologists agree that the isostatic theory fits the gravity anomaly due to variations of the Moho well. The Moho is one of the main sources of regional anomalies in mountainous areas. We can therefore use isostatic corrections to separate the anomaly caused by the Moho and the anomalies of the structures above the Moho.

### *Filtering Method*

Band pass-filters and Wiener filters are often used for separation of anomalies when the geological structures are not well-known. The reason is that the power spectrum can be used to estimate the anomaly components which are caused by sources with different depths, and then a band-pass filter or Wiener filter can be designed to separate the anomalies with different source depths. The output of a band-pass filter is always smoothed, but the main features and amplitudes of anomalies are reasonable.

### *Upward Continuation*

This method is a special case of the filtering method. It is based on differing attenuations between deep and shallow structures, and the output has explicitly physical meaning (Jacobsen, 1987). Therefore this method is often used to separate regional and local anomalies.

One of problems of this method is determining how high the anomalies of a source at a given depth should be upward continued. With the help of the filtering method, this problem can be solved.

The procedure for anomaly separation

Based on the above analysis, a procedure for anomaly separation was established. The procedure includes these

steps:

1. Study the geological environment, and set up a general geological model.
2. Compute the power spectrum of the data set, and separate segments of the spectrum based on the general geological model.
3. Design a band-pass filter or a Wiener filter to filter the data set. Analyze the regional anomaly map to identify the main features and the amplitudes of the anomalies.
4. Reprocess the data set using the upward continuation method until the main features and amplitudes are similar to those in the filtered data.

#### Gravity anomaly separation

Gravity data from the Klamaths and Cascades areas are taken as an example for separation of regional and local anomalies.

#### Geological model

This area is a rugged mountainous area (Figure 2). The highest peak is Mount Shasta, about 4200 m, and the lowest elevation is about 413 m. To the west of the area is the Pacific Ocean and to the east is a mountainous area, so

isostatic equilibrium requires displacement of the Moho subsurface. Thus, the Moho is one of the main sources of regional anomalies in the region.

Based on the analysis of Chapter 2, there are two geologic provinces; the Klamath Mountains and the Cascade Range. The rocks of the Klamath Mountains are mainly mafic and ultramafic rocks. The Cascade Range is mainly composed of volcanic rocks. In the Cascade Range, the basement is the layers of the Klamath Mountains. The thickness of volcanic rocks in the Cascade Range is about 5-7 km. Generally, the densities of the mafic and ultramafic rocks are high, about  $2.7-3.0 \text{ g/cm}^3$ , and the densities of the volcanic rocks are low, about  $2.2-2.6 \text{ g/cm}^3$ . Therefore, the basement is the other source of the regional gravity anomaly in the Cascade Range area.

Thus, there are two major subsurface density contrasts in the study area: the Moho surface and the basement surface. These are the sources of the regional anomaly in the area.

#### Separation of Anomalies

Based on the geological analysis, an isostatic correction was used to separate the Moho effect from the Bouguer anomaly (Figure 9). The parameters used were: crustal thickness at sea level, 31 km; topographic density,

2.65 g/cm<sup>3</sup>; density contrast across the base of the crust, 0.6 g/cm<sup>3</sup>. Figure 22 is a contour map of the isostatic anomalies using Airy-Heiskanen isostatic theory, and Figure 23 is a map of the residual anomalies after isostatic correction. The map is very similar to the one constructed by Jachens and Griscom (1985).

The residual anomalies include the basement anomalies and the anomalies due to shallow structure. Figure 24 is the power spectrum of the residual anomalies. Our main purpose is to separate the anomalies due to the basement. The volcanic and sedimentary series is less than 10 km thick, so a band-pass filter with a 250-80 km wavelength pass band was designed to separate the basement and shallow anomalies. The result is shown in Figure 25.

The regional anomalies in the band-pass filter map are smoothed. There is a main gravity low at the center of the map, and the gravity highs are in the Klamaths area. A band of gravity highs is located to the east of the gravity low. This band of gravity highs passes through the Medicine Lake Highland. The amplitude of the main gravity low is -40 mgal.

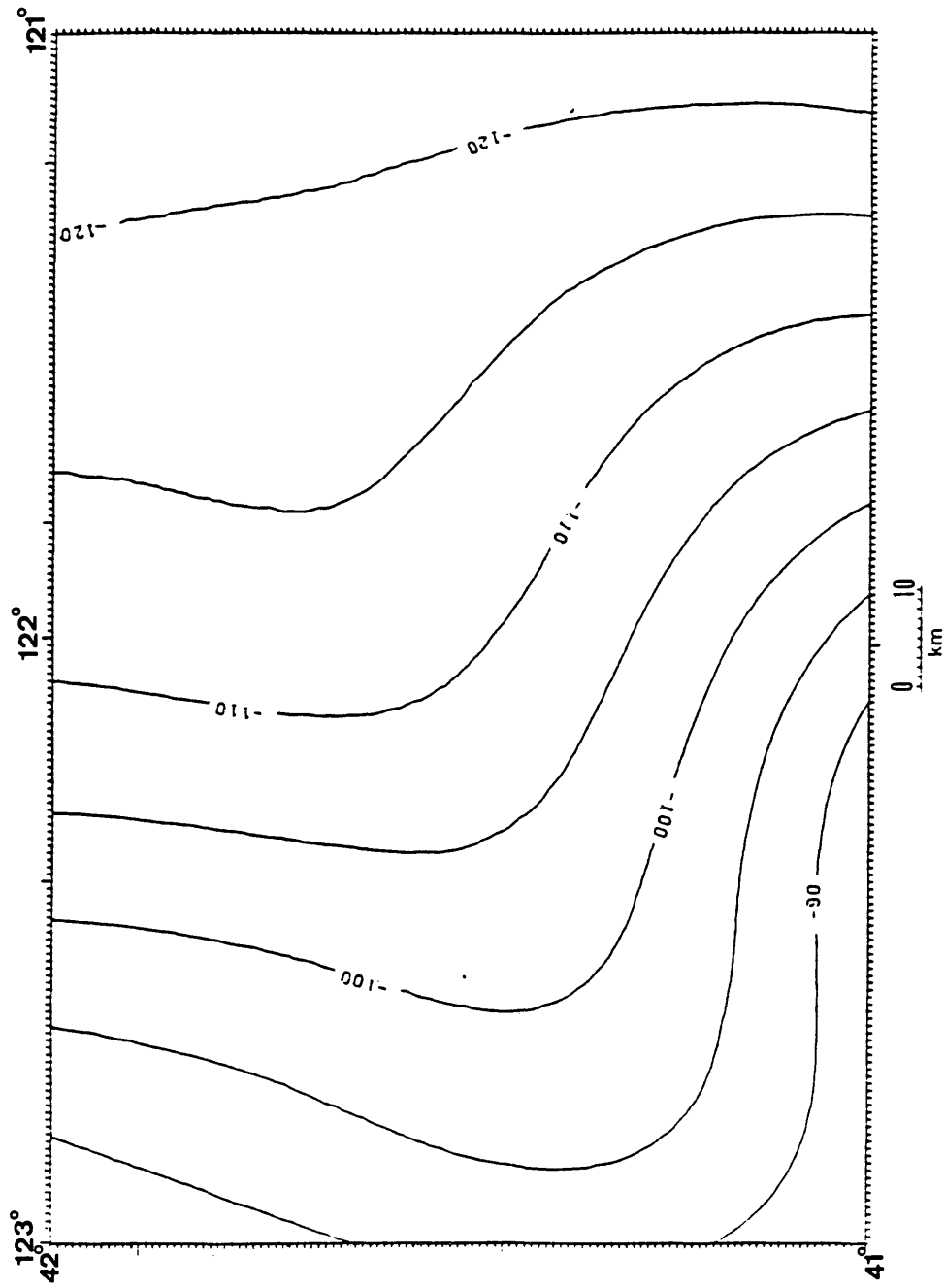


Figure 22. Isostatic anomaly map of the study area. Contour interval: 5 mGal.

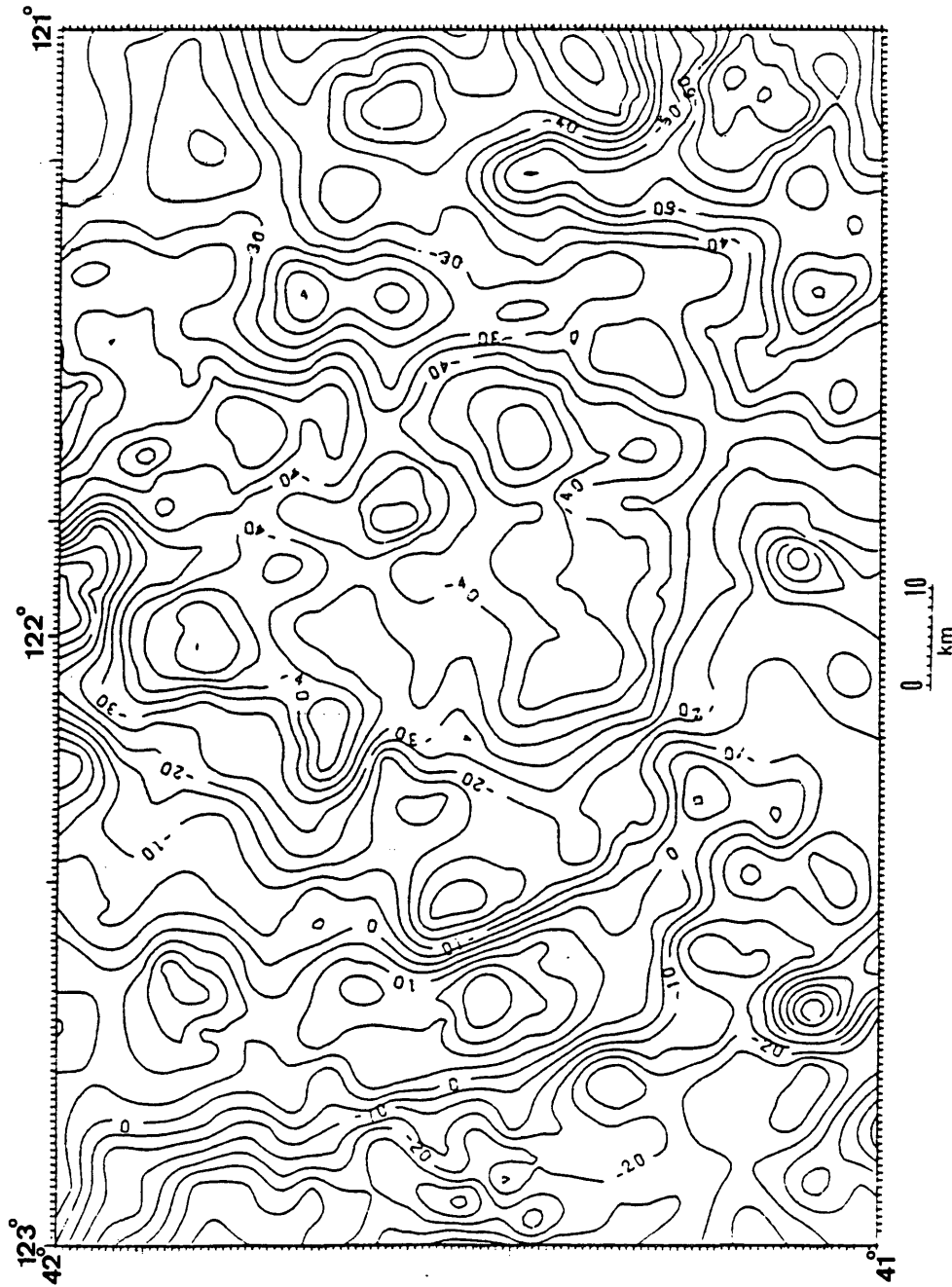


Figure 23. Isostatic residual anomaly map in the study area.  
Contour interval: 5 mGal.



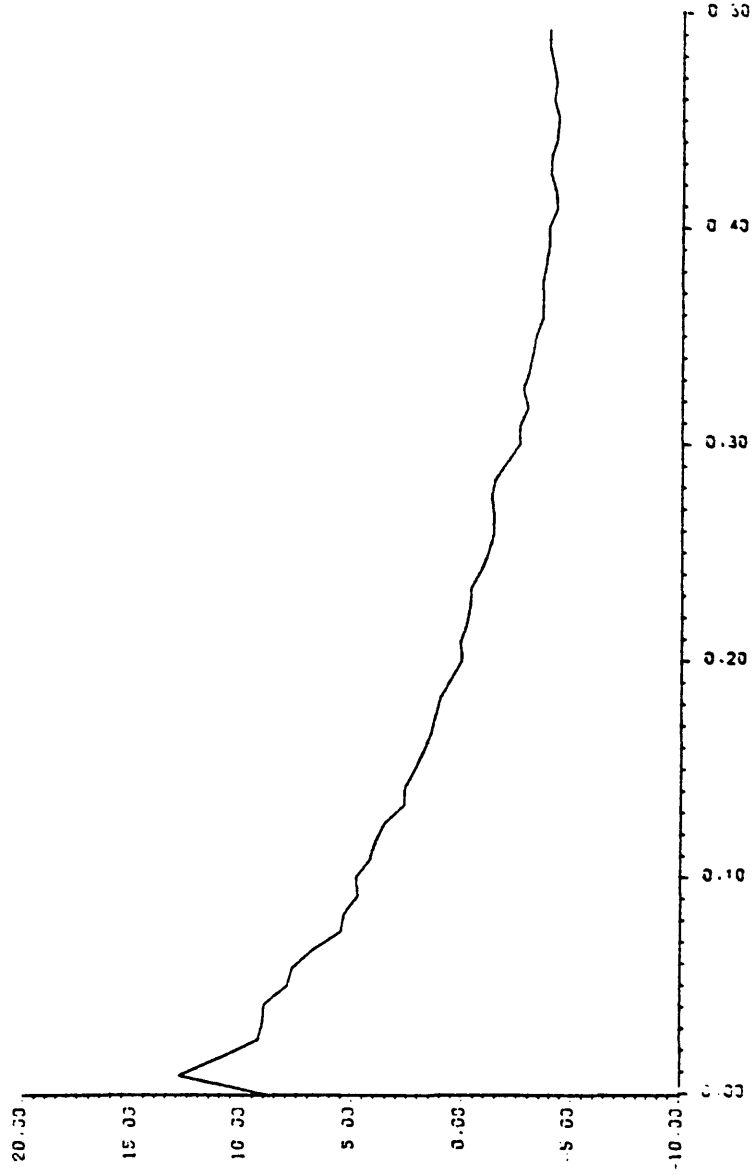


Figure 24. Radially average power spectrum of the isostatic residual anomaly of the study area.

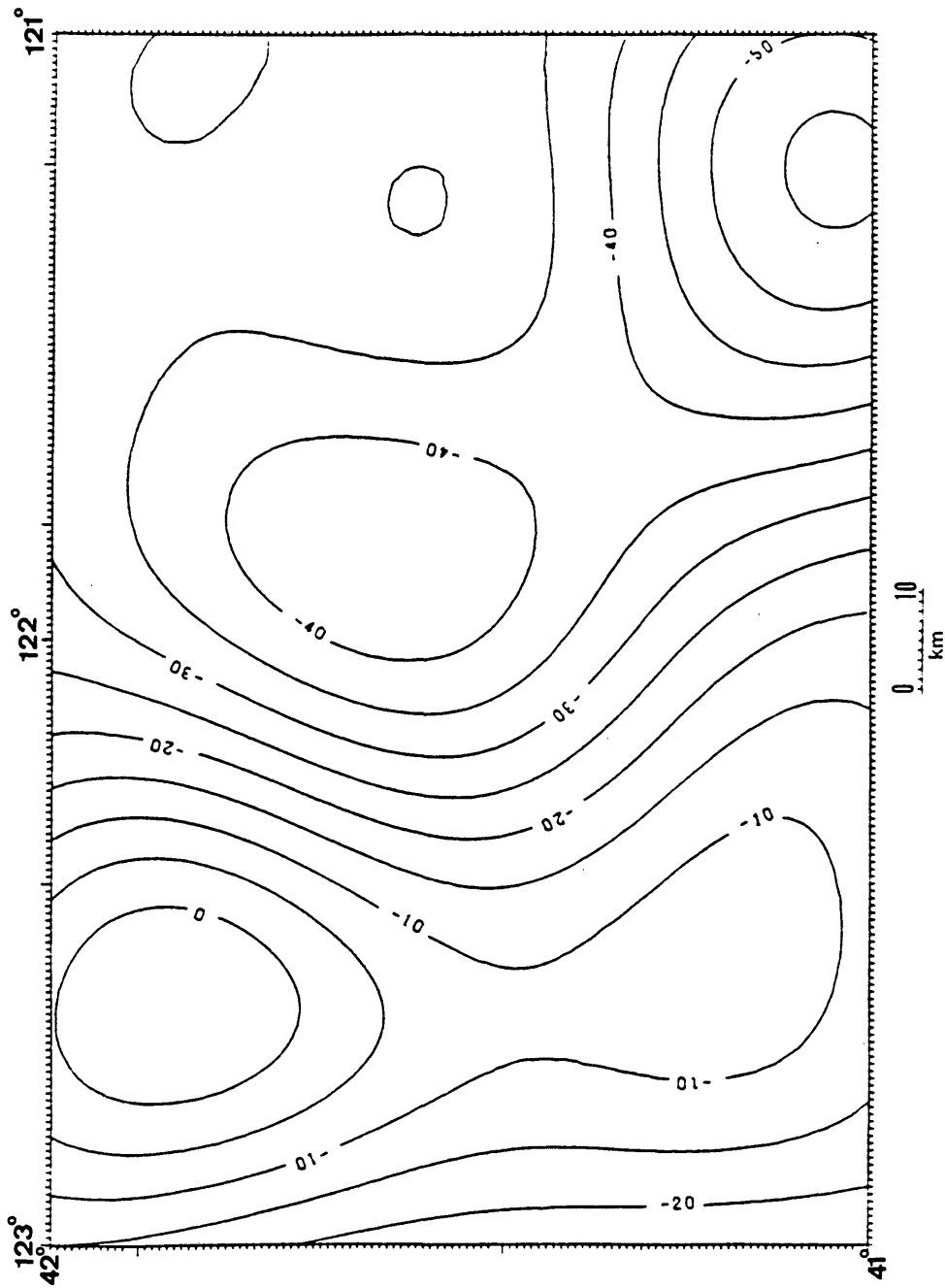


Figure 25. Filtered gravity anomaly map of the isostatic residual anomaly for the study area (filter pass band: 250-80 km). Contour interval: 5 mGal.

Based on the band-pass filter result, the data were upward continued to several levels. The main features and relative amplitudes of the data continued to a 7.5 km level are very close to those of the band-pass filter, so this continuation level was selected for separation. The separated basement anomalies are shown on Figure 26. There is a gravity low at the center of the map. The two sides of the gravity low are sharply defined, and coincide with the normal faults along the two sides of the basin. This map was used to interpret the basement structure in the Cascade Range region.

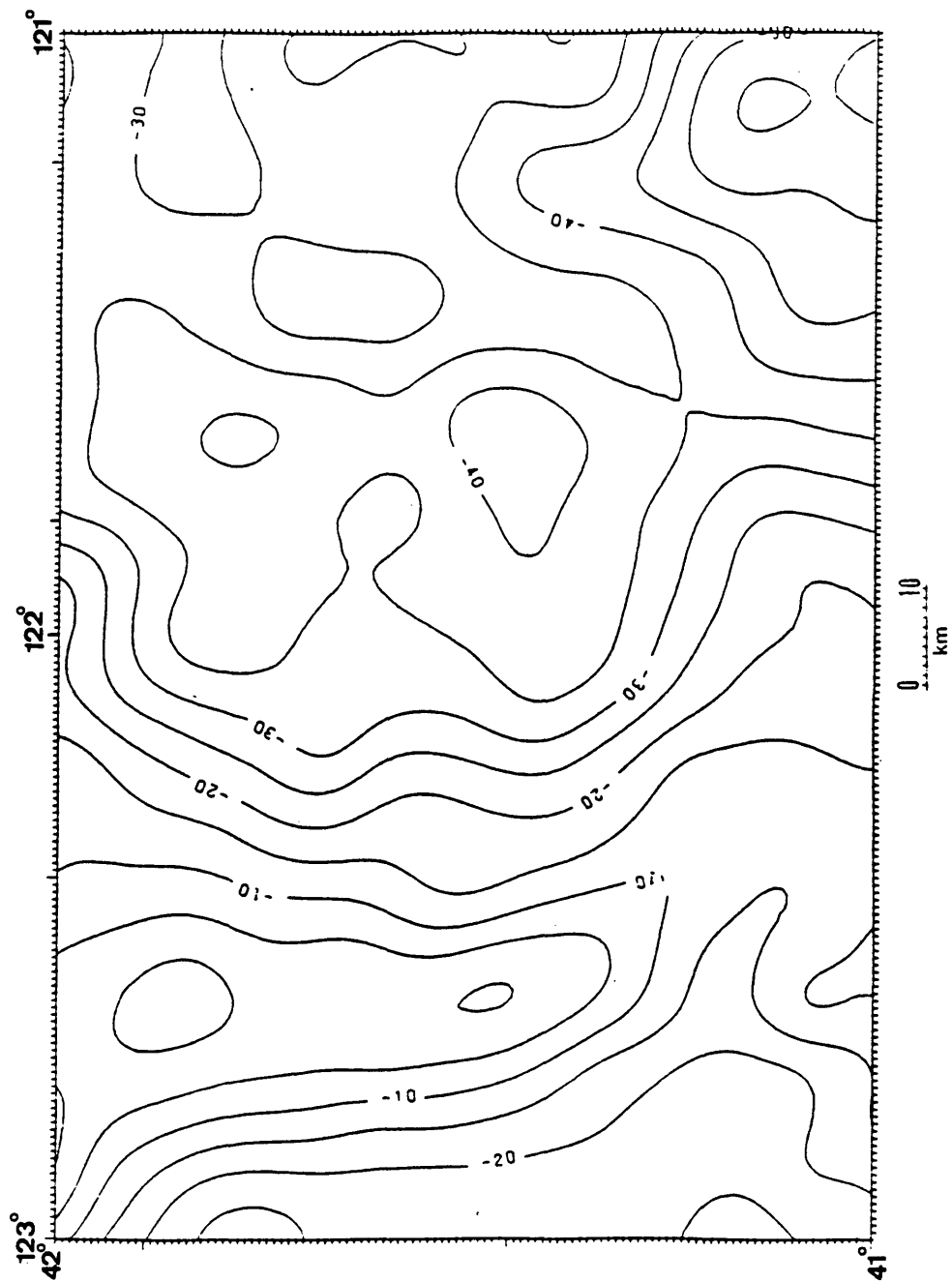


Figure 26. Gravity anomaly on 7.5 km plane above sea level.  
Contour interval: 5 mGal.

## INTEGRATED INTERPRETATION

Gravity, surface density, magnetic, refraction, magnetotelluric, and heat flow data are available for interpretation in the Klamaths and Cascades area. Among these data, the gravity and aeromagnetic data are continuously distributed on the whole area. The others are isolated profile data or scattered point data.

## Features of geophysical methods

Each geophysical method is based on certain physical properties; thus each method is able to resolve some specific properties of the subsurface. The gravity method is based on lateral density contrast and has a serious ambiguity problem. However, the data are continuously distributed over the whole area. Therefore, with the help of geologic and other geophysical data, we are able to interpret the entire area.

The aeromagnetic method is based on the susceptibility contrast above the Curie point depth. In this area, the Curie point depth is about 10 km (Xia, 1986). Thus, we can only use aeromagnetic data to study the magnetized bodies which are located at depths less than 10 km.

The refraction method is based on seismic refraction phenomena. Refraction happens only where the velocity of a

layer is less than the velocity of the underlying layer. There exists a blind zone around a shot point; the deeper the refracting layer, the bigger the blind zone. The refraction data in the area are in the form of several profiles. Although the refraction data are more direct than all of the other data in the area, they provide data only on isolated profiles and contain a shallow blind zone. Thus, this data must be used with other methods.

The magnetotelluric method is based on resistivity contrasts. In the area, there is only one section, with 8 stations, so the magnetotelluric data only provide a very rough resistivity model.

Heat flow data are sensitive to the presence of volcanic cones and to the high permeability, for example, of extensional fault zones. However, some areas have low heat flow, perhaps because the Quaternary volcanic rocks have high permeability, and the ground water percolates downward. Thus, when heat flow data are used, some distortion must be expected.

Based on this analysis, we can use specific groups of methods to solve different geological problems.

#### Geophysical data

##### *Gravity data*

The gravity data set is from NOAA/NGS gravity data

base. The data base in the study area was edited by California Division of Mines and Geology (Chong & Blank, 1972; Chapman & Bishop, 1967). The data are from different sources: Everden (1963), Humble Oil and Refining Company (1964), California Department of Water Resources (1964), LaFehr (1965), LaFehr (1966), U.S. Naval Oceanographic Office (1968-1969).

Finn (1981) and Finn and Spydell (1982) made a more detailed gravity survey in the Medicine Lake Highland area to study intrusion there. Smith (1984) did a gravity survey consisting of 133 stations to map the boundary between the Klamath Mountains and the Cascade Range.

All of the data were reduced to complete Bouguer anomalies, using a standard reduction density of  $2.67 \text{ g/cm}^3$ . Terrain corrections were computed by means of templates for Hayford-Bowie inner zones (A-F) (Smith, 1984), and the computer terrain correction program of Plouff (1966) was applied out to the standard radius of 166.7 km (through Hayford-Bowie zone O). About 30% of stations had terrain corrections in excess of 10 mgal. The International Ellipsoid formula (1930) was used for the normal correction.

$$g = 978.049(1 + 0.0052284 \sin\theta - 0.0000059 \sin^2(2\theta)) \text{ Gals.}$$

Density data are the basis for interpreting gravity

anomalies. The density data used are from different sources, as edited by Chapman and Bishop (1967) and Chong and Blank (1972). A reduction density map was also generated in this research during the course of calculating the variable density terrain corrections. The two density data sets from different methods coincide very well. A new gravity anomaly map using terrain corrections with variable density distributions was generated as part of the research. This new gravity map will be interpreted comprehensively.

#### *Aeromagnetic data*

Huppunen (1983) conducted an aeromagnetic survey in the area between  $40^{\circ}15'$  and  $42^{\circ}15'$  N latitude and  $120^{\circ}45'$  and  $122^{\circ}45'$  W longitude. A flight elevation of 2.74 km was chosen to allow maximum areal coverage with minimum terrain clearance.

#### *Refraction data*

In 1981, the U.S. Geological Survey (Zucca and others, 1986) conducted a seismic refraction survey of northern California designed both to characterize the structure in four of the geologic provinces of that region - the Klamath Mountains, Cascade Range, Modoc Plateau, and Basin and Range provinces (Figure 27) - and to establish the geologic relations between these provinces. It was also intended to



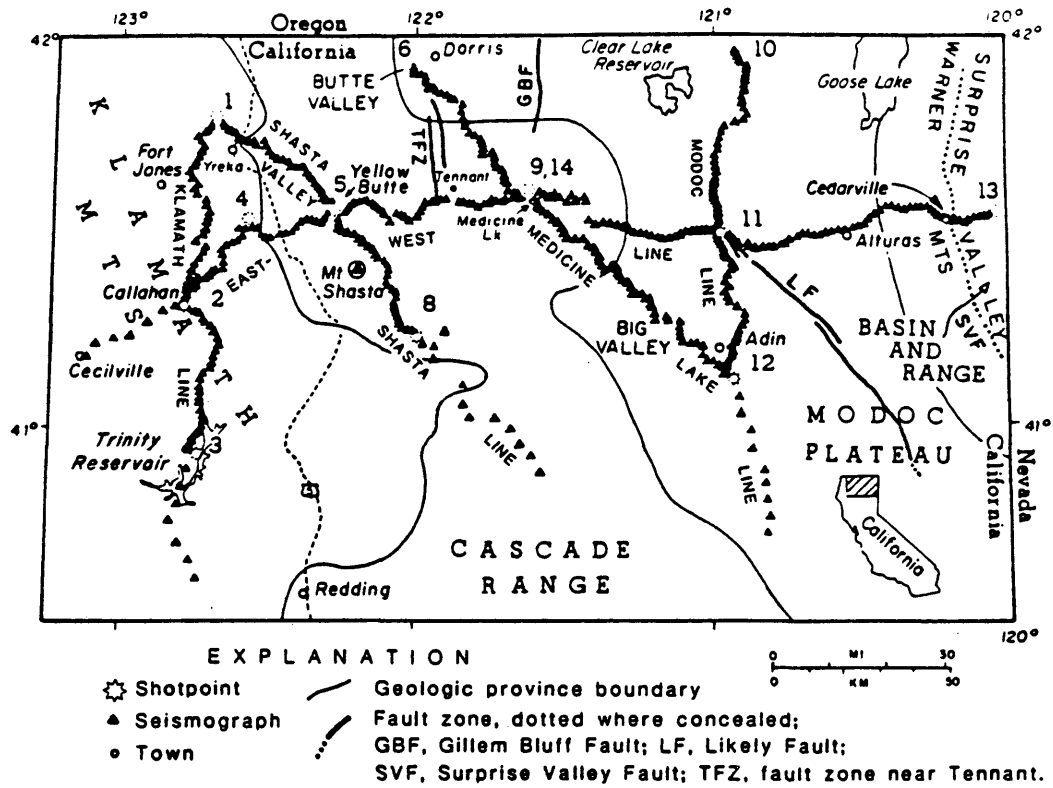


Figure 27. Northern California refraction line location map of Northern California (after Zucca and others, 1987).

define the structural setting of the two large Cascade Range volcanoes in the area, Mount Shasta and Medicine Lake Highland.

*Other geophysical data*

In 1982, the U.S. Geological Survey (Stanley, 1982) conducted a regional magnetotelluric survey for a geothermal program in the Cascade Range, but only one line, with 8 stations, is in the study area. The soundings consisted of tensor resistivity measurements over a frequency range from 0.002 to 100 Hz. These data provide an outline of the regional structure with a three-layer model.

In 1979, the U.S. Geological Survey (Mass and others, 1982) began a systematic program of temperature-gradient and heat-flow measurements. Temperature data were obtained from all wells and drill holes in the region. The status of heat-flow observations is illustrated in Figure 28.

Analysis of the density data

A partial compilation of measured densities for rock units in the Klamaths and Cascades area is given in Table 2. Only a few density values for Tertiary and Quaternary sedimentary rocks are available in the area; these average about  $2.0 \text{ g/cm}^3$ , but diatomaceous sediments, which are

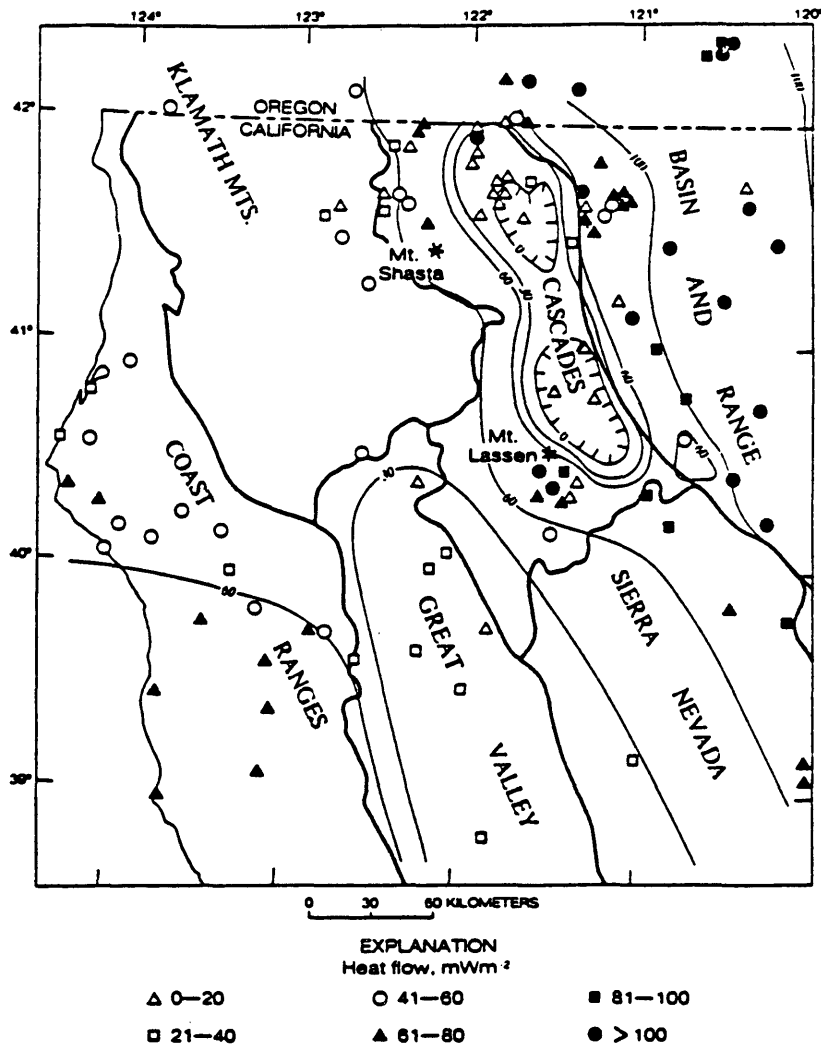


Figure 28. Heat flow map of Northern California (after Mass and others, 1982).

Table 2. Rock sample densities in the Klamath Mountains and Cascade Range area (after Chong and Blank, 1972).

<i>Province or Subprovince</i>	<i>Formation</i>	<i>Rock Type</i>	<i>Number of Samples</i>	<i>Density Range (g/cm<sup>3</sup>)</i>	<i>Average Density (g/cm<sup>3</sup>)</i>	<i>Source</i>
COAST RANGES	Franciscan (California)	Graywacke	857		2.65	Irwin (1961)
	Franciscan (Weed Sheet)	Graywacke	9		2.68	Bailey and others (1964)
	Dothan	Graywacke	31		2.67	Doct (1965)
	Dothan	Graywacke and Argillite	6		2.64	Kays and Bruemmer (1964)
	Franciscan	Graywacke and Argillite	6	2.57-2.72	2.65	This paper
KLAMATH MTS. WESTERN JURASSIC	Galice	Sedimentary	5	2.50-2.72	2.58	This paper
	Galice	Sandstone	6		2.61	Doct (1965)
	Galice	Sedimentary and volcanic	5		2.69	Kays and Bruemmer (1964)
	Galice (Oregon)	Recrystallized sedimentary and volcanic	6		2.85	Kays and Bruemmer (1964)
	Galice (Weed Sheet)	Recrystallized sedimentary and volcanic	5	2.89-3.00	2.93	This paper
KLAMATH MTS. WESTERN PALEOZOIC AND TRIASSIC		Metavolcanic	4	2.83-2.91	2.88	This paper
		Metamorphic, almadia-amphibolite facies, vicinity of Condrey Mountain	6	2.78-3.17	3.02	This paper
	(Condrey Mountain area)	Metamorphic, "old schist" of Wells and others	5	2.53-2.78	2.66	This paper
	(Exclusive of Condrey Mountain area)	Metamorphic	7	2.68-2.96	2.76	This paper
KLAMATH MTS. CENTRAL METAMORPHIC		Metavolcanic	2	3.00-3.03	3.02	This paper
		Metasedimentary	4	2.44-2.72	2.63	This paper
KLAMATH MTS. EASTERN KLAMATH		"Basement rocks"	50		2.72	LaFehr (1966)
KLAMATH MTS.		Ultramafic	14	2.41-3.18	2.72	This paper
KLAMATH MTS.		Mafic intrusive	4	2.83-3.16	3.05	This paper
KLAMATH MTS.		Granitic	7	2.85-3.15	2.78	This paper
CASCADE RANGE		"Tertiary volcanic rocks"	58		2.52	LaFehr (1966)

locally abundant, may be distinctly lower than this figure (Chapman and Bishop, 1967). Although the values listed are in many cases based on a small number of samples and are not necessarily representative, they do provide an indication of density contrasts and are useful for qualitative interpretation.

Zucca and others (1985) converted the east-west model based on refraction data to a density model (Figure 29). The velocity-density relationships cited by Dobrin (1976, p.53) were used approximately for the upper crust, and of Birch (1961) for all of the lower crust. The density values for Quaternary volcanic rocks are 2.10 to 2.25 g/cm<sup>3</sup>; the values for intrusions are 2.67 to 2.73 g/cm<sup>3</sup>. The other densities on the density section are from the data of LaFehr (1965).

The reduction density map provides average densities of rocks in the study area. In the Klamath Mountains area, the rock densities of the Trinity sheets in the Eastern Klamath plate and the Central Metamorphic plate are very high, from 2.7-3.05 g/cm<sup>3</sup>. The rock densities in the Western Jurassic plate are low, about 2.6 g/cm<sup>3</sup>. The rock densities in the Western Paleozoic and Triassic plate are intermediate, about 2.7 g/cm<sup>3</sup>. Table 3 contains reduction density data for .

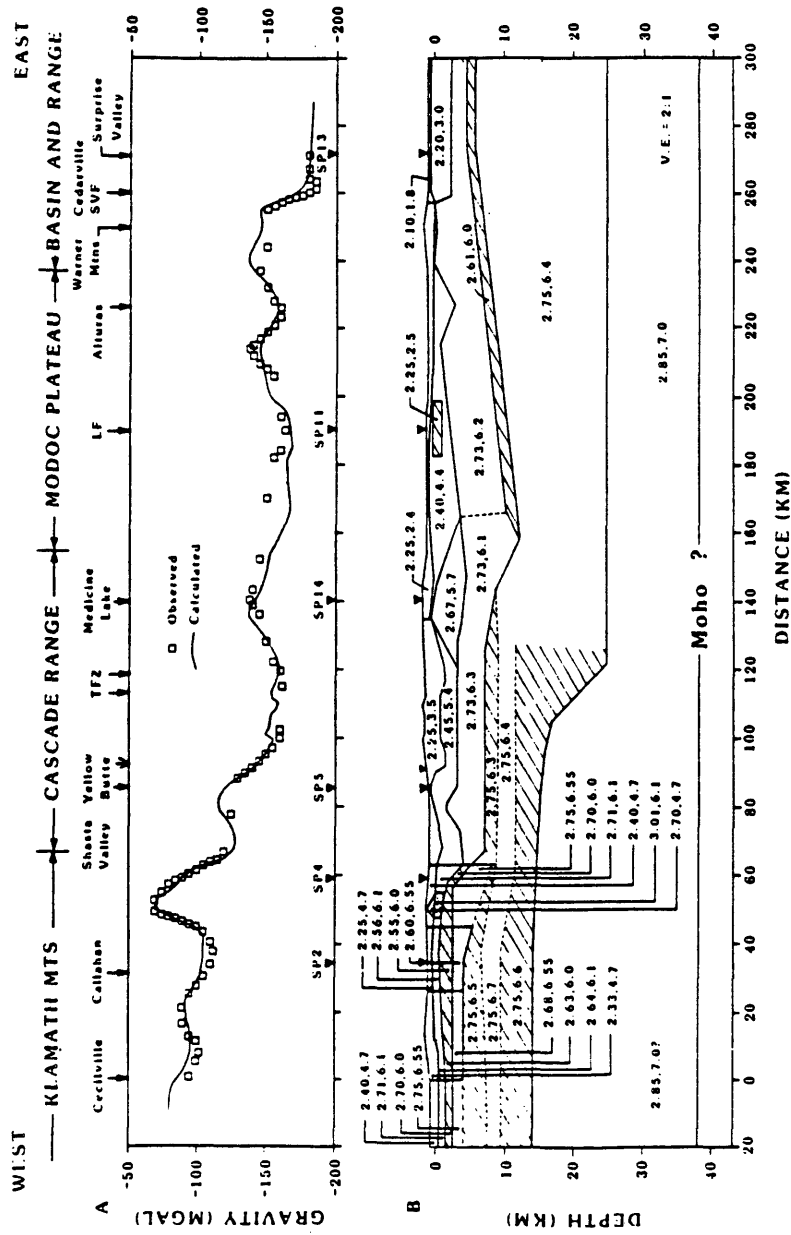


Figure 29. Calculated density section of Klamath Mountains and Cascade Range area (after Zucca and others, 1986).

Table 3. Rock densities in the Klamath Mountains and Cascade distribution map.

PLACE NAME	ROCK TYPE	DENSITY(g/cm <sup>3</sup> )
Goose Nest	Qrv <sup>a</sup> , Qrv <sup>P</sup>	2.0-2.4
Little Deer Mountain	Qrv <sup>b</sup> , Qrv <sup>P</sup>	2.6-2.8
Yellow Butte	Qrv <sup>P</sup>	2.0-2.2
Mountain Shasta	Qrv <sup>a</sup> , Qrv <sup>P</sup> , Qrv <sup>b</sup>	2.2-2.4
Orr Mountain	Qrv <sup>b</sup>	2.2
Wild Horse Mountain	Qrv <sup>b</sup>	2.2
Garna Mountain	Qpv <sup>a</sup> , Qpv <sup>r</sup>	2.2
Horse Peak	Qpv <sup>a</sup>	2.2
Medicine Lake	Qpv <sup>b</sup> , Qpv <sup>a</sup> , Qpv <sup>r</sup> ,	
Highland	Qpv <sup>P</sup>	2.6-3.0
Toad Mountain	Qpv <sup>b</sup>	2.8-3.0
Willow Creek Mountain	Pv <sup>b</sup>	2.8
Mountain Dome	Pv <sup>b</sup>	3.0
Fourmile Hill	Pv <sup>a</sup>	2.8
Nebb Flat Reservoir	Mv <sup>b</sup>	2.8-3.0
Bear Mountain	Tv <sup>b</sup>	2.8-3.0
Black Fox Mountain	Tv <sup>b</sup>	2.6-2.8
Big Valley Mountains	Tv <sup>b</sup>	3.0
Along boundary between Klamath and Cascades	Tv	2.6-2.8
Little Shasta	Tv <sup>r</sup>	2.8

Time:

Qrv-Recent volcanic; Qpv-Pleistocene volcanic;

Pv-Pliocene volcanic; Mv-Miocene volcanic;

Tv-Tertiary volcanic;

Rock (superscript):

r-rhyolite; a-andesite; b-basalt; p-pyroclastics.

twenty places in the Cascade Range. Based on an analysis of Table 3, we can conclude that there are two factors which dominate density. One is rock type and the other is time. The sequence of rock densities, from low to high, is: pyroclastics - rhyolite - andesite - basalt. The younger the rock is, the lower the density. Therefore, the gravity anomalies in the Western Cascade Range are generally larger than the anomalies in the High Cascades.

The three density data sets point out two main density contrasts. The first density contrast is  $0.2 - 0.4 \text{ g/cm}^3$  between the eastern Klamath Plate and the Cascade Range. This density contrast is one of the sources of the gravity regional caused by basement in the Cascade Range area. The second density contrast is between the Western Jurassic Plate and the Central Metamorphic Plate, about  $0.3-0.4 \text{ g/cm}^3$ . The other local density contrast is between intrusive and country rocks; these contrast values are variable. For example, the contrast is  $0.2-0.4 \text{ g/cm}^3$  in the Medicine Lake Highland, and  $0.3 \text{ g/cm}^3$  in the China Mountain areas. The deepest density contrast is at Moho surface, about  $0.45 \text{ g/cm}^3$ . This is the main source of the regional anomaly in the study area.



## Interpretation of regional anomalies

### *Moho and deep crust*

The numerical values of the model parameters used to construct the isostatic map (Figure 21) are: (1) topographic density of  $2.67 \text{ g/cm}^3$ , (2) sea level crust thickness of 25 km, based on the results of seismic refraction surveys near San Francisco (Healy, 1963); and (3) a density contrast across the base of the crust of  $0.4 \text{ g/cm}^3$ . Based on the isostatic map, the Moho surface in the study area is an eastward-dipping slope. The Moho dominates the regional anomaly in the area. Based on the empirical formula:

$$H = H_0 * (1 - 0.1 * g)$$

where  $H_0$ , 25 km, is the crustal thickness at the coast and  $g$  is the isostatic anomaly at the point being computed. The refraction data and magnetotelluric data define the location of the subsurface between the lower crust and upper crust. Rocks are generally granitic above the interface and basaltic below it (Figure 30).

These are the main sources of the regional anomaly in the study area. They cause an eastward-dipping slope in the regional anomaly.

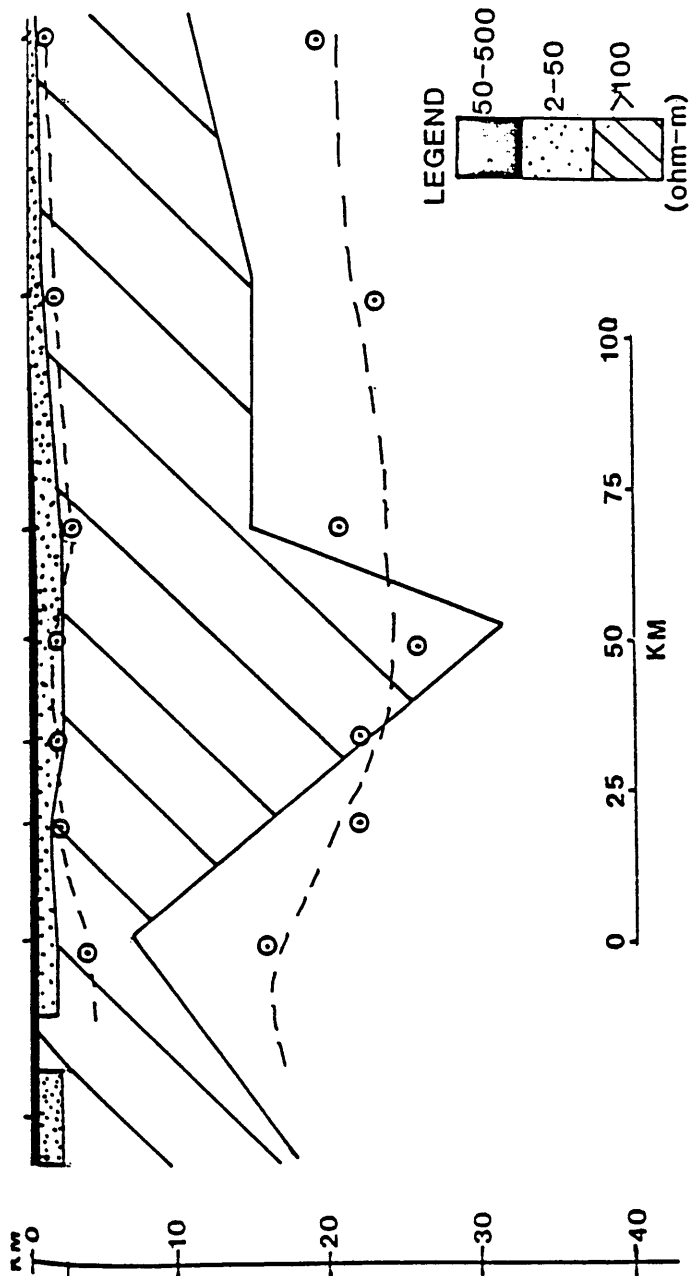


Figure 30. Interpreted section from magnetotelluric data in Northern California (after Stanley, 1982).

*Klamath Mountains*

A north-south trending gravity high predominates the gravity anomalies in the Klamath Mountain area. The gravity high runs continuously from Badger Mountain, Antelope Mountain and China Mountain to Red Mountain. The main gravity high is located at China Mountain, with a maximum amplitude of about 35 mGal.

Two flanks of the gravity high are high-gradient zones. The eastern zone is the boundary between the Klamath Mountains and the Western Cascades. The western zone separates the Central Metamorphic plate, The Eastern Klamath plate and the Western Paleozoic and Triassic plate, and the Western Jurassic plate. To the west of the high-gradient zone are gravity lows. The main difference between the variable-density data and the constant-density data in the Klamath Mountains area is an amplitude reduction of about 20 mGal.

The gravity high coincides with the Trinity sheet of the eastern Klamath plate and the Central Metamorphic plate. The rocks of these plates are ophiolites; most ophiolites are basic and ultrabasic rocks. The densities range from 2.7-3.00 g/cm<sup>3</sup>. It is impossible to map the boundary between the eastern Klamath plate and the Central

Metamorphic plate. However, the high-gradient zone on the west side of the gravity high separates the Western Paleozoic and Triassic Plate and the the Western Jurassic Plate. The densities of these plates are about 2.7 and 2.6 g/cm<sup>3</sup>, respectively.

There is a group of magnetic highs on the aeromagnetic map n the Klamath Mountains province (Figure 31). The anomalies trend north-south. The map of the filtered anomaly reduced to the pole gives evidence for the eastward dipping of the plates. The magnetic anomalies are originally associated with gravity anomalies. However, after filtering using a low-pass filter to suppress wavelengths shorter than 20 km (Figure 32), the group of magnetic anomalies becomes four magnetic highs with a north-south trend and are displaced to the east. The axes of the gravity anomalies and magnetic anomalies are separated by about 10 km. The source of the filtered magnetic anomalies is deeper than that of the unfiltered gravity data. Therefore, the axis separation implies that the source is eastward-dipping; that is, that the eastern Klamath Plate and the Central Metamorphic Plate are eastward-dipping.

After upward continuation of the magnetic data to 7.5 km (Figure 33), the series of magnetic anomalies becomes an

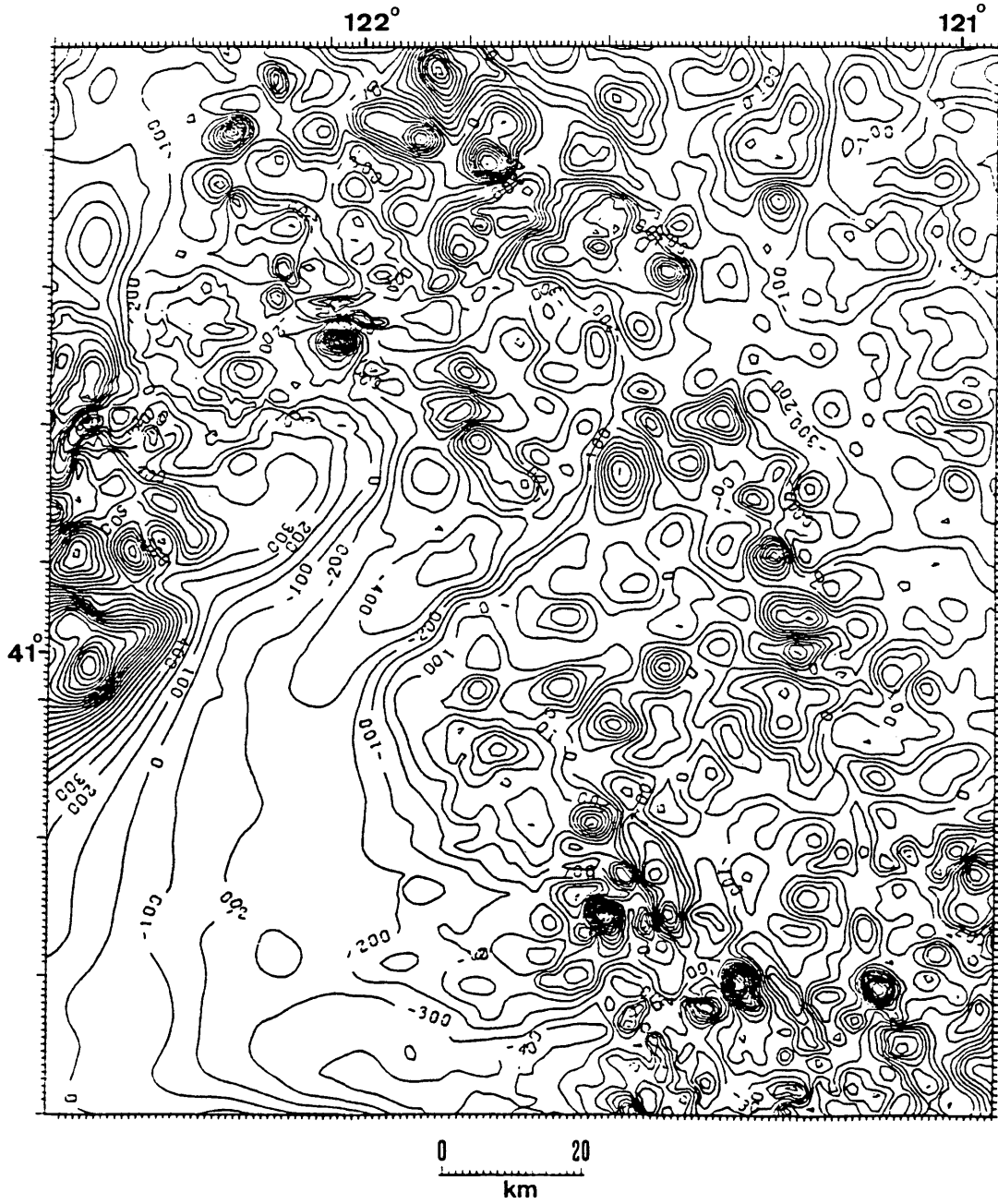


Figure 31. Aeromagnetic anomaly map of Northern California. Contour interval: 100 nT.

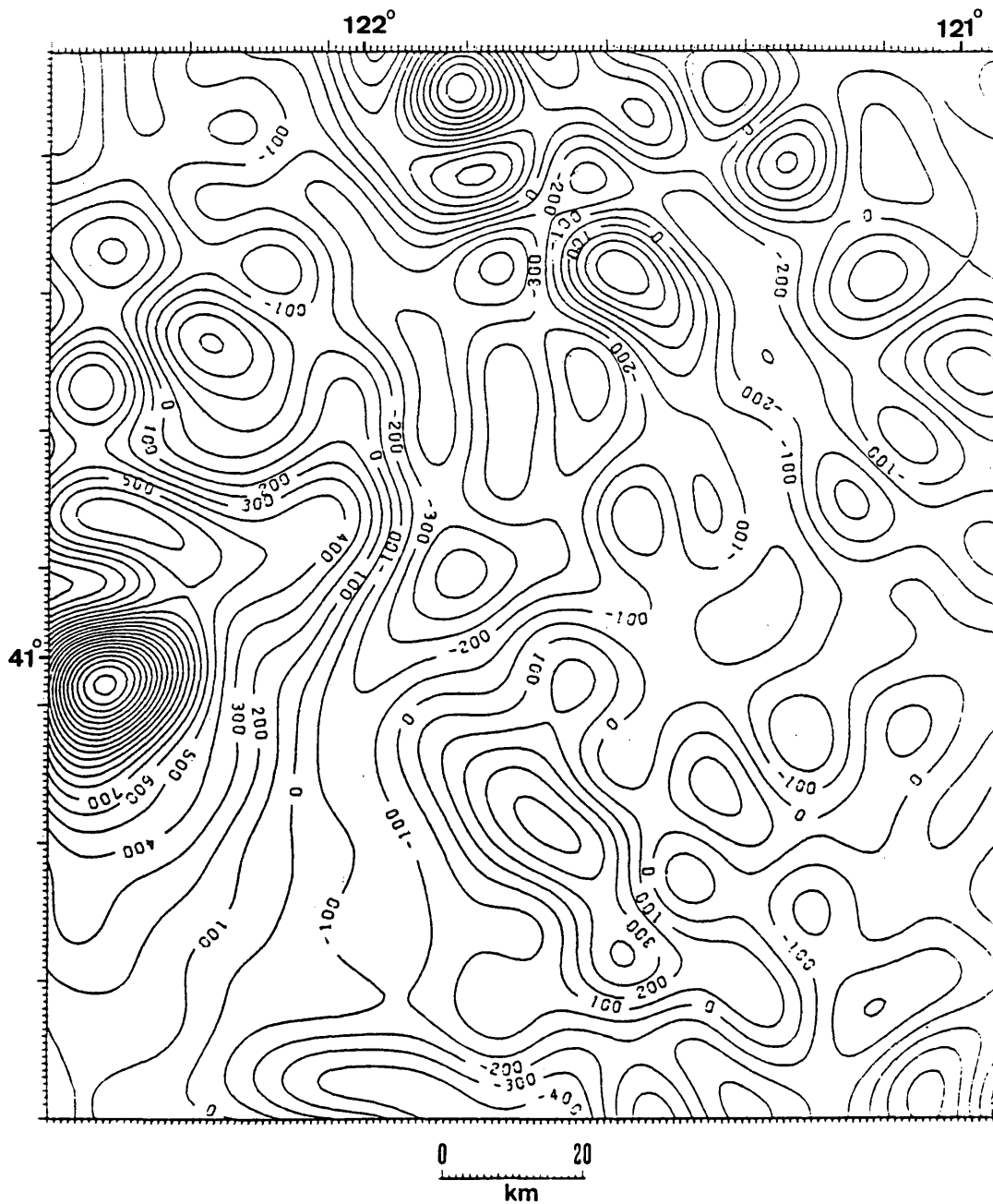


Figure 32. Filtered, reduced-to-pole aeromagnetic anomalies for Northern California (filter pass band: 1000-20 km). Contour interval: 100 nT.

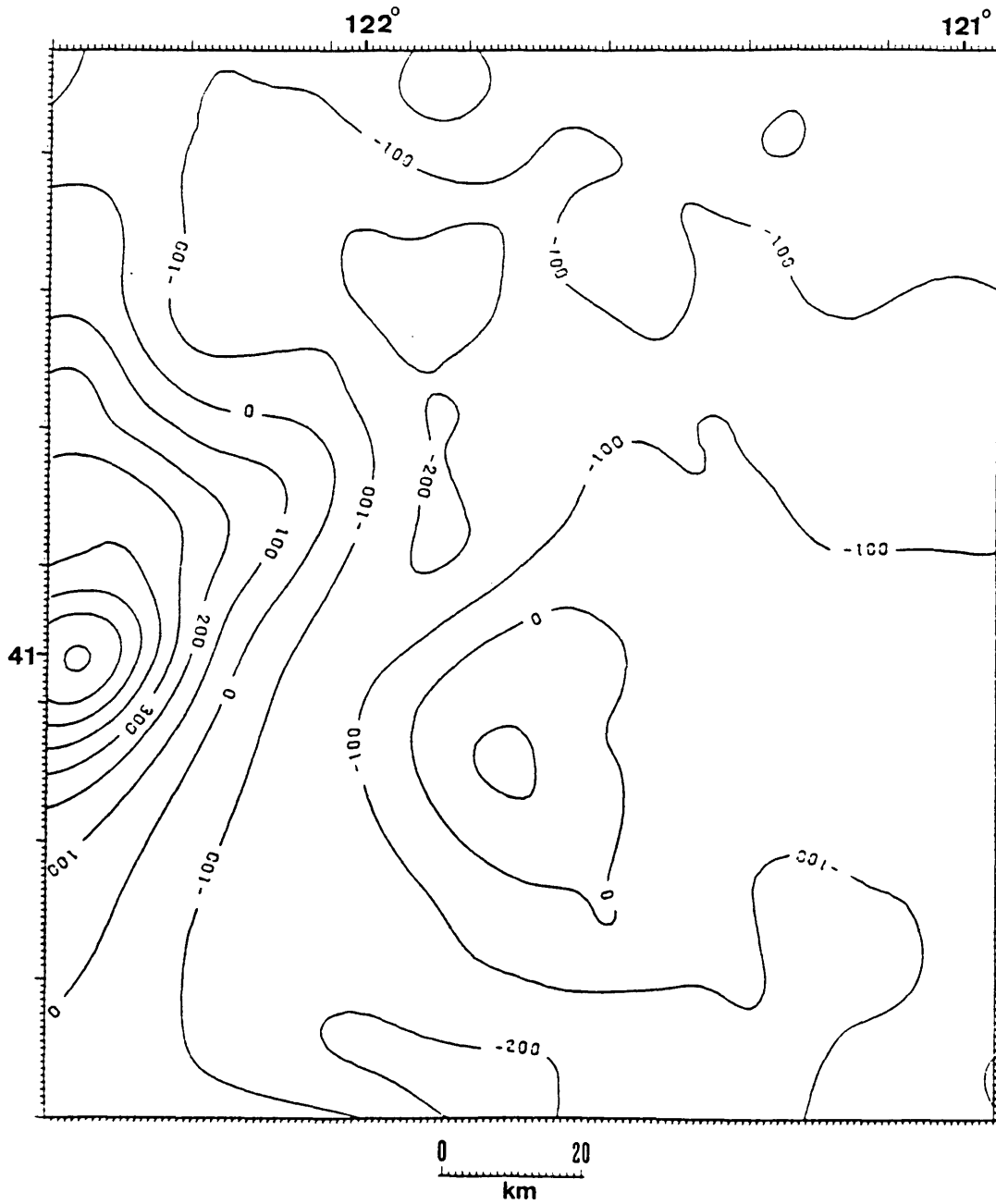


Figure 33. Aeromagnetic anomalies on 7.5 km plane above sea level.  
Contour interval: 100 nT.

elliptical anomaly with a north-south long axis. The center of the anomaly is at  $41^{\circ}$  latitude, just at the southern edge of the study area. The China Mountain anomaly becomes an edge of the magnetic high. This implies that the ultramafic complex extends northward at relatively shallow depth beneath Ordovician and Silurian rocks. This inference is in agreement with early interpretations by LaFehr (1966) and Itwin and Bath (1962).

Thus, most of the gravity anomalies in the Klamath Mountains province result from density distributions of different plates and rock sheets.

#### *Cascade Range*

In the Cascade Range area, a large gravity low dominates the features on the complete Bouguer anomaly map made with a constant reduction density. The shape of the anomaly is a triangle, the three corners of which are Mount Shasta, Medicine Lake Highland and Butte Reservoir. The lowest value is located at Mount Shasta, about 165 mGal. There are several gravity lows which are coincident with topographic highs: Mount Shasta, Deer Mountain, Little Deer Mountain, Cedar Mountain, Hebpon Mountain, Bonita Butte, and Stephens Butte. Specifically, the Mount Shasta gravity low has strong coherence with topography. Three gravity highs are located to the east of large gravity lows: Mammoth



siding, Medicine Lake Highland, and Indian Spring Mountain. These highs are discontinuous, but seem to form a north-south trend. There is also a discontinuous set of gravity lows with a northwest-southeast trend from Lower Klamath Lake to Big Valley.

On the complete Bouguer anomaly map made with variable reduction density, there are several differences: 1) The gravity lows correlated with topography disappear. 2) Mount Shasta, originally a gravity low (the lowest value on the map), is now on a flank of a high-gradient zone. This zone separates the Western Cascades and the High Cascades. 3) The gravity high of the Medicine Lake Highland is combined with the other three gravity highs to form a gravity high ridge with a north-south trend. The western part of the Medicine Lake Highland anomaly is reduced to a gravity low, like a camel back.

The aeromagnetic anomaly map is very complex in the Cascade Range. Many small magnetic anomalies are scattered in the area. Most of them are associated with topography, but they are distributed along a northwest trend. The amplitudes of these anomalies are less than 1000 nT, typically 300-500 nT.

The aeromagnetic data were processed by routine methods. First, a low-pass filter passing wavelengths

greater than 4 km was used to reduce the random noise. Then, the filtered data were reduced to the pole from an inclination of  $62.5^{\circ}$  and a declination of  $17^{\circ}$ . After these steps, a low-pass filter, passing wavelengths greater than 20 km, was used to filter the reduced-to-the-pole data. The features of the processed data have a very strong northwest trend. The anomalies belonging to this trend range from Butte Reservoir to Big Valley. The Medicine Lake Highland anomaly and another anomaly located northeast of the anomaly became one bigger anomaly and were displaced northeastward.

The high-gradient zone on the east side of the Klamath Mountains was interpreted as a normal fault based on constant density data (Smith 1984). However, Mount Shasta is in a high-gradient zone with a north-south trend on the variable density data map, but is a gravity low on the constant-density map. This high-gradient zone is moved eastward in the variable density map, and is separated more widely from the high-gradient zone on the east side of the China Mountain. There are gravity lows between the two high-gradient zones. This area is the Western Cascades. The heat flow data show that there is low heat flow ( $0-60 \text{ mWm}^2$ ) along the high-gradient zone to the east of China Mountain, and high heat flow ( $61-100 \text{ mWm}^2$ ) along the

high-gradient zone passing through Mount Shasta. Therefore, I prefer to interpret the high-gradient belt of the east side of the Klamaths as the sum of effects of the Trinity plate anomaly and an old fault. The Western Cascade volcanic rocks are deposited on the eastern Klamath Plate (Magill and Cox, 1980). The normal fault zone with a north-south trend may coincide with the Mount Shasta high-gradient zone. This normal fault zone is the boundary between the Western Cascade and the High Cascade, and is probably the passageway for the High Cascade volcanics.

On the east of the Medicine Lake Highland, there is a gravity high with a north-south trend. The gravity values on the east side of the anomaly are lower than those on the west side. These may indicate another normal fault zone. The magma may have intruded or erupted along this fault zone. The Medicine Lake Highland intrusion may also result from the fault zone.

It is obvious that the gravity anomalies decrease from west to east on the isostatic residual map; the shape of the anomalies suggest steps. This indicates that the regional structures are an eastward-dipping graben structure in the study area bounded by the normal fault zones. The heat flow value along the two zones are 61-100 mWm<sup>2</sup>. These data

provide the other evidence to prove that the normal faults exist.

On the gravity map, density map, and aeromagnetic map, three strong northwest trends exist: 1) Horn Brook-Mount Shasta-McArthur Swamp, 2) Butte Reservoir-Medicine Lake-Big Valley, 3) Tulelake Sump-Beeler Reservoir. This is especially clear on the filtered aeromagnetic data (with the wavelengths less than 20 km suppressed). Mount Shasta and Medicine Lake Highland are located at the intersection between the northwest trend and the normal fault zone. These trends indicated a northwest-trending strike-slip fault zone. These faults are believed to have developed concurrently with the older northwest fold pattern.

Based on this interpretation, we may generate a regional structural model. The Cascade Range is a graben structure. The graben results from normal fault zones with north-south trends. Then, the grabens were filled by volcanic rocks. Based on an understanding of the geologic model, we can use the regional gravity anomaly (upward continued to a 7.5 km level) to obtain the basement structure with help of inversion techniques.

A two-dimensional rectangular model and a Marquardt inversion method were used to compute the basement depths.

The horizontal derivative was used to determine the edges of the volcanic basin. Eleven rectangles were used to model each profile. To minimize edge effects, a half-step model was used at the eastern edge of each profile, instead of a rectangular model. The profiles are west-east in direction. A north-south profile was used as a tie line to adjust the depths between the west-east profiles. Figure 34 is the basement depth contour map constructed in this way.

To give a quantitative concept of the regional structure, a forward model section was generated along a west-east direction through the China Mountain, Mount Shasta and south of Medicine Lake. The deep parts of the forward model were based on seismic refraction data, and the surficial parts were based on surface geology and surficial density data. The computed result of the forward model was fitted to the variable density data on 4 km datum (Figure 35). Because the variable-density data were used, the forward models for the bodies above sea level should be assigned different density contrasts, based on the variable reduction densities. This reveals a disadvantage of the variable-density terrain correction: it makes modeling work more complicated. Figure 36 is the result of forward modeling of the regional structure section.

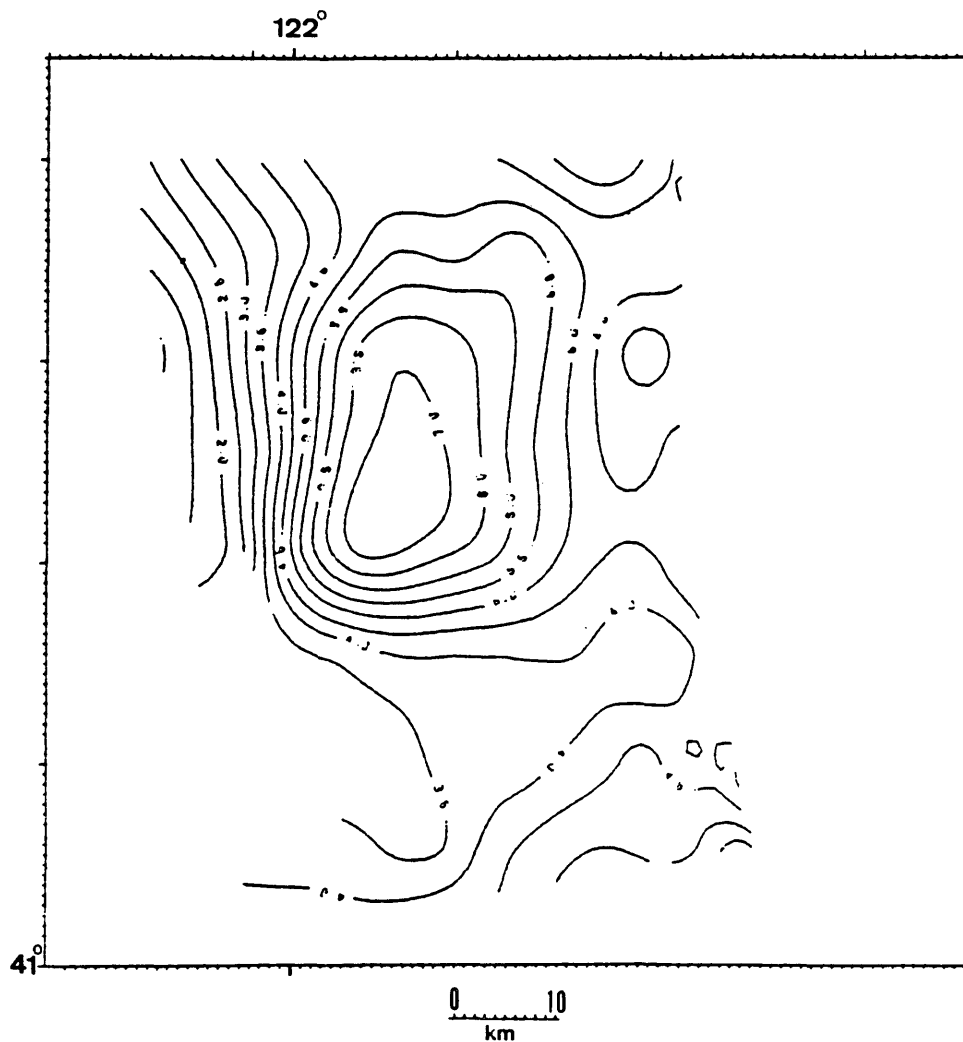


Figure 34. Basement depth contour map of Cascade Range.  
Contour interval: 0.5 km

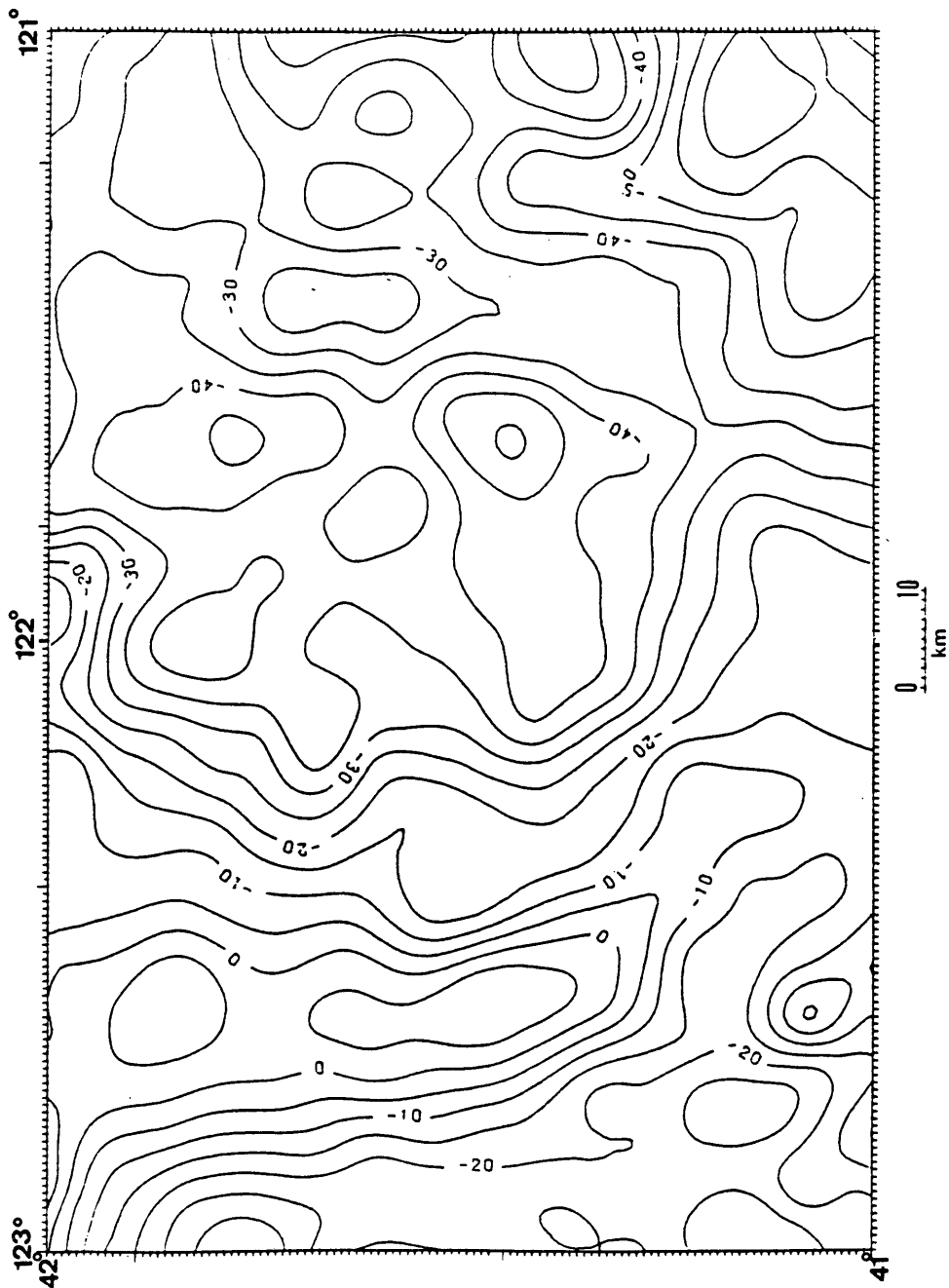


Figure 35. Reduced gravity anomaly on 4 km datum above sea level. Contour interval 5 mGal.

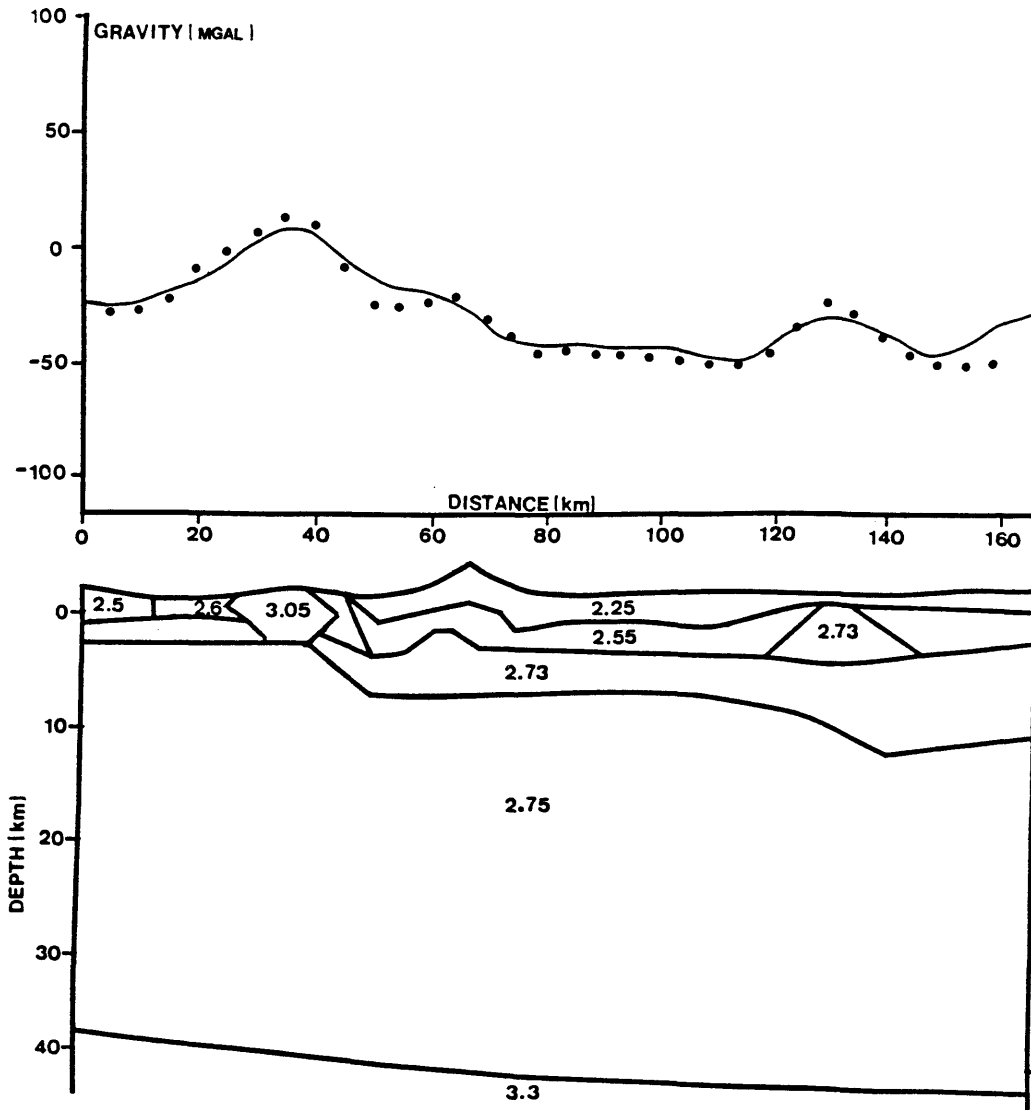


Figure 36. Forward model section of regional structure in Klamath Mountains and Cascade Range. Solid line: reduced anomaly reduced to 4 km datum; dotted line: calculated anomaly.



*Medicine Lake Highland gravity high:*

There is a gravity high in the Medicine Lake Highland area on both the constant-density map and variable-density maps. The amplitude of this anomaly is about 10 mGal. The center of the gravity high is near Medicine Lake on the constant-density map. On the variable-density map, the gravity anomaly is combined with the belt of gravity highs, and the center of the anomaly is displaced northeast about 8 km. The western part of the Medicine Lake gravity high becomes a relative gravity low, like a camel back. Comparison between the two maps reveals a problem of the variable-density reduction: that this method may erase the anomalies in which we are interested, which are correlated with topography. However, if we use the two data sets to make a joint interpretation, it may allow us to estimate the bottom depth of the sources.

This gravity high was studied by Finn and Williams (1985). Finn (1981) made a local gravity survey in the area (Figure 37). Fuis and other (1986) made a seismic refraction survey; two sections pass through the area. Catchings (1983) modeled the seismic data in his MS thesis.

On the aeromagnetic map, Medicine Lake is a local magnetic high which is composed of three sub-anomalies.

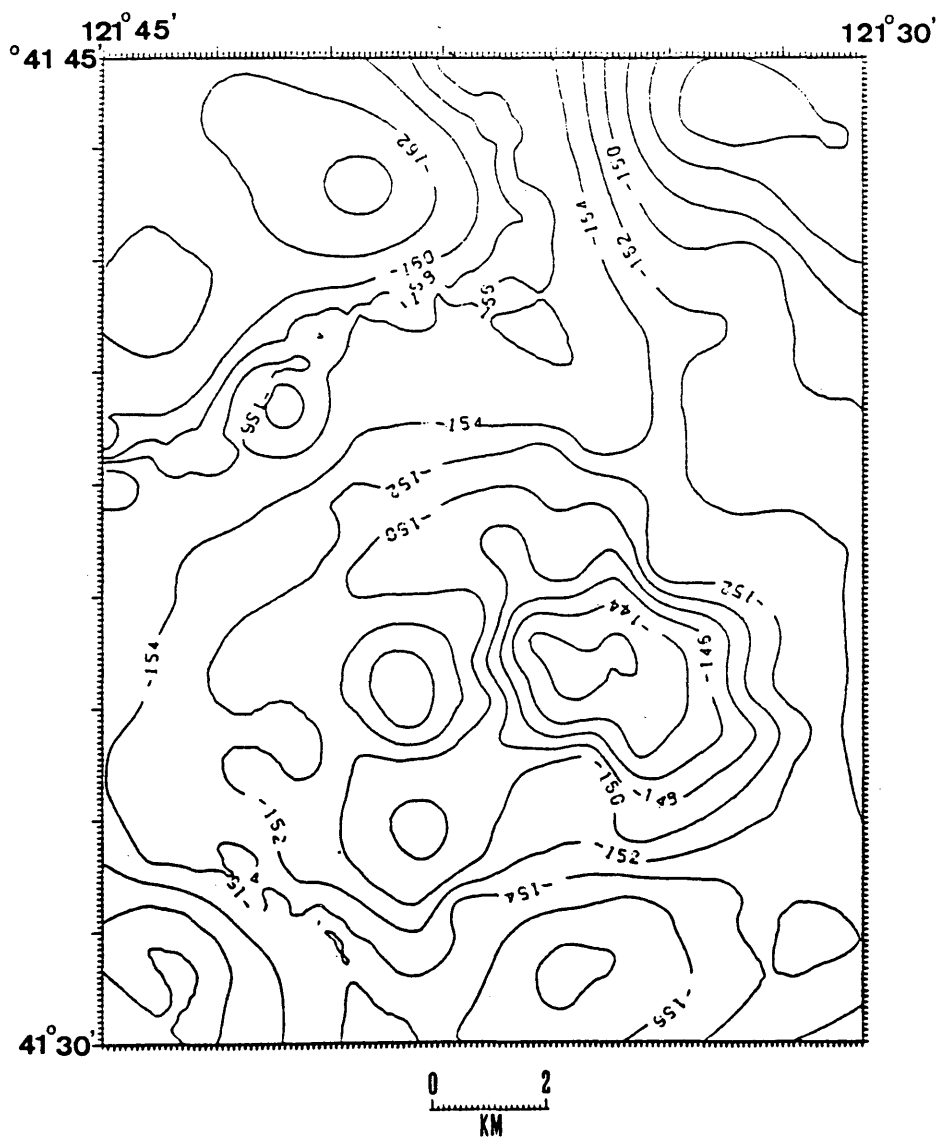


Figure 37. Gravity anomaly map of Medicine Lake Highland. Contour interval: 2 mGal.

After cutting wavelengths less than 20 km, this anomaly is joined with the other anomaly located northeast of Medicine Lake, and is displaced to northeast; its amplitude is about 500 nT.

Two seismic refraction sections pass through the Medicine Lake Highland; one is a west-east regional line, the other is the northwest Medicine Lake line. The two seismic lines provide evidence that the anomaly is caused by an intrusive body. The depth of the body top is very shallow, about 1 km. Along the Medicine Lake line, there are gravity survey data, and the seismic line is more continuous. Therefore, this section was used to construct a forward model. Based on Catchings' (1983) model and Fuis' (1986) model, a forward model was generated along the Medicine Lake line. The densities of the layers and the intrusion were adjusted based on reduction density and both sets of seismic data. Figure 38 shows the result of forward modeling for the Medicine Lake Highland intrusion.

Based on the above analysis, the Medicine Lake Highland gravity high can be interpreted as follows. The main magma chamber is located to the northeast of the Medicine Lake. The normal fault with north-south trend provides the probably passageway for the magma to intrude and erupt. At

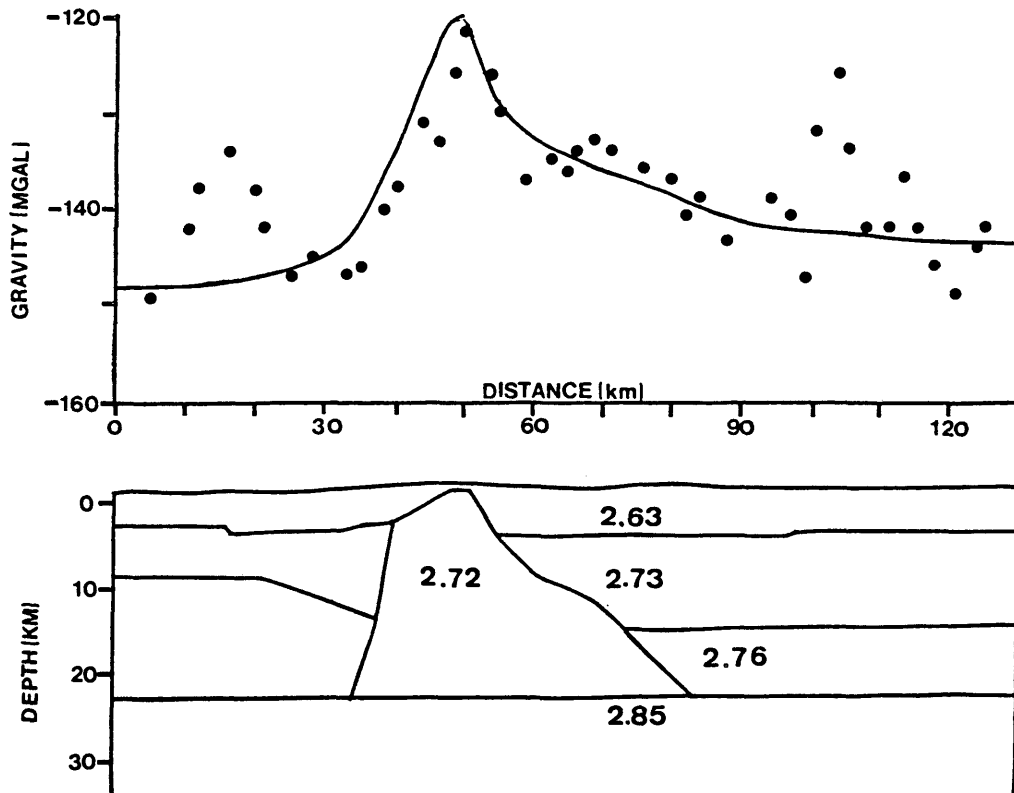


Figure 38. Forward model profile through Medicine Lake Highland. Solid line: calculated anomaly; dotted line: observed anomaly.

Medicine Lake, the magma also intruded into the strike-slip fault. However, the bottom of the western part of the Medicine Lake intrusion is not deep.

Finn and Williams (1985) studied several subintrusions in the western United States. They concluded that there is a relationship between caldera size and the density of the intrusion. Larger calderas (diameters greater than 15 km) have relatively low-density intrusions beneath them, while small calderas (diameters less than 15 km) have relatively high-density intrusions beneath them. The density contrasts that produce the observed anomalies occur between the intrusion, whose density is usually greater than  $2.6 \text{ g/cm}^3$ , and the country rock. Commonly, the shallow country rock is an older volcanic layer with a density less than  $2.5 \text{ g/cm}^3$ . The result of the density contrast is a positive anomaly over the intrusion. For larger calderas, the surrounding volcanic layer is thin and overlies the dense metamorphic and plutonic country rocks. The intrusion is commonly less dense than country rock. The result is a negative anomaly. This conclusion is coincident with chemical features of magma bodies. A magma with low density is often highly silicic. Such magma is thin; thus, it is easy for the magma to spread into a large caldera. Mafic magma is of high

density and is thick. It is hard for such magma to spread before it condenses. Therefore, it forms a small caldera. Figure 39 is a statistical curve of the relationship between caldera diameter and gravity anomaly, and chemical components.

We can use Finn and Williams' (1985) conclusion to interpret the Medicine Lake gravity high geologically. The Medicine Lake intrusion has a broad, elliptical top roughly 5 by 9 km in size. The thickness of the intrusion is thicker than the thickness of the volcanic layer that it intruded in the eastern part, and it penetrated the base of the volcanic edifice. The density contrast of the intrusion is  $0.3 \text{ g/cm}^3$  (the intrusion is  $2.73 \text{ g/cm}^3$ , and the older volcanic rock is  $2.4\text{-}2.6 \text{ g/cm}^3$ ). The intrusion of Medicine Lake must be more mafic, with higher density. Thus, the caldera on the surface of Medicine Lake is small; its diameter is less than 10 km.

The main result of integrated interpretation of the variable reduction density map is a tectonic model of the Klamath Mountains and the Cascade Range. Three high-gradient zones indicate the plate boundary in the Klamath Mountains area and the boundary between the Klamath Mountains and Cascade Range, as well as a normal fault zone

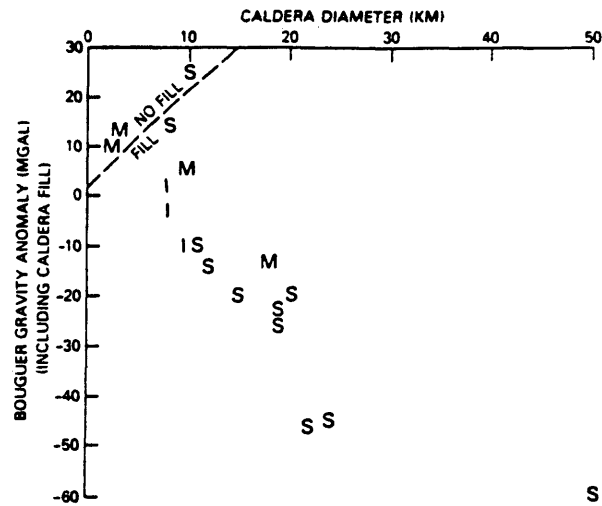


Figure 39. Diameter versus Bouguer gravity anomaly for 18 calderas. M: mafic rock; I: intermediate rock; S: silicic rock (after Finn and Williams, 1985).

near Mount Shasta. Heat flow data point out that the boundary between the Klamath Mountains and the Cascade Range is not a normal fault - the normal fault zone is located near Mount Shasta. This fault zone is probably the passageway for Mount Shasta volcanic activity. The ridge of gravity highs on the east of Medicine Lake indicates another normal fault zone which is probably the passageway for Medicine Lake volcanic activity. The two normal fault zones form a half graben structure in the Cascade Range area. This graben dominates the geologic features in the Cascade Range. The aeromagnetic data and gravity data indicate strike-slip faults with northwest trend in the Cascade Range area. Figure 40 is a regional geologic profile based on the integrated interpretation.



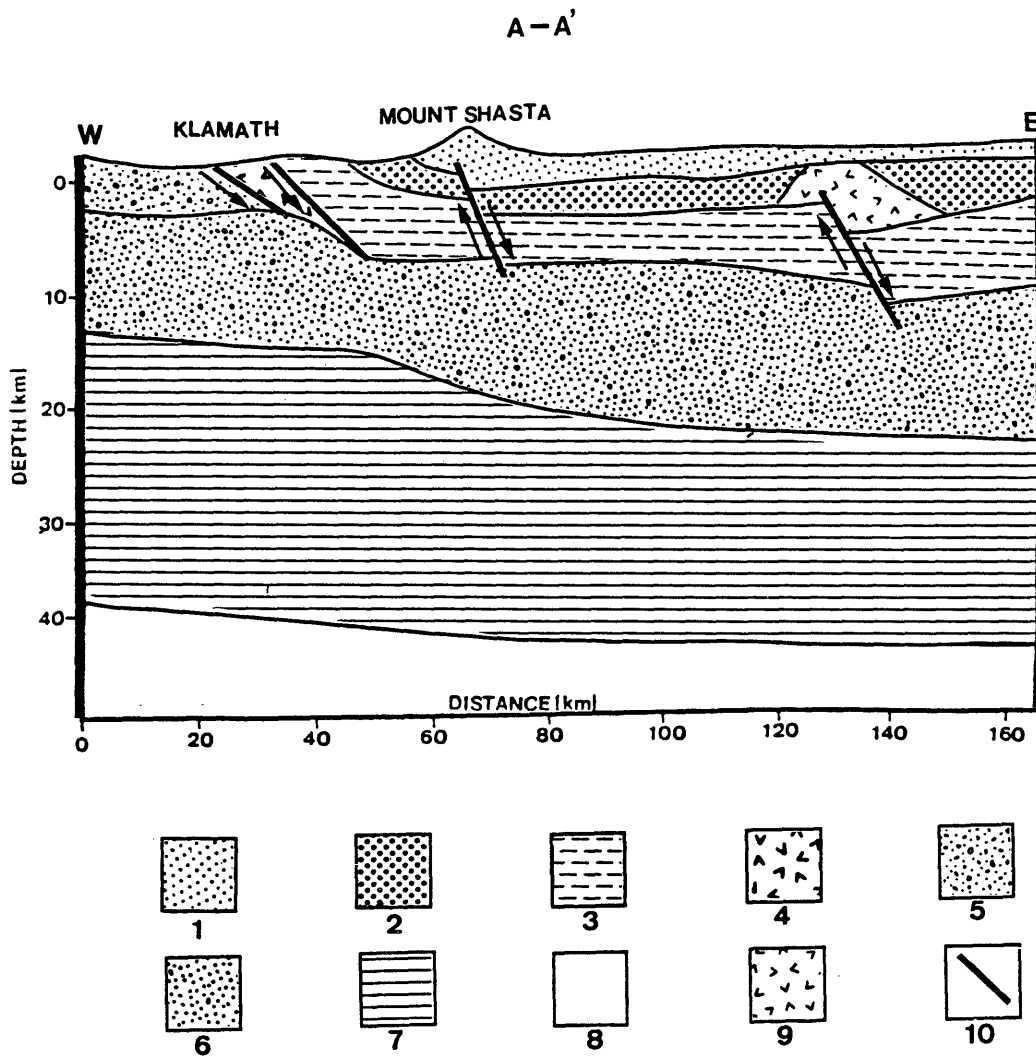


Figure 40. Geologic model profile of Klamath Mountains and Cascade Range area. 1) High Cascades, 2) Western Cascades, 3) Eastern Klamath plate, 4) Central Metamorphic plate, 5) Western Paleozoic and Triassic plate, 6) Granite, 7) Basalt, 8) Upper Mantle, 9) Intrusion, 10) Fault.

## CONCLUSIONS AND FUTURE WORK

## Conclusions

In areas of rugged topography, we often encounter three problems: the need for terrain corrections with variable density distributions, the need to reduce data to a datum, and the difficulty of anomaly separation. In this thesis, these three problems have been studied and lead to the following conclusions:

- 1) Nettleton density profiling is an effective method for calculating reduction densities, and linear regression can be used to model the density profiles. To reduce the effects of the regional anomalies in the Nettleton profiles, derivatives of elevations and gravity anomalies should be used to compute the correlation coefficients instead of elevations and gravity anomalies. The resulting density map in the Klamath Mountains and Cascade Range area coincides with the geologic map, and the gravity anomalies are less correlated with the topography than those with constant reduction density.
- 2) The Dampney method is the most accurate of the three methods tested for reducing data to a common datum. However, a supercomputer should be used to

reduce the data. The algorithm of Bhattacharyya and Chan converges very fast. However, an accurate numerical integral method should be used to treat carefully the places where the datum is too close to the station elevations.

- 3) A geologic structural model is the basis for separating regional and residual anomalies. In rugged mountainous areas, the isostatic correction should be used to separate effect of Moho undulations. Upward continuation has physical meaning, and can be used to separate regional and local anomalies. With help of the low-pass-filter method, an optimal height of upward continuation may be obtained.
- 4) With help of other geophysical data, the complete Bouguer anomaly map with variable reduction density was interpreted to obtain following results:
  - a) The sources of the gravity high in the Klamath Mountain province are the Trinity sheet of the Western Klamath plate and the Central Metamorphic plate. They are ophiolitic.
  - b) The relationship between the Cascade Range and the Klamath Mountains is a depositional

contact, not a normal fault contact.

- c) There is a graben-style structure in the Cascade Range. Two normal fault zones with eastward dip formed the graben structure. These normal faults are the probable vents for High Cascade volcanic activity.

#### Future research work

The key to terrain corrections with variable reduction density is the quality of the variable reduction density distribution map. The reduction density map in the thesis is reasonably accurate, but it is not perfect. The shortcoming of the density map is that the density data samples are not uniformly distributed through the study area. Therefore, there are some density zones with east-west trends on the density map. The reasons for these shortcomings are perhaps the following:

- 1) The linear regression model does not fit well in places where the terrain correction values are very large, for example, Mount Shasta (about 120 mgal). In such places, a parabolic model should be used.
- 2) The density calculations are only based on peaks in the topography on the Nettleton profile. As a matter of fact, styles of topography are variable.

Different topographic models, for example, trough and slope models, might be studied for calculating density to improve the quality of the reduction densities. Based on this study, this is the key to improving the quality of the reduction density map.

- 3) The density calculations are based on two-dimensional data and the geologic environment was not considered as a factor in computing the reduction density.

Therefore, the following future research would be desirable:

- 1) Use parabolic regression in the places where the terrain correction values are large.
- 2) Use different topographic models in the Nettleton profile to compute the reduction densities.
- 3) Test two-dimensional data and add geologic factors to the density calculation algorithm.

The gravity data with variable-reduction-density terrain corrections have shown advantages in the Klamath Mountain and Cascade Range area, but pitfalls exist also. So far, there are three apparent pitfalls. First, some target anomalies caused by bodies with anomaly densities correlated with the topography are reduced or disappear: for example, the anomaly in the Medicine Lake Highland. Second, the terrain correction with variable reduction density makes

forward modeling more complicated; we have to assign different density contrasts to different units above sea level. Third, it is more difficult to join data with the adjacent data areas. Thus, the use of the variable reduction densities and the interpretation of gravity data with variable reduction density are important subjects for future research work.

## REFERENCES

- Airy, G.B., 1855, Phil. Trans. R. Soc. Lond., 145, 101-104.
- Bhattacharyya, B.K., and Chan, K.C., 1977, Reduction of magnetic and gravity data on an arbitrary surface acquired in a region of high topographic relief: Geophysics, 41, 1411-1430.
- Birch, F. 1961, The velocity of compressional waves in rocks to 1 to kilobars, part 2: Journal of Geophysical Research, 66, 2199-2224
- Bulina, L.V., 1961, The use of airborne magnetic prospecting data in deep seated structure of earth crust with the Siberian platform: Sovetskaya Geologiya, 5, 134-138.
- California Department of Water Resources, 1963, Northern counties round water investigation: Calf. Dept. Water Resources Bull., 98, 223.
- Catchings, R., 1983, Crustal structure from seismic refraction in the Medicine Lake area of the Cascades Range and Modoc plateau: M.S. thesis, University of Wisconsin, Medicine.
- Chapman R.H., and Bishop C.C., 1967, Bouguer gravity map of California, Alturas sheet: California Division of Mines and Geology.
- Chong K.Kim, and Blank J.R., 1972, Bouguer gravity map of California, Weed sheet: California Division of Mines and Geology.
- Cordell, L., and Grauch, V.J.S., 1984, Mapping basement magnetization zones from aeromagnetic data in the San Juan Basin, New Mexico, in Hinze, W.J., ed., The utility of regional gravity and magnetic anomaly maps: Society of Exploration Geophysics, Tulsa, 181-197.
- Dampney, C.N.G., 1969, The equivalent source technique: Geophysics, 34, 39-53.
- Dickinson, W.R., 1976, Sedimentary basins Developed During evolution of Mesozoic-Cenozoic arc-trench system in Western North America: Can. J. Earth Sci., 13, 1268-1287.

- Dobrin, M.B., 1976, Introduction to geophysical prospecting: New York, McGraw-Hill.
- Emilia, D.A., 1973, Equivalent sources used as an analytic base for processing total magnetic field profiles: Geophysics, 38, 339-348.
- Evernden, J.F., 1963, Unpublished gravity data in Kim, C.K., and Blank, H.R., ed. 1973, Bouguer gravity map of California, Weed sheet, California Division of Mines and Geology.
- Evjen, H.M., 1936, The place of the vertical gradient in gravitational interpretation: Geophysics, 1, 127-136.
- Finn, C., 1981, Complete Bouguer map of Medicine Lake, California, 15' topographic quadrangle: U.S. Geol. Sur. Open-file report 81-0098.
- Finn, C., and Williams, David L., 1982, gravity evidence for a shallow intrusion under medicine Lake Volcano: Geology, 10, 503-507.
- Finn, C., and Spydell, D.R., 1982, Principle facts for seventy-four gravity stations in the Northern California, Cascade Mountains; U.S.G.S. Open File Report 82-1080.
- Forsberg, R., 1985, Gravity field terrain effect computations by fast Fourier transform techniques: Presented at the AGU meeting, Baltimore.
- Francine R., Jean-Claude E., and Lakshmanan J., 1987, Variable density Bouguer processing of gravity data from Herault, France: First Break, 5, 9-13.
- Fuis, G.S., Zucca, J.J., Mooney, W.D., and Milkereit, B., 1987, A geologic interpretation of seismic refraction results in Northern California: Geological Society of America Bulletin, 98, 63-65.
- Grant, F.S., and Elsharty, A.F., 1962, Bouguer gravity corrections using a variable density: Geophysics, 27, 616-626.
- Gupta, V.K., and Ramani, N., 1980, Some aspects of regional-residual separation of gravity anomalies in a Precambrian terrain: Geophysics, 45, 1412-1426.
- Hammer, S., 1939, Terrain correction for gravimeter stations Geophysics, 4, 184-194.



- Hammond, P.E., 1979, A tectonic model for evolution of the Cascade Range, in Armentrout, J.M., Cole, M.R., and Terbert, Jr., H., eds., Cenozoic Paleogeography of the Western United States: Soc. of Econ. Paleon. and Mineral., Pacific Section, Pac. Coast Paleogeo. Sym., 3, 219-237.
- Hansen, R.O., and Miyazaki, Y., 1984, Continuation of potential fields between arbitrary surfaces: Geophysics, 49, 787-795.
- Harkness, W., 1889, On the solar parallax and its related constants: Washington, House Misc, Doc.51-1, 38, Serial Set 2797.
- Healy, J.H., 1963, Crustal structure along the coast of California from seismic refraction measurements: Jour. Geophys. Res., 86, 5777-5787.
- Heiskanen, W.A., and Vening Meinesz, F.A., 1958, The earth and its gravity field: McGraw-Hill, New York.
- Henderson, R.G., and Cordell, L., 1971, Reduction of unevenly spaced potential field data to a horizontal plane by means of finite harmonic series: Geophysics, 36, 856-866.
- Humble Oil and Refining Company, 1964, Unpublished gravity data in Champman and Bishop ed., Bouguer gravity map of California, Alturas sheet, 1967, California Division of Mines and Geology.
- Huppunen J.L., 1983, Analysis and interpretation of magnetic anomalies observed in North-Central California: Ph.D. thesis, Oregon State University.
- Irwin, W.P., and Bath, G.D., 1962, Magnetic anomalies and Ultramafic rocks in Northern California: U.S.G.S. Professional Paper 450, B65-B67.
- Irwin, W.P., 1981, Tectonic accretion of the Klamath Mountains, in Ernst, W.G., ed., The geotectonic development of California (W.W. Rubey Volume no.1): Prentice Hall, New York, 30-49.
- Jachens, R.C., and Griscom, A., 1985, An isostatic residual gravity map of California - A residual map for interpretation of anomalies from intracrustal sources: in Hinze, W.T., ed., The utility of regional gravity and magnetic anomaly maps, Society of Exploration Geophysicists, Tulsa, 347-360.

- Jacobsen, B.H., 1987, A case for upward continuation as a standard separation filter for potential-field maps: *Geophysics*, 52, 1138-1148.
- LaFehr, T.R., 1965, Gravity, isostasy, and crustal structure in the southern Cascade Range: *Jour. of Geophys. Res.*, 70, 5561-5597.
- LaFehr, T.R., 1966, Gravity in the Klamath Mountains, California: *Bull. Geol. Soc. Amer.*, 77, 1177-1190.
- MacDonald, G.A., 1966, Geology of the Cascade Range and Modus plateau, in Bailey, E.H., ed., *Geology of Northern California: Calif. Div. of Mines and Geol. Bull.*, 190, 65-96.
- Magill, J. and Cox, A., 1980, Tectonic rotation of Oregon Western Cascades: Oregon Dept. Geol. Min. Indus. Special Paper 10, Portland, Oregon, 67 pp.
- Mass, C.W., Sass, J.W., and Lachenbruch, A.H., 1982, Preliminary heat-flow investigation of the California Cascades: U.S. geol. Sur. Open-File Report 82-150.
- Moritz, H., 1980, *Advanced physical geodesy*: Herbert Wichmann Verlag, Karlsruhe, Abacus Press, Turnbridge Wells.
- Nettleton, L.L., 1939, Determination of density for the reduction of gravimeter observations: *Geophysics*, 4, 176-183.
- Nettleton, L.L., 1954, Regionals, residuals, and structures: *Geophysics*, 19, 1-22.
- Pawlowski, R.P., 1986, A program for continuing three-dimension potential fields: Unpublished report, Center for Potential Fields Studies, Colorado School of Mines, Golden.
- Plouff, D., 1966, Digital terrain corrections based on geographic coordinates (abstract): *Geophysics*, 31, 1208.
- Pratt, J.H., 1855, On the attraction of the Himalaya Mountains and of the elevated regions beyond upon the plumb-line in India; on computations of the effect of the attraction of the mountain masses as disturbing the apparent astronomical latitude of stations in geodetic surveys: *Phil. Trans. R. Soc. Lond.* 145, 53-55.

- Sideris, M.G., 1984, Computation of gravimetric terrain corrections using fast Fourier transform techniques: M.S. Thesis, Univ. of Calgary.
- Smith, B., 1984, A gravity study of the geologic boundary separating the Klamath Mountains and Cascade Range provinces in Northern California: M.S. Thesis, Colorado School of Mines.
- Stanley, W.D., 1982, A regional magnetotelluric survey of the Cascade Mountains region: U.S. Geol. Sur. Open-File Report 82-126.
- U.S. Naval Oceanographic Office, 1968-1969, Unpublished compilation (NAVOCEANO).
- Vajk, R., 1956, Bouguer corrections with varying surface density: Geophysics, 21, 1004-1020.
- Woollard, G.P., 1966, Regional isostatic relations in the United States, in Steinhart, J.S. and Smith, T.J., eds., The earth beneath continents: Geophys. Mono. 10, Am. Geophys. Union, 557-594.
- Xia, H., and Dewhurst, W.T., 1986, Terrain correction with variable density distribution: Presented at Society of Explorations 65th International Meeting & Exposition, Nov. 2-6.
- Xia, H., 1986, Curie point depths of the Klamath/Cascades area of Northern California: Unpublished report, Center for Potential Fields Studies, Colorado School of Mines, Golden.
- Zucca, J.J., Fuis, G.S., Milkereit, B., Mooney, W.D., and Catchings, R.D., 1986, Crustal structure of Northeastern California: Jour. Geophys. Res., 91, 7359-7382.

APPENDIX

```

*****
* THIS PROGRAM FOR COMPUTATION OF DENSITY
* INPUT DATA:
*   1. GRIDDED ELEVATION DATA,
*   2. GRIDDED FREE AIR DATA,
*   3. GRIDDED TERRAIN CORRECTION DATA.
* OUTPUT DATA: A DENSITY DATA FILE
*****
PARAMETER ( ISIZE=350)
CHARACTER ANS*1,ANS1*1
CHARACTER RIDENT*56,PGM*8
CHARACTER*30 IFILE1,IFILE2,IFILE3,OFILE(2)
DIMENSION HH( ISIZE, ISIZE),GFF( ISIZE, ISIZE),GTT( ISIZE, ISIZE)
DIMENSION H( ISIZE),GF( ISIZE),GT( ISIZE),GA( ISIZE, ISIZE),XOUT(20)
*****
* THIS PROGRAM FOR COMPUTING DENSITY AUTOMATICLY VARIABLE DENSITY
* CALCUNATION.
* INPUT DATA:
*   1. GRIDING DATA OF ELEVATION
*   2. GRIDING DATA OF FREE AIR ANOMALY
*   3. GRIDING DATA OF TERRAIN CORRECTION VALUE
* OUTPUT DATA: A DENSITY DATA FILE
*****
PARAMETER ( ISIZE=350)
CHARACTER ANS*1,ANS1*1
CHARACTER RIDENT*56,PGM*8
CHARACTER*30 IFILE1,IFILE2,IFILE3,OFILE(2)
DIMENSION HH( ISIZE, ISIZE),GFF( ISIZE, ISIZE),GTT( ISIZE, ISIZE)
DIMENSION H( ISIZE),GF( ISIZE),GT( ISIZE),GA( ISIZE, ISIZE),XOUT(20)
DIMENSION SH( ISIZE),SGF( ISIZE),SGT( ISIZE),Y(12, ISIZE),SGA( ISIZE)
DIMENSION REGRES(21),DD(21),DSH(100),DGA(100),WORK( ISIZE)
INTEGER FTYPE
COMMON/MINC/RIDENT,PGM,NC,NR,NZ,XO,DX,YO,DY,ANGLE
DATA NIN,NOUT,NN/5,6,0/
-----
C INPUT H,FG,TG DATA
C
PRINT*, ' ENTER: INPUT H DATA FILE NAME: '
READ(5,1) IFILE1
1  FORMAT(A)

PRINT*, ' ENTER: INPUT FREE AIR DATA FILE NAME: '
READ(5,1) IFILE2

PRINT*, ' ENTER: INPUT TERRAIN CORRECTION DATA FILE NAME: '
READ(5,1) IFILE3

PRINT*, ' ** WHAT IS THE UNIT OF ELEVATION? '
PRINT*, '   1. FEET '
PRINT*, '   2. METER '
READ(5,*) IUNIT

```

```

PRINT*, ' ENTER: OUTPUT DENSITY NAME ON ROW DIRECTION!'
READ(5,1) OFILE(1)

PRINT*, ' ENTER: OUTPUT DENSITY NAME ON COLUMN DIRECTION!'
READ(5,1) OFILE(2)

CALL GREAD(HH,IFILE1)
CALL GREAD(GFF,IFILE2)
CALL GREAD(GTT,IFILE3)

WRITE(6,2)RIDENT,PGM,NC,NR,XO,DX,YO,DY
2  FORMAT(//,1X,'IDENTIFIER:      ',A56,/,
1    1X,'GRID ROUTINE:      ',A8,/,
2    1X,'# COLUMNS:      ',I10,/,
3    1X,'# ROWS:      ',I10,/,
4    1X,'X-ZERO:      ',F10.4,/,
5    1X,'X INCREMENT:      ',F10.4,/,
6    1X,'Y-ZERO:      ',F10.4,/,
7    1X,'Y INCREMENT:      ',F10.4,///)

C
C CHANGE METER INTO FEET
C
  IF(IUNIT.EQ.2)THEN
    DO 100 I=1,NR
      DO 100 J=1,NC
        HH(I,J)=HH(I,J)/0.3048
100  CONTINUE
  ENDIF
C
  CALL VMIN2(NR,NC,HH,HMIN)
  WRITE(6,3) HMIN
3  FORMAT(/////,'      MINIMUM ELEVATION:',F8.2)

-----

DO 1000 III=1,2
  OPEN(8,FILE=OFILE(III))

  IF(III.EQ.1)THEN
    IIEND=NR
  ELSE
    IIEND=NC
  ENDIF

C-----
C EXTRACT A ROW/COLUMN
C
  DO 1100 II=1,IIEND,4
    NMIN=0

```

```
CALL SCTN(III,II,NR,NC,IP,NN,HH,GFF,GTT,H,GF,GT)
```

```
C-----
C DETERMINE NUMBER OF SEGMENTS
C
  DO 1200 I=1,NN
    IF(I.EQ.1)THEN
      TMIN=MIN(H(I),H(I+1))
      GO TO 1250
    ENDIF
    IF(I.EQ.NN)H(I+1)=H(I)
    TMIN=MIN(H(I-1),H(I),H(I+1))
1250  IF(TMIN.EQ.H(I))THEN
      NMIN=NMIN+1
      XOUT(NMIN)=I
      PRINT*,NMIN,XOUT(NMIN)
    ENDIF
1200  CONTINUE

C-----
C SEGMENTS LOOP
C
  LL=NMIN-1
  I2=1
1300  IF(LL) 1100,1100,1400
1400  I1=I2
      I2=I1+1
      SL=XOUT(I1)
      SR=XOUT(I2)

C
C EXTRACT EACH SEGMENT
C
  CALL SEGMENT(NN,SL,SR,H,GF,GT,K,SH,SGF,SGT)
C
C K: THE NUMBER OF POINTS IN A SEGMENT
C
  IF(I.EQ.1)THEN
    PRINT*, ' THIS IS ROW ',II, ', TOTAL SEMENT:',NMIN-1
  ELSE
    PRINT*, ' THIS IS COLUMN ',II, ', TOTAL SEMENT:',NMIN-1
  ENDIF
  PRINT*, ' THIS IS SGMENT ',I1, ', TOTAL POINTS:',K
  IF(K.LE.1)THEN
    LL=LL-1
    GO TO 1300
  ENDIF

C
C COPUTE DENSITY
C
  D=1.5
  DELTA=0.1
```

```

DO 1500 I=1,21
  CALL BOUG(K,D,HMIN,SH,SGF,SGT,SGA)
  CALL DERIVA(K,SH,K-1,DSH)
  CALL DERIVA(K,SGA,K-1,DGA)
  CALL REG(K,DSH,K,DGA,R)
  REGRES(I)=ABS(R)
  DD(I)=D
  D=D+DELTA
1500  CONTINUE
C
C SHOW THE DENSITY ON SCREEN
C
  CALL VMIN(21,REGRES,AMIN)
  WRITE(6,4)
4    FORMAT(//,'  D', '          R',/)
  DO 1600 I=1,21
    PRINT*,DD(I),REGRES(I)
    IF(REGRES(I).EQ.AMIN)THEN
      DDD=DD(I)
      ENDIF
1600  CONTINUE

C
C DETERMINE IF THE DENSITY REASONABLE?
C
  IF(DDD.LE.1.8.OR.DDD.GE.3.35)THEN
    WRITE(6,5) DDD
5    FORMAT(//,'DENSITY:',F5.2,', NOT REASONABLE!')
    LL=LL-1
    GO TO 1300
  ELSE

C
  WRITE(6,6) DDD
6    FORMAT(//,'DENSITY:',F5.2,' REASONABLE!')
C
  ISL=INT(SL)
  ISR=INT(SR)

C
  IF(III.EQ.1)THEN
    RLA=YO+IP
  ELSE
    RLO=XO+IP
  ENDIF

C
C SAVE DENSITY ON OUTPUT FILE
C
  DO 1700 I=ISL,ISR,5
    IF(III.EQ.1)THEN
      RLO=XO+I
    ELSE
      RLA=YO+I

```



```

        ENDIF
        WRITE(8,7) RLO,RLA,DDD
7       FORMAT(F8.4,X,F9.4,X,F4.2)
1700    CONTINUE
C
        LL=LL-1
        GO TO 1300
        ENDIF
C
1100    CONTINUE
C
        CLOSE(8)
C
1000    CONTINUE
C
        STOP
        END
C
*****
* FIND THE MINIMUM VALUE FROM A 2-D METRIC
*****
        SUBROUTINE VMIN2(L,M,A,RMIN)
        PARAMETER( ISIZE=350)
        REAL A( ISIZE, ISIZE)
        RMIN=1.E36
        DO 1 I=1,L
        DO 1 J=1,M
1       RMIN=MIN(RMIN,A(I,J))
        RETURN
        END

```

```

*****
* 1. INPUT GRIDDED DATA FILE
*****
      SUBROUTINE GREAD(A,IFILE)
      REAL A(350,350)
      CHARACTER RIDENT*56,PGM*8,IFILE*20
      COMMON/MINC/RIDENT,PGM,NC,NR,NZ,XO,DX,YO,DY,ANGLE
      DATA NIN,NOUT/5,6/
C
      OPEN(UNIT=10,FILE=IFILE,STATUS='OLD',FORM='UNFORMATTED',
1     RECL=1816)
      READ(10)RIDENT,PGM,NC,NR,NZ,XO,DX,YO,DY,ANGLE
      DO 10 I=1,NR
      READ(10)IGER,(A(I,J),J=1,NC)
10     CONTINUE
      CLOSE(10)
      RETURN
      END
*****
* 2. GET THREE SECTIONS OF ELEVATION, FREE AIR AND TERRAIN CORRECTION
*****
      SUBROUTINE SCTN(III,II,NR,NC,IP,NP,HH,GFF,GTT,H,GF,GT)
      PARAMETER(ISIZE=350)
      DIMENSION HH(ISIZE,ISIZE),H(ISIZE)
      DIMENSION GFF(ISIZE,ISIZE),GF(ISIZE)
      DIMENSION GTT(ISIZE,ISIZE),GT(ISIZE)
C
      IF(III-1)10,10,20
10     IR=II
      CALL GLOPRO(NR,NC,IR,HH,H)
      CALL GLOPRO(NR,NC,IR,GFF,GF)
      CALL GLOPRO(NR,NC,IR,GTT,GT)
      IP=IR
      NP=NC
      GO TO 30
20     IC=II
      CALL GLAPRO(NR,NC,IC,HH,H)
      CALL GLAPRO(NR,NC,IC,GFF,GF)
      CALL GLAPRO(NR,NC,IC,GTT,GT)
      IP=IC
      NP=NR
30     RETURN
      END
C
*****
* 3. READ A PROFILE FROM A TWO DIMENSION ARRAY ALONG LONGITUDE
*****
      SUBROUTINE GLOPRO(NR,NC,IR,AA,A)
      PARAMETER(ISIZE=350)
      REAL AA(ISIZE,ISIZE),A(ISIZE)
      DO 1 I=1,NC

```

```

      A(I)=AA(IR,I)
1     CONTINUE
      END
*****
* 4. READ A PROFILE FROM A TWO DIMENSION ARRAY ALONG LATITUDE
*****
      SUBROUTINE GLAPRO(NR,NC,IN,AA,A)
      PARAMETER( ISIZE=350)
      REAL AA( ISIZE, ISIZE),A( ISIZE)
      DO 1 I=1,NR
      A(I)=AA(I,IN)
1     CONTINUE
      END
*****
* 5. FIND MINIMUM VANUE FROM A 1-D METRIC
*****
      SUBROUTINE VMIN(L,A,RMIN)
      REAL A(L)
      RMIN=1.E10
      DO 1 I=1,L
1     RMIN=MIN(RMIN,A(I))
      END
*****
* 6. FIND MAXMUM VANUE FROM A 1-D METRIX
*****
      SUBROUTINE VMAX(L,A,RMAX)
      REAL A(L)
      RMAX=-1.E10
      DO 1 I=1,L
1     RMAX=MAX(RMAX,A(I))
      END
*****
* 7. EXTRACT SEGMENT
*****
      SUBROUTINE SEGMNT(NC,SL,SR,H,GF,GT,K,SH,SGF,SGT)
      PARAMETER( ISIZE=100)
      DIMENSION H(NC),GF(NC),GT(NC)
      DIMENSION SH( ISIZE),SGF( ISIZE),SGT( ISIZE)
      K=0
      DO 1 I=1,NC
      IF(I.GE.SL.AND.I.LE.SR) THEN
      K=K+1
      SH(K)=H(I)
      SGF(K)=GF(I)
      SGT(K)=GT(I)
      END IF
1     CONTINUE
      END
*****
* 8. BOUGUER CORRECTION
*****

```

```

SUBROUTINE BOUG(L,D,HMIN,H,GF,GT,GA)
REAL H(L),GF(L),GT(L),GA(L)
TEM1=0.01277*HMIN
TEM2=0.01277*D
TEM3=D/2.67
DH=TEM1*(2.67-D)
HD=TEM1*D
DO 1 J=1,L
  GA(J)=GF(J)-TEM2*H(J)+HD-DH+GT(J)*TEM3
1 CONTINUE
END

```

```

*-----
* 9. THIS SUBROUTINE TO COMPUTE DERIVATIVE
*-----

```

```

SUBROUTINE DERIVA(NA,A,NB,B)
REAL A(NA),B(NB)
DO 1 I=1,NA-1
  B(I)=A(I)-A(I+1)
1 CONTINUE
END

```

```

*-----
* 10. THE SUBROUTINE FOR CALCULATING REGRESSION
*-----

```

```

SUBROUTINE REG(NX,X,NY,Y,R)
* R: REGRESSION COEFFICIENT
* S: REGRESSION ERROR COEFFICIENT
* A1: REGRESSING EQUATION CONSTANT a
* B1: REGRESSING EQUATION CONSTANT b
* REGRESSING EQUATION: a+bX
REAL X(NX),Y(NY)
XM=0
YM=0
A=0
B=0
C=0
DO 1 I=1,NX
  XM=XM+X(I)
  YM=YM+Y(I)
1 CONTINUE
TEM=REAL(NX)
XM=XM/TEM
YM=YM/TEM
DO 2 I=1,NX
  A=A+ABS(X(I)-XM)*ABS(Y(I)-YM)
  B=B+(X(I)-XM)**2
  C=C+(Y(I)-YM)**2
2 CONTINUE
IF(B.EQ.0) RETURN
R=A/SQRT(B*C)
END

```

C

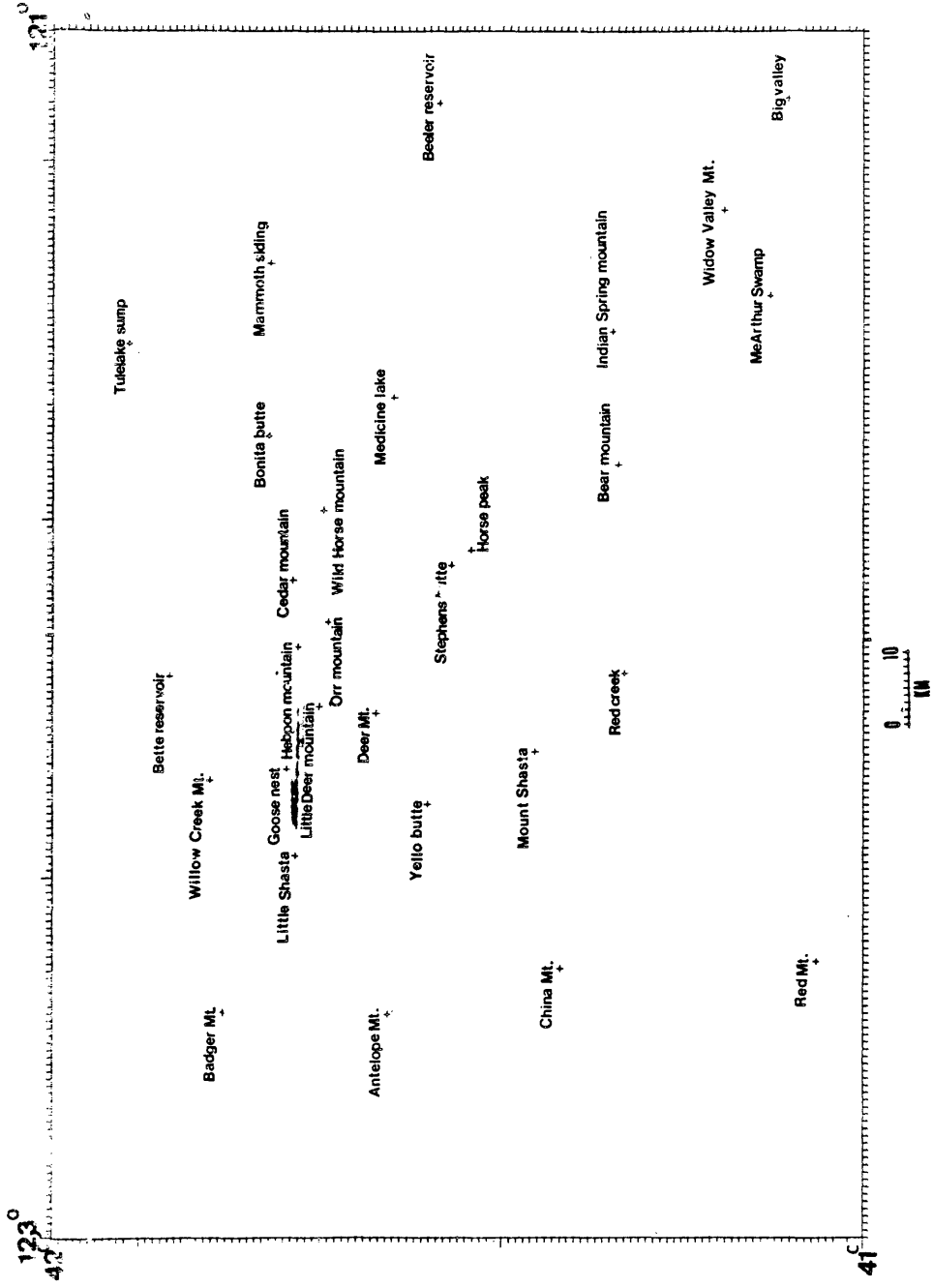


Figure 41. Place Location Map.